Spring 2023

# Applied Geochemistry, Geochronology and Biostratigraphy: Case Studies from the 38th Parallel Structures in Missouri and Orange Basin, Offshore Western South Africa

Marissa Kay Spencer
*Missouri University of Science and Technology*



Department: Geosciences and Geological and Petroleum Engineering

# APPLIED GEOCHEMISTRY, GEOCHRONOLOGY AND BIOSTRATIGRAPHY: CASE STUDIES FROM 38TH PARALLEL STRUCTURES IN MISSOURI AND ORANGE BASIN, OFFSHORE WESTERN SOUTH AFRICA

by

MARISSA KAY SPENCER

A DISSERTATION

Presented to the Graduate Faculty of the

MISSOURI UNIVERSITY OF SCIENCE AND TECHNOLOGY

In Partial Fulfillment of the Requirements for the Degree

DOCTOR OF PHILOSOPHY

in

GEOLOGY AND GEOPHYSICS

2023

Approved by:

Francisca Oboh-Ikuenobe, Advisor
Jonathon Obrist-Farner
Leslie Gertsch
Sophie Warny
Wan Yang

## PUBLICATION DISSERTATION OPTION

This dissertation consists of the following three articles, formatted in the style used by the Missouri University of Science and Technology:

Paper I, found on pages found on pages 2–23, is intended for submission to *Geology*.

Paper II, found on pages 24–53, is intended for submission to *Palaeogeography, Palaeoclimatology, Palaeoecology*.

Paper III, found on pages 54–94, has been published by Springer in *Advances in Petroleum Source Rock Characterizations: Integrated Methods and Case Studies – A Multidisciplinary Source Rock Approach* (Edited by H. El Atfy and B.I. Ghassal).

# ABSTRACT

The unique alignment of the Decaturville, Crooked Creek, and Weaubleau geological structures in central Missouri, three of nine known such structures along the 38$^{th}$ parallel in Illinois, Missouri, and Kansas, has puzzled geoscientists for decades. Research using palynology (palynomorphs and particulate organic matter) and radiometric dating of impact spherules were used to constrain age and a relationship between these enigmatic structures and infer their paleoenvironmental conditions. Novel melting damages, unique to impact, were documented in the palynomorphs in all the three structures. Early Ordovician acritarchs with melted processes correlate with $^{40}$Ar-$^{39}$Ar stepwise heating age of impact spherules from the Crooked Creek structure. This age is coeval with a large clustering event that was responsible for other craters in North America and globally during the Ordovician. The presence of melted acritarchs and palynological material of mixed ages and environments reflect the effects of meteorite impact on the sedimentary environments and stratigraphy.

Another study utilized the palynomorph, palynofacies and foraminiferal contents of 43 samples from four wells in the Orange Basin located offshore western South Africa. The aim was to constrain paleoenvironmental conditions and evaluate the hydrocarbon potential of an understudied area of this offshore frontier basin. Key biostratigraphic and palynofacies information provided evidence for a Cenomanian age for the studied interval, inner to middle shelf settings, and an arid hinterland at the time of deposition of the studied interval. This case study also suggested that the sediments were characterized primarily by gas-prone type III kerogen and some oil-prone type II kerogen.

# ACKNOWLEDGMENTS

Above all, to God be the glory, for truly without Him, no understanding or achievement may be reached. My gratitude is extended to my advisor Dr. Francisca Oboh-Ikuenobe for her guidance. I am also very grateful for the support and mentorship provided by Missouri University of Science and Technology (Missouri S&T) staff and faculty, including Dr. John Hogan, Dr. Clarissa Wisner, Dr. Marek Locmelis, and Dr. David Rogers, committee members, Dr. Sophie Warny, Dr. Leslie Gertsch, Dr. Wan Yang, and Dr. Jonathon Obrist-Farner as well as Dr. Laura Webb of the University of Vermont, and Dr. Joachim Dorsch, and Carl Campbell of St. Louis Community College.

Financial support and contributions by the Department of Geosciences and Geological and Petroleum Engineering at Missouri S&T made it possible to pursue and complete this project. Additional contributions, resources and support provided by Jerry Prewett, Patrick Mulvaney, Tracey Mason, Matthew Barrand of the Missouri Geological Survey are also gratefully acknowledged. Scholarships provided by the Geological Society of America's Continental Drilling Research Grant and the Dr. Alfred Spreng Graduate Research Award (Missouri S&T's Geology and Geophysics Program) were also essential for the completion of this project. Additional thanks are extended to a gracious property owner who provided access and samples to a key area of study.

Last, but not least, I am grateful to my family and friends for their love, patience and support which has helped me to persevere to a better me. Through it all, the never-ending love of my children (Megan, Ryan, and Aaron) and grandchildren (Levi, Lucas, Lydia, Levi, and Eli) has sustained me.

# TABLE OF CONTENTS

Page

# LIST OF ILLUSTRATIONS

PAPER I Page



PAPER II



PAPER III

# LIST OF TABLES

PAPER II Page

# NOMENCLATURE

| Symbol | Description |
|---|---|
| ~ | Approximately |
| ℙ | Pennsylvanian period |
| € | Cambrian period |
| p€ | Precambrian Eon |
| ₸ | Triassic period |
| ● | Ordovician – confirmed impact structure |
| ○ | Ordovician – suspected impact structure |
| ⋆ | 38$^{th}$ parallel – confirmed impact structure |
| ☆ | 38$^{th}$ parallel – suspected impact structure |
| ▵ | 38th Parallel – geological structure |
| ✷ | palynological samples |
| ⊗ | Spherule samples |
| µm | micrometer |
| + | present but not counted |

# 1. INTRODUCTION

Palynology, a branch of paleontology, is a comprehensive tool that is used in several areas of study. Applications of this valuable proxy include modern and past uses in forensics, allergy studies, honey evaluation, archaeology, geochronology, evolutionary and paleoenvironmental studies, paleoecology, climate studies, and hydrocarbon potential.

The aim of this work is to demonstrate various applications of palynology using case studies from two areas of the world, namely central Missouri (USA) and offshore western South Africa. In these case studies, palynology is used: 1) as a biochronology tool; 2) to link uniquely damaged (melted) palynomorphs to meteorite impact; 3) to document the effects of terrestrial meteorite impact on palynomorphs and particulate organic matter; 4) to evaluate the hydrocarbon potential of a frontier basin; and 5) to reconstruct paleoenvironmental conditions.

The results of this project will be presented in separate sections with self-contained components (abstract, introduction, results, discussion, and conclusions). References will also be grouped separately at the end of each independent section. All the sections have been separately disseminated to the scientific community through conference abstracts, planned journal articles, and as a chapter in a published Springer book. Publication citations are given in the footnote of the first page of each section.

## PAPER

# I. GOLDILOCKS FOSSILS AND THREE MISSOURI 38TH PARALLEL STRUCTURES: A TALE OF ORDOVICIAN IMPACT CLUSTERING*[1,2]

Marissa K. Spencer[1], Francisca E. Oboh-Ikuenobe[1], and Laura E. Webb[2]

[1]Department of Geosciences and Geological and Petroleum Engineering, Missouri University of Science and Technology, 1400 N. Bishop, Rolla, MO 65409, USA

[2]Department of Geography and Geosciences, University of Vermont, 180 Colchester Avenue, Burlington, Vermont 05405, USA

## ABSTRACT

A decades-long debate centers on a series vs. clustering origin of aligned 38th parallel geologic structures in the central U.S. Novel methods may resolve the timing and origin of three structures in Missouri (Crooked Creek, Decaturville, Weaubleau) and add to an impact clustering event with global and regional implications. Impact can destroy biota and rocks, but where preserved, affected rocks and fossils provide timing evidence. Although palynomorph damage can result from other earth processes, features attributed to melting, such as in Goldilocks fossils (melted but identifiable) are unique to impact and indicate areal and temporal event proximity. Correlation of melted acritarchs and impact spherule $^{40}Ar/^{39}Ar$ step-heating ages better constrain 38th parallel impact timing

* 1. This manuscript is intended for submission to *Geology*.
2. Spencer, M., Oboh-Ikuenobe, F.E., and Webb, L.E., 2021. The Ordovician meteor event: evidence from impact-damaged acritarchs and the 40Ar/39Ar date of impact spherules from the Crooked Creek Structure. Geological Society of America Abstracts with Programs, 109 (7).

and suggests a link with an L-chondrite asteroid breakup and subsequent Ordovician meteorite clustering event.

## 1. INTRODUCTION

The 38th Parallel structures (38PS) are geological structures along the 38th latitude in the central U.S. (Figure 1) with debate about their genesis (Snyder and Gerdemann, 1965; Heyl, 1972; Rampino and Volk, 1996; Luczaj, 1998). Although visually comparable to comet fragments that impacted Jupiter (National Aeronautics and Space Administration, 2019), evidence suggests an alternate perspective and scale, including connection to the Ordovician Meteor Event (OME). They extend E-W >1000 km over the sediment-covered igneous and metamorphic rocks of the North American craton, and are shaped by Paleozoic geologic events, including the Midcontinent Rift System, Sloss sequences, Ozark Uplift, Nemaha Uplift, and Appalachian and Ouachita orogenies (Sloss, 1963, 1988; Dolton and Finn, 1989; Hatcher et al., 1989; van Schmus, 1992; Hatcher, 2010).

The three Missouri 38PS (MO38PS), Crooked Creek, Decaturville, and Weaubleau, have intense faulting, folding, and brecciation with variable sizes, features, and geology (Figure 1) and are classified as complex craters by size and morphology (Melosh, 1989). At the center of the Cuba and Palmer fault zone (Anderson, 1983; Heyl, 1983; Luczaj, 1998), the Crooked Creek crater is ~7 km wide with a partially collapsed central uplift bordered by high-angle normal faults and divided by a narrow irregular

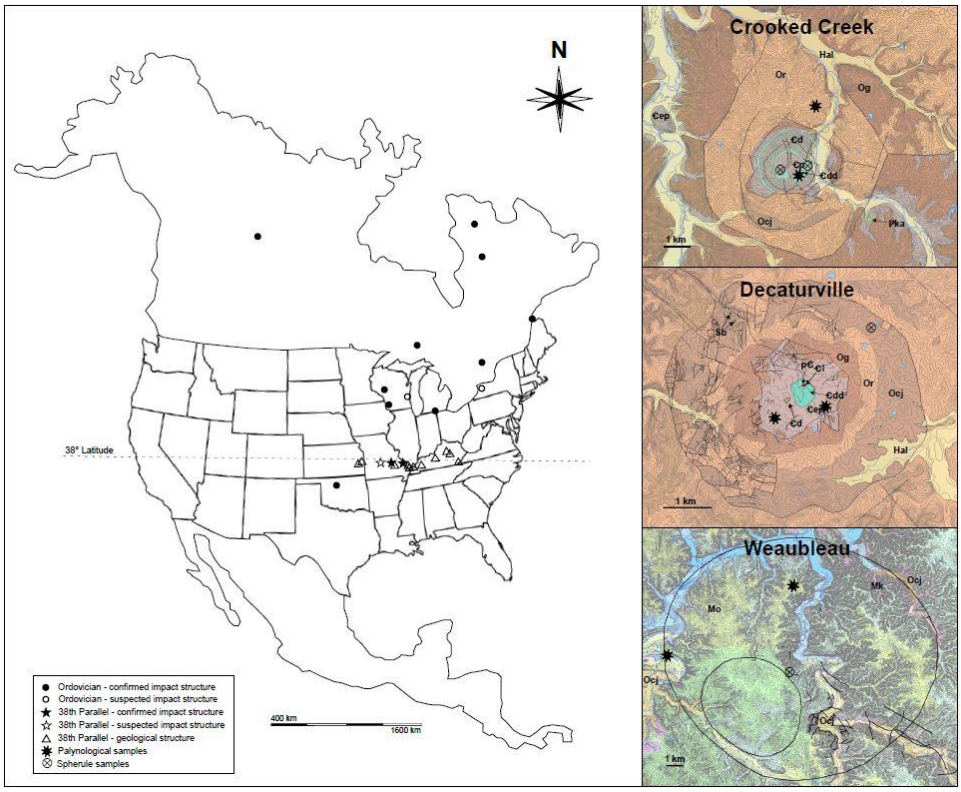


Figure 1. Locations and geological maps of Missouri 38th parallel structures (Crooked Creek, Decaturville, and Weaubleau). Holocene (Hal: alluvium), Pennsylvanian (ℙka: Cherokee Group, Krebs Subgroup, Atokan Stage), Mississippian (Mo: Osagean, Mk: Kinderhookian), Ordovician (Or: Roubidoux, Og: Gasconade, Ocj: Cotter-Jefferson City), Cambrian (Cl: Lamotte, Cd: Davis, Cdd: Derby-Doe Run, Cep: Eminence-Potosi, Cp: Potosi), pC: Precambrian granite bedrock, palynology samples represented by circle with cross, and impact spherule sample location represented by spiked circles.

horst (Hendriks, 1954). The rocks are sedimentary with the oldest displaced stratigraphically upward ~300 m (Hendriks, 1954). Surrounded by a normal ring fault, Decaturville extends ~5.5 km and has a central uplift with crosscutting radial low angle thrust faults (Offield and Pohn, 1979). The rocks include central uplift Precambrian blocks displaced from ~540 m and discontinuous sedimentary outcrops with lateral bedding variation (Offield and Pohn, 1977). Weaubleau is shallow and large at ~19 km in diameter with sedimentary rocks and bedrock granite only as clasts in breccia (Evans et

al., 2003). Streams reveal potential ring and rim faulting, with mapping hindered by short fault extent, lack of pre-Pennsylvanian outcrops (Beveridge, 1951), and well-log data paucity. Crooked Creek and Decaturville are confirmed impact structures (Hendriks, 1954; Offield and Pohn, 1979) based on shatter cone exclusivity at nuclear blasts and meteorite impact (Osinski and Ferrière, 2016), although planar features in resistant minerals also document shock metamorphism (French, 1998). Planar features are documented in quartz in Crooked Creek (Dietz and Lambert, 1980; Poelchau and Kenkmann, 2011), Decaturville (Offield and Pohn, 1979), and Weaubleau (Morrow and Evans, 2007).

MO38PS timing estimates vary with lingering uncertainty. Early Ordovician-Pennsylvanian timing is assumed for Crooked Creek (Hendriks, 1954; Luczaj, 1998; Schmieder and Kring, 2020) based on deformed Lower Ordovician rocks (Snyder and Gerdemann, 1965) and undeformed Pennsylvanian-aged rocks (Luczaj, 1998), although Miller et al. (2007) offers a Mississippian-Pennsylvanian age from unaltered fossils in float breccia. Apatite fission track dating of uplifted granite yielded disparate Late Triassic-Late Jurassic ages for Decaturville (Offield and Pohn, 1979), while paleomagnetism and mineralization suggest post-Pennsylvanian to younger timing (Offield and Pohn, 1979; Elmore and Dulin, 2007; Schmieder and Kring, 2020). A Late Mississippian-late Paleozoic age is suggested for Weaubleau based on unaltered and unconformable interthrusted Mississippian and Pennsylvanian-aged rocks and fossils in breccias (Beveridge, 1951; Snyder and Gerdemann, 1965; Rampino and Volk, 1996; Mickus et al., 2005; Evans et al., 2008). An Osagean-Meramecian timing is proposed

from paleomagnetism and unaltered fossils in breccia (Dulin and Elmore, 2007; Miller et al., 2010).

Building upon these contributions, correlation of impact-affected material (melted acritarchs, impact spherule $^{40}Ar/^{39}Ar$ ages) in the three MO38PS will provide a stronger case for impact timing and mitigates challenges of 1) complex stratigraphy, 2) facies limitations, 3) limited impact-affected material, and 4) prolonged and ongoing post-impact effects. These results may broaden the number of Ordovician clusters and the understanding of planetary body interactions and U.S. midcontinent geology, including mineral deposits associated with impact (Mathur et al., 2021; James et al., 2022).

## 2. METHODS

### 2.1. PALYNOLOGY

Oxidized and unoxidized organic residue slides were prepared by Global Geolab from samples (Appendix A) using standard palynological processing (Traverse, 2007). Slides were scanned using transmission light microscopy and palynomorphs photographed using a Nikon polarizing microscope with Nikon Q-Imaging MicroPublisher 3.3 RTV digital camera. Palynomorphs were grouped by melt-damage severity (not melted; melted but recognizable; too damaged to discern) and environment – terrestrial (spores, pollen, fungal remains) and aquatic (chitinozoans and acritarchs) – and named where possible. Data was supplemented with photographs and palynological data obtained from literature (e.g., Jansonius and Hills, 1976; Fensome et al., 1990;

Balme, 1995; Punt et al., 2007; Williams et al., 2017). Palynomorph age ranges are from Palynodata and White (White, 2008).

### 2.2. $^{40}$AR/$^{39}$AR LASER STEPWISE HEATING OF SPHERULES

Crooked Creek, Decaturville, and Weaubleau samples (see Appendix B) were crushed, and spherules picked, washed (10% HCL), rinsed with deionized water, measured, and imaged with a Nikon microscope. Scanning electron microscopy (SEM; Hitachi S4700 and FEI Helios Nanolab 600) with electron dispersive spectroscopy (EDS; Oxford Instruments) was used for semi-quantitative elemental analysis. Individual spherules were then analyzed by $^{40}$Ar/$^{39}$Ar laser step heating analyses in the argon geochronology laboratory at the University of Vermont. Data were obtained from 11 analyses of single spherules from 7 samples, 4 of which were replicates (i.e., a second single spherule was analyzed). Details regarding $^{40}$Ar/$^{39}$Ar methods and complete data tables are provided (see Appendix C).

## 3. RESULTS

Palynology samples (Appendix A) had low palynomorph recovery but were diverse in type and age (Figures 2, 3). Ages range from Cambrian to Holocene with Cretaceous palynomorphs notable since Cretaceous rocks only occur in the Mississippian Embayment in Missouri (Spencer, 2001). Palynomorphs include terrestrial (cryptospores, spores, pollen, fungal hyphae, and spores) and aquatic (chitinozoans, acritarchs) types.

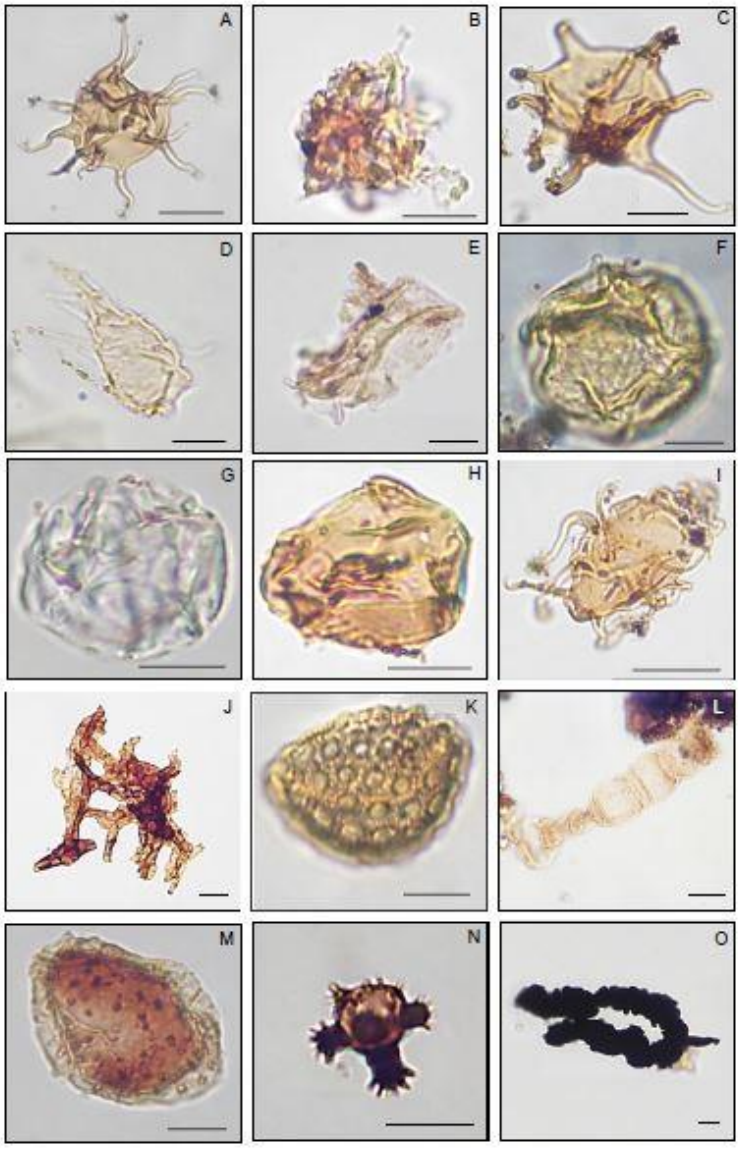


Figure 2. Photomicrographs of select palynomorphs of mixed ages, environments, and damage effects from within Crooked Creek (CC), Decaturville (D) and Weaubleau (W) impact structures. Included are the sample slide number, and Lovins Field Finder (LF) or England Finder (EF) coordinates. Scale bars = 10 μm. A, *Baltisphaeridium bystrentos*, W1-1690-NS1, LF 3G36. B, unidentified acritarch, D2-3198-C57, LF 2U29. C, *Baltisphaeridium perclarum*, W1-1690-NS1, LF 3J24. D, *Cornuferifusa* sp.?, CC-2505-CC795, LF 3L42. E, unidentified acritarch, D2-3198-C57, LF 2U28. F, *Polygonium gracile*?, D1-2506-D771, LF 1G32. G, *Multiplicisphaeridium* sp.?, CC2-2505-CC795, EF 62, 10.1, H, *Veryhachium cymosum*?, W1-1690-NS1, LF 2L31, I, *Acanthodiacrodium* sp., W1, EF 19.2, 48.9. J, Fungal mycelium, W2-9652, LF 4C38, K, *Stellatopollis* sp.?, D1-2506-D771, LF 2M45. L, *Desmochitina minor*, D2-3198-C57, LF 1F28. M, *Aneurospora geriennei* cf., W2-9652, LF 2F40. N, *Baltisphaeridium jardiniae*, CC2-2505-CC795, LF 3J44. O. Opaque tubule, CC2-2505-CC795, LF 3L37.

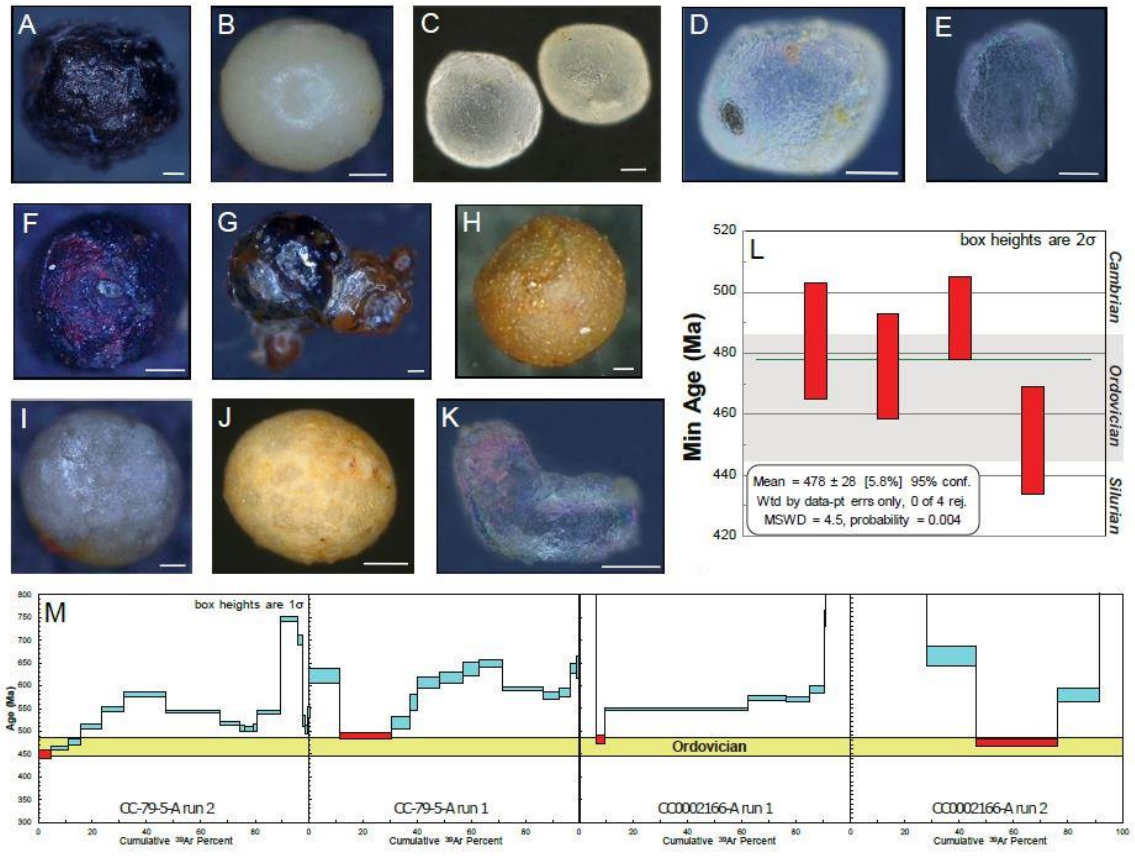


Figure 3. Impact spherules from Crooked Creek, Decaturville, and Weaubleau impact structures, and $^{40}Ar/^{39}Ar$ stepwise heating age results from Crooked Creek spherules.

Particulate organic matter (POM) also represents aquatic (marine and non-marine amorphous organic matter, filamentous algae) and terrestrial (degraded, structured, structureless, and opaque phytoclasts) detritus.

Palynomorphs and POM range from well-preserved to severely damaged (Figure 2). Impact damages include vesicular, smoothed, or frosted wall surface alteration; beaded, frayed, missing, and fused processes; and extreme body damage (ghosted, brecciated). The acritarchs have diverse shapes and processes with variable damage even among the same type. The only melted palynomorphs in all three structures are

Ordovician acritarchs (i.e., Baltisphaeridium perclarum, Acanthodiacrodium tadlaense, Veryhachium oklahomense, Goniosphaeridium polygonale, Vermimarginata barbata, Veryhachium trispinosum) (Figure 2).

Spherules occur in the Decaturville rim, Weaubleau center polymict breccia outcrops, and dolomites in the Crooked Creek center (Figures 1, 3; Appendix B). Spherules were not found in Pennsylvanian rocks around any of the three structures (see Appendix D). Spherules vary in size (0.2-2 mm), morphology, and texture with aerodynamic shapes (spherical, egg, football, diamond, triangular, dumbbell) and fused and aggregate forms. Spherules have ied colors (white, black, gray, yellow, red, brown, orange) and textures (smooth, botryoidal, framboidal, frosted, crystalline, acicular, leopard-spot). They have hollow and compact forms, internal patterns (concentric, radial), and thin veneers with irregular surface pitting common. Spherule compositions are silicate and rarely glassy (see Appendix B).

Laser $^{40}Ar/^{39}Ar$ stepwise heating of individual spherules yielded complex apparent age spectra (Figure 3) rather than simple plateaus. Instead of a simple mixing relationship between trapped (e.g., atmospheric) and radiogenic argon components, scatter in the inverse isochron plots (see Appendix C) suggest multiple radiogenic and trapped components. Steps releasing 4% or more of the total 39Ar from each sample provided minimum ages from c. 391 to 593 Ma. Four minimum ages from six analyses (from two samples, each with two runs) are Ordovician or are concordant within error. Thus, there are four apparent age spectra for Crooked Creek spherules with minimum age convergence. These four minimum step ages yield a 478 ±28 Ma combined mean age at the 95% confidence interval, interpreted as a timing estimate for partial resetting of

inherited age domains by the Crooked Creek impact. Decaturville and Weaubleau spherules had lower potassium and apparent age spectra with tilde or saddle shapes without plateaus. Inverse isochrons likewise yielded poor fits, if at all, with data spread suggesting contributions from multiple radiogenic and trapped components. Minimum ages obtained from these samples did not converge and ranged from c. 43 Ma to 1.4 Ga.

The pattern of zinc and copper mineralization present surrounding the three MO38PS at distances between 95-160 km (see Appendix E), is likely due to post-impact hydrothermal processes, like that discovered at Chixculub impact (Mathur 2021).

# 4. DISCUSSION

## 4.1. IMPACT DATING CHALLENGES

Impact geochronology is challenging, particularly in sedimentary targets (Osinski et al., 2007). Impact is dynamic and intense with variable shock and temperature effects resulting in variable and complex sedimentology and stratigraphy (Christeson et al., 2021) that is poorly understood (Keller, 2007). Sedimentary impactite studies are few (Beauford, 2012) and impact-affected material suitable for radiometric dating is limited in the MO38PS. Sediments are migmatized, intruded by multi-generations of dike and breccia from phreatic eruptions and prolonged volcanism (Ubide et al., 2017) and subjected to ongoing alteration processes (Ames et al., 2004; James et al., 2022), including hydrothermal effects (Bao et al., 2009; Schmieder et al., 2018; Jiang et al., 2021) that result in mixed, condensed, and partially or completely altered sediments (Grieve, 1991; See et al., 1998; Dressler and Reimold, 2001; Naumov, 2002; Koeberl et

al., 2012; Osinski et al., 2020). Slumping due to crater morphology and gravity is ongoing and may result in post-impact sedimentary breccia formation (Shukla and Sharma, 2018). The silicified (Reimold et al., 2005) and hardened structures may function as a barrier to preserve remnant unaltered post-impact fossils in sink fill or sediment drape. In situ MO38PS rocks are Cambro-Ordovician, with unaltered younger sediment input after impact. Biostratigraphy is valuable for age; however, facies may limit faunal types, and unconformities limit context. Missouri Phanerozoic biostratigraphy focuses on facies-dependent microfossils, unlike palynology which offers expanded relative age and paleoenvironment. Biostratigraphic evidence includes unaltered Ordovician-Carboniferous-aged fossils in float breccias (Miller et al., 2006, 2007) possibly from debris flows after impact. Remagnetization affects paleomagnetism, common in dolomites like those present in the structures (Chang et al., 1987; McCabe and Elmore, 1989; Elmore et al., 2012; Zhang et al., 2018). Establishing an impact link and placing the results in context is key for the most cogent interpretation.

### 4.2. OVERCOMING CHALLENGES WITH NOVEL METHODS

Impact biostratigraphy presents unique damage-related challenges. Although resistant, palynomorphs may be damaged by other earth processes. Melting distinguishes impact-related damage; however, fossils may be damaged (Edwards and Powars, 2003; Edwards, 2012) or destroyed (Smith et al., 2021) thus hindering age interpretation. ‘Goldilocks fossils’ relate this challenge with the story of Goldilocks and the Three Bears, and a quest to find items that were “just right”. Sorting palynomorphs by those that are 1) too damaged to discern, 2) not melted, and 3) “just right” (melted but still

recognizable) revealed wide-ranging palynomorph ages but only Ordovician acritarchs that melted (Figures 2, 4). The melted palynomorph ages in each structure are correlative to the Crooked Creek impact spherule $^{40}Ar/^{39}Ar$ age. Also, acritarchs occur in marine environment as the MO38PS sedimentary rocks and align with regional and global geology interpretations.

### 4.3. CORRELATION WITH IMPACT SPHERULE $^{40}AR/^{39}AR$ AGE

$^{40}Ar/^{39}Ar$ dating is useful for impact interpretation (Reimold et al., 1990; Koeberl et al., 2001; Sherlock et al., 2005), particularly for complex thermal histories with extraneous argon inputs from rapidly cooling impact melt and vapor condensates where radiogenic argon may not escape completely and result in inherited $^{40}Ar$ (Pickersgill et al., 2020). $^{40}Ar/^{39}Ar$ enables measurement of smaller amounts with precision, key for heterogeneous material requiring argon source, alteration, and outgassing differentiation (Sherlock et al., 2005). While concordant apparent age spectra defining plateaus are ideal, reproducibility among minimum ages interpreted in geological context and consistent with other supporting data can yield important constraints on event timing subject to partial resetting (Klepeis et al., 2019).

Impact spherules form as ejecta or vapor condensation (Johnson and Melosh, 2012) in a dynamic and high-temperature environment (Bunch et al., 2012). Impact timing may be inferred since radiometric age resets with cooling; however, interpretation can be complex due to impact related-partial melting or recrystallization (Kenny et al., 2020) and potential for overprinting (Jourdan et al., 2012). Spherules are a product of 1) target rock, 2) trace meteorite projectile, and 3) impact geochemical processes with

further influence by diagenesis. Although a silicate composition aligns with MO38PS sedimentary rocks, spherules may be compositionally inhomogeneous and inconsistently reset due to partial melting or crystallization. Decaturville and Weaubleau spherule apparent age spectra are complex and discordant with spectral shapes indicative of partial crystallization and hydrothermal alteration (Alexandrov et al., 2002; Kelley, 2002) related to impact. The inverse isochron data scatter reflects a mix of radiogenic and trapped components resulting from a long-lived crystallization, inherited heterogeneity, or partial radiogenic $^{40}$Ar loss attributed to retrograde reactions, thermal diffusion, deformation, or chemical alteration (Schaen et al., 2021) all common to impact and subsequent weathering (Berry and McDougall, 1986; Alexandrov et al., 2002; Schaen et al., 2021). Decaturville and Weaubleau spherules are from polymict breccias likely formed in a hot, highly energetic environment (Offield and Pohn, 1979; Morrow and Evans, 2007; Newman and Osinski, 2018), while Crooked Creek spherules found in dolomites near the central uplift, potentially formed as ejecta, were quickly covered by sedimentation and further protected by uplift fault structure and thus provided relevant steps with a combined mean age of 478 ±28 Ma. coeval with the melted fossil ages.

### 4.4. ORDOVICIAN CLUSTERING LINK

The break-up of a ~200 km diameter L-chondrite asteroid (c. 470 Ma), produced fragments intersecting Earth's orbit over ~2 m.y. (Ormö et al., 2015), and more craters than any other clustering event on Earth (Schmieder and Kring, 2020). OME craters occur in Sweden, Estonia, Canada, and the U.S. with in-situ L-chondrite meteorites and extraterrestrial chromite documented in Sweden (Schmitz et al., 2001, 2019). In addition

to timing and proximity to other OME craters, theoretic physics suggests chains are improbable, and most break-up processes result in clusters rather than chains (Melosh, 1989).

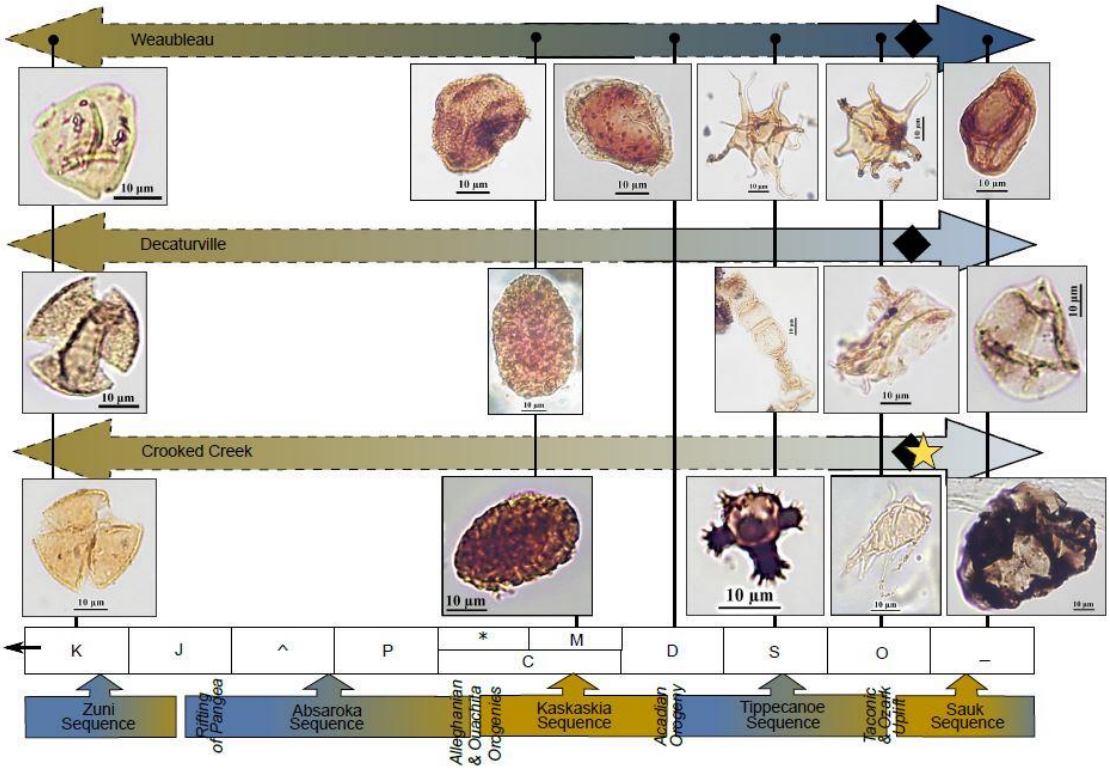


Figure 4. Combined relative and absolute age evidence in context with regional geologic events. Diamonds represent melted acritarch age ranges, and the star represents $^{40}Ar/^{39}Ar$ age for Crooked Creek.

## 5. CONCLUSIONS

Age correlation of melted acritarchs and impact spherules (Figure 4) provide an unexpected relationship for the MO38PS. Impact timing appears to be coeval to the OME which suggests the MO38PS resulted from L-chondrite asteroid fragment impacts in a

marine environment. Absolute and relative age dating of impact-affected material suggests the Crooked Creek, Decaturville, and Weaubleau impact structures were likely formed in the Early Ordovician as part of impact clustering.

## REFERENCES

Alexandrov, P., Ruffet, G., and Cheilletz, A., 2002, Muscovite recrystallization and saddle-shaped 40 Ar/ 39 Ar age spectra: example from the Blond granite (Massif Central, France): Geochimica et Cosmochimica Acta, v. 66, p. 1793–1807, doi:10.1016/S0016-7037(01)00895-X.

Ames, D.E., Kjarsgaard, I.M., Pope, K.O., Dressler, B., and Pilkington, M., 2004, Secondary alteration of the impactite and mineralization in the basal Tertiary sequence, Yaxcopoil-1, Chicxulub impact crater, Mexico: Meteoritics & Planetary Science, v. 39, p. 1145–1167, doi:10.1111/j.1945-5100.2004.tb01134.x.

Anderson, J.L., 1983, Proterozoic anorogenic granite plutonism of North America, *in* p. 133–154, doi:10.1130/MEM161-p133.

Balme, B.E., 1995, Fossil in situ spores and pollen grains: an annotated catalogue: Review of Palaeobotany and Palynology, v. 87, p. 81–323, doi:10.1016/0034-6667(95)93235-X.

Bao, Z., Wang, Q., Bai, G., and Zhao, Z., 2009, Impact of hydrothermal alteration on the U-Pb isotopic system of zircons from the Fangcheng syenites in the Qinling orogen, Henan Province, China: Chinese Journal of Geochemistry, v. 28, p. 163–171, doi:10.1007/s11631-009-0163-1.

Beauford, R.E., 2012, Carbonate melts and sedimentary impactite variation at Crooked Creek and Decaturville Impact Craters, Missouri, USA, *in* 43rd Lunar and Planetary Science Conference, The Woodlands, Lunar and Planetary Science.

Berry, R.F., and McDougall, I., 1986, Interpretation of 40Ar/39Ar and K/Ar dating evidence from the Aileu Formation, East Timor, Indonesia: Chemical Geology: Isotope Geoscience section, v. 59, p. 43–58, doi:10.1016/0168-9622(86)90056-4.

Beveridge, T.R., 1951, The geology of the Weaubleau Creek area, Missouri: Missouri Division of Geological Survey and Water Resources, Rolla, Missouri.

Bunch, T.E. et al., 2012, Very high-temperature impact melt products as evidence for cosmic airbursts and impacts 12,900 years ago: Proceedings of the National Academy of Sciences, v. 109, doi:10.1073/pnas.1204453109.

Chang, S.-B.R., Kirschvink, J.L., and Stolz, J.F., 1987, Biogenic magnetite as a primary remanence carrier in limestone deposits: Physics of the Earth and Planetary Interiors, v. 46, p. 289–303, doi:10.1016/0031-9201(87)90191-9.

Christeson, G.L., Morgan, J. v., and Gulick, S.P.S., 2021, Mapping the Chicxulub impact stratigraphy and peak ring using drilling and seismic data: Journal of Geophysical Research: Planets, v. 126, doi:10.1029/2021JE006938.

Dietz, R.S., and Lambert, P., 1980, Shock metamorphism at Crooked Creek cryptoexplosion structure, MO: Meteoritics, v. 15, p. 281–282.

Dolton, G.L., and Finn, T.M., 1989, Petroleum geology of the Nemaha Uplift, Central Midcontinent, U.S. Geological Survey Open-File Report 88-450D.:

Dressler, B.O., and Reimold, W.U., 2001, Terrestrial impact melt rocks and glasses: Earth-Science Reviews, v. 56, p. 205–284, doi:10.1016/S0012-8252(01)00064-2.

Dulin, S., and Elmore, R.D., 2007, Paleomagnetism of the Weaubleau structure, southwestern Missouri, *in* Special Paper 437: The Sedimentary Record of Meteorite Impacts, Geological Society of America, p. 55–64, doi:10.1130/2008.2437(04).

Edwards, L.E., 2012, Dinocyst taphonomy, impact craters, cyst ghosts and the Paleocene–Eocene thermal maximum (PETM): Palynology, v. 36, p. 80–95, doi:10.1080/01916122.2012.679205.

Edwards, L.E., and Powars, D.S., 2003, Impact damage to dinocysts from the Late Eocene Chesapeake Bay Event: PALAIOS, v. 18, p. 275–285, doi:10.1669/0883-1351(2003)018<0275:IDTDFT>2.0.CO;2.

Elmore, R.D., and Dulin, S., 2007, New paleomagnetic age constraints on the Decaturville impact structure and Weaubleau structure along the 38th parallel in Missouri (North America): Geophysical Research Letters, v. 34, doi:10.1029/2007GL030113.

Elmore, R.D., Muxworthy, A.R., and Aldana, M., 2012, Remagnetization and chemical alteration of sedimentary rocks: Geological Society, London, Special Publications, v. 371, p. 1–21, doi:10.1144/SP371.15.

Evans, K., Davis, G., Miao, X., Mickus, K., Miller, J., and Morrow, J., 2008, Re-evaluating the 38th Parallel serial impact hypothesis, *in* AGU Fall Meeting Abstracts, American Geophysical Union.

Evans, K.R., Rovey, C.W., II., Mickus, K.L., Miller, J.F., Plymate, T.G., and Thomson, K.C., 2003, Weaublea-Osceola Structure, Missouri: Deformation, event stratification, and shock metamorphism of a mid-carboniferous impact site, *in* Third International Conference on Large Meteorite Impacts, Nördlingen, Germany.

Fensome, R.A., Williams, G.L., Barss, M.S., Freeman, J.M., and Hill, J.M., 1990, Acritarchs and fossil prasinophytes: an index to genera, species and infraspecific taxa: v. 25, p. 771.

French, B., 1998, Traces of catastrophe: a handbook of shock-metamorphic effects in terrestrial meteorite impact structures: Washington, DC, Smithsonian Institute, 31–60 p.

Grieve, R.A.F., 1991, Terrestrial impact: the record in the rocks: Meteoritics, v. 26, p. 175–194, doi:10.1111/j.1945-5100.1991.tb01038.x.

Hatcher, R.D., 2010, The Appalachian Orogen: a brief summary, *in* From Rodinia to Pangea: The Lithotectonic Record of the Appalachian Region, Geological Society of America, doi:10.1130/2010.1206(01).

Hatcher, R.D., Thomas, W.A., and Viele, G.W., 1989, The Appalachian-Ouachita Orogen in the United States (R. D. Hatcher, W. A. Thomas, & G. W. Viele, Eds.): Boulder, Colorado 80301, Geological Society of America, doi:10.1130/DNAG-GNA-F2.

Hendriks, H.E., 1954, The Geology of the Steelville Quadrangle Missouri : Jefferson City, Missouri Geological Survey and Water Resources, v. 36, 1–88 p.

Heyl, A. v., 1983, Some major lineaments reflecting deep-seated fracture zones in the central United States, and mineral districts related to the zones: Global Tectonics and Metallogeny, v. 2, p. 75–89, doi:10.1127/gtm/2/1983/75.

Heyl, A. v., 1972, The 38th Parallel Lineament and its relationship to ore deposits: Economic Geology, v. 67, p. 879–894, doi:10.2113/gsecongeo.67.7.879.

James, S., Chandran, S.R., Santosh, M., Pradeepkumar, A.P., Praveen, M.N., and Sajinkumar, K.S., 2022, Meteorite impact craters as hotspots for mineral resources and energy fuels: a global review: Energy Geoscience, v. 3, p. 136–146, doi:10.1016/j.engeos.2021.12.006.

Jansonius, J., and Hills, L.V., 1976, Genera file of fossil spores and pollen (with supplements): Special Publication, Department of Geology, University of Calgary, Canada,.

Jiang, Q., Jourdan, F., Olierook, H.K.H., Merle, R.E., Verati, C., and Mayers, C., 2021, 40Ar/39Ar dating of basaltic rocks and the pitfalls of plagioclase alteration: Geochimica et Cosmochimica Acta, v. 314, p. 334–357, doi:10.1016/j.gca.2021.08.016.

Johnson, B.C., and Melosh, H.J., 2012, Formation of spherules in impact produced vapor plumes: Icarus, v. 217, p. 416–430, doi:10.1016/j.icarus.2011.11.020.

Jourdan, F., Reimold, W.U., and Deutsch, A., 2012, Dating terrestrial impact structures: Elements, v. 8, p. 49–53, doi:10.2113/gselements.8.1.49.

Keller, G., 2007, Impact stratigraphy: old principle, new reality, *in* Special Paper 437: The Sedimentary Record of Meteorite Impacts, Geological Society of America, p. 147–178, doi:10.1130/2008.2437(09).

Kelley, S., 2002, Excess argon in K–Ar and Ar–Ar geochronology: Chemical Geology, v. 188, p. 1–22, doi:10.1016/S0009-2541(02)00064-5.

Kenny, G.G., Karlsson, A., Schmieder, M., Whitehouse, M.J., Nemchin, A.A., and Bellucci, J.J., 2020, Recrystallization and chemical changes in apatite in response to hypervelocity impact: Geology, v. 48, p. 19–23, doi:10.1130/G46575.1.

Klepeis, K.A., Webb, L.E., Blatchford, H.J., Jongens, R., Turnbull, R.E., and Schwartz, J.J., 2019, The age and origin of Miocene-Pliocene fault reactivations in the upper plate of an incipient subduction zone, Puysegur Margin, New Zealand: Tectonics, v. 38, p. 3237–3260, doi:10.1029/2019TC005674.

Koeberl, C., Claeys, P., Hecht, L., and McDonald, I., 2012, Geochemistry of impactites: Elements, v. 8, p. 37–42, doi:10.2113/gselements.8.1.37.

Koeberl, C., Reimold, W.U., and Kelley, S.P., 2001, Petrography, geochemistry, and argon-40/argon-39 ages of impact-melt rocks and breccias from the Ames impact structure, Oklahoma: The Nicor Chestnut 18-4 drill core: Meteoritics & Planetary Science, v. 36, p. 651–669, doi:10.1111/j.1945-5100.2001.tb01907.x.

Luczaj, J., 1998, Argument supporting explosive igneous activity for the origin of “cryptoexplosion” structures in the midcontinent, United States: Geology, v. 26, p. 295, doi:10.1130/0091-7613(1998)026<0295:ASEIAF>2.3.CO;2.

Mathur, R., Mahan, B., Spencer, M., Godfrey, L., Landman, N., Garb, M., Graham Pearson, D., Liu, S.-A., and Oboh-Ikuenobe, F.E., 2021, Fingerprinting the Cretaceous-Paleogene boundary impact with Zn isotopes: Nature Communications, v. 12, p. 4128, doi:10.1038/s41467-021-24419-8.

McCabe, C., and Elmore, R.D., 1989, The occurrence and origin of Late Paleozoic remagnetization in the sedimentary rocks of North America: Reviews of Geophysics, v. 27, p. 471, doi:10.1029/RG027i004p00471.

Melosh, H.J., 1989, Impact cratering: a geologic process: Oxford University Press, 245 p.

Mickus, K.L., Evans, K.R., and Rovey, C.W., II., 2005, Gravity and magnetic analysis of the Weaubleau Osceola structure, Missouri, *in* SEPM Conference on the Sedimentary Record of Meteorite Impacts, Springfield, Society for Sedimentary Geology.

Miller, J.F., 2010, Conodonts and other fossils from cores in the resurge breccia at the Weaubleau Impact Structure St. Clair County, Missouri, *in* Geological Society of America North-Central Section (44th Annual) and South-Central Section (44th Annual) Joint Meeting (11–13 April 2010), Abstracts with Programs. Vol. 42, No. 2, p.50, Geological Society of America.

Miller, J.F., Evans, K.R., Ethington, R.L., Repetski, J.E., Sandberg, C.A., and Thompson, T.L., 2007, Critical stratigraphic data from reworked conodonts in impact breccias across Missouri's Ozark Dome, *in* Geological Society of America Annual Meeting, Geological Society of America.

Miller, J.F., Evans, K.R., Kurtz, V.R., Thompson, T.L., Mulvany, P.S., Sandberg, C.S., Repetski, J.E., and Ethington, R.L., 2006, Using conodonts and other fossils to determine the age of Missouri's 38th Parallel structures and some "lost horizons" of the Ozark Dome, *in* Geological Society of America, 2006 Philadelphia Annual Meeting (22–25 October 2006), Abstracts with Programs, Geological Society of America.

Morrow, J., and Evans, K., 2007, Preliminary shocked-quartz petrography, upper Weaubleau breccia, Missouri, USA, *in* Meteoritical Society 2007 Annual Meeting, Meteoritical Society.

National Aeronautics and Space Administration, 2019, How historic Jupiter comet impact led to planetary defense:

Naumov, M.V., 2002, Impact-generated hydrothermal systems: data from Popigai, Kara, and Puchezh-Katunki impact structures, *in* p. 117–171, doi:10.1007/978-3-662-05010-1_6.

Newman, J.D., and Osinski, G.R., 2018, Investigation of carbonate-rich breccias and their emplacement in the central uplift of the Decaturville Impact Structure, Missouri, *in* 49th Lunar and Planetary Science Conference, Lunar and Planetary Institute.

Offield, T.W., and Pohn, H.A., 1977, Deformation at the Decaturville impact structure, Missouri, *in* Impact and explosion cratering: Planetary and terrestrial implications; Proceedings of the Symposium on Planetary Cratering Mechanics, p. 321–341.

Offield, T., and Pohn, H., 1979, Geology of the Decaturville impact structure, Missouri: United States Geological Survey, Washington, DC.

Ormö, J., Sturkell, E., Alwmark, C., and Melosh, J., 2015, First known terrestrial impact of a binary asteroid from a main belt breakup event: Scientific Reports, v. 4, p. 6724, doi:10.1038/srep06724.

Osinski, G.R., Cockell, C.S., Pontefract, A., and Sapers, H.M., 2020, The role of meteorite impacts in the origin of life: Astrobiology, v. 20, p. 1121–1149, doi:10.1089/ast.2019.2203.

Osinski, G.R., and Ferrière, L., 2016, Shatter cones: (mis)understood? Science Advances, v. 2, doi:10.1126/sciadv.1600616.

Osinski, G.R., Spray, J.G., and Grieve, R.A.F., 2007, Impact melting in sedimentary target rocks: an assessment, *in* Special Paper 437: The Sedimentary Record of Meteorite Impacts, Geological Society of America, p. 1–18, doi:10.1130/2008.2437(01).

Pickersgill, A.E., Mark, D.F., Lee, M.R., and Osinski, G.R., 2020, 40Ar/39Ar systematics of melt lithologies and target rocks from the Gow Lake impact structure, Canada: Geochimica et Cosmochimica Acta, v. 274, p. 317–332, doi:10.1016/j.gca.2020.01.025.

Poelchau, M.H., and Kenkmann, T., 2011, Feather features: a low-shock-pressure indicator in quartz: Journal of Geophysical Research: Solid Earth, v. 116, doi:10.1029/2010JB007803.

Punt, W., Hoen, P.P., Blackmore, S., Nilsson†, S., and le Thomas, A., 2007, Glossary of pollen and spore terminology: Review of Palaeobotany and Palynology, v. 143, p. 1–81, doi:10.1016/j.revpalbo.2006.06.008.

Rampino, M.R., and Volk, T., 1996, Multiple impact event in the Paleozoic: collision with a string of comets or asteroids? Geophysical Research Letters, v. 23, p. 49–52, doi:10.1029/95GL03605.

Reimold, W.U., Jessberger, E.K., and Stephan, T., 1990, 40Ar/39Ar dating of pseudotachylite from the Vredefort dome, South Africa: a progress report: Tectonophysics, v. 171, p. 139–152, doi:10.1016/0040-1951(90)90095-P.

Reimold, W.U., Koeberl, C., Gibson, R.L., and Dressler, B.O., 2005, Economic mineral deposits in impact structures: a review, *in* Impact Tectonics, Berlin/Heidelberg, Springer-Verlag, p. 479–552, doi:10.1007/3-540-27548-7_20.

Schaen, A.J. et al., 2021, Interpreting and reporting 40Ar/39Ar geochronologic data: GSA Bulletin, v. 133, p. 461–487, doi:10.1130/B35560.1.

Schmieder, M., Kennedy, T., Jourdan, F., Buchner, E., and Reimold, W.U., 2018, A high-precision 40Ar/39Ar age for the Nördlinger Ries impact crater, Germany, and implications for the accurate dating of terrestrial impact events: Geochimica et Cosmochimica Acta, v. 220, p. 146–157, doi:10.1016/j.gca.2017.09.036.

Schmieder, M., and Kring, D.A., 2020, Earth's Impact Events Through Geologic Time: A List of Recommended Ages for Terrestrial Impact Structures and Deposits: Astrobiology, v. 20, p. 91–141, doi:10.1089/ast.2019.2085.

Schmitz, B. et al., 2019, An extraterrestrial trigger for the mid-Ordovician ice age: Dust from the breakup of the L-chondrite parent body: Science Advances, v. 5, doi:10.1126/sciadv.aax4184.

Schmitz, B., Tassinari, M., and Peucker-Ehrenbrink, B., 2001, A rain of ordinary chondritic meteorites in the early Ordovician: Earth and Planetary Science Letters, v. 194, p. 1–15, doi:10.1016/S0012-821X(01)00559-3.

van Schmus, W.R., 1992, Tectonic setting of the Midcontinent Rift System: Tectonophysics, v. 213, p. 1–15, doi:10.1016/0040-1951(92)90247-4.

See, T.H., Wagstaff, J., Yang, V., Hörz, F., and McKay, G.A., 1998, Compositional variation and mixing of impact melts on microscopic scales: Meteoritics & Planetary Science, v. 33, p. 937–948, doi:10.1111/j.1945-5100.1998.tb01698.x.

Sherlock, S.C., Kelley, S.P., Parnell, J., Green, P., Lee, P., Osinski, G.R., and Cockell, C.S., 2005, Re-evaluating the age of the Haughton impact event: Meteoritics & Planetary Science, v. 40, p. 1777–1787, doi:10.1111/j.1945-5100.2005.tb00146.x.

Shukla, M.K., and Sharma, A., 2018, A brief review on breccia: it's contrasting origin and diagnostic signatures: Solid Earth Sciences, v. 3, p. 50–59, doi:10.1016/j.sesci.2018.03.001.

Sloss, L.L., 1988, Sedimentary cover—North American Craton (L. L. Sloss, Ed.): Boulder, Colorado, Geological Society of America, doi:10.1130/DNAG-GNA-D2.

Sloss, L.L., 1963, Sequences in the cratonic interior of North America: GSA Bulletin, v. 74, p. 93–114, doi:10.1130/0016-7606(1963)74[93:SITCIO]2.0.CO;2.

Smith, V., Warny, S., Vellekoop, J., Vajda, V., Escarguel, G., and Jarzen, D.M., 2021, Palynology from ground zero of the Chicxulub impact, southern Gulf of Mexico: Palynology, v. 45, p. 283–299, doi:10.1080/01916122.2020.1813826.

Snyder, F.G., and Gerdemann, P.E., 1965, Explosive igneous activity along an Illinois-Missouri-Kansas axis: American Journal of Science, v. 263, p. 465–493, doi:10.2475/ajs.263.6.465.

Spencer, C.G., 2001, Roadside geology of Missouri: Mountain Press, 288 p.

Traverse, A., 2007, Paleopalynology: Dordrecht, Springer Netherlands, doi:10.1007/978-1-4020-5610-9.

Ubide, T., Guyett, P.C., Kenny, G.G., O'Sullivan, E.M., Ames, D.E., Petrus, J.A., Riggs, N., and Kamber, B.S., 2017, Protracted volcanism after large impacts: evidence from the Sudbury impact basin: Journal of Geophysical Research: Planets, v. 122, p. 701–728, doi:10.1002/2016JE005085.

White, J.M., 2008, Palynodata Datafile: 2006 version:, doi:10.4095/225704.

Williams, G.L., Fensome, R.A., and MacRae, R.A., 2017, The Lentin and Williams index of fossil dinoflagellates 2017 edition.:

Zhang, Y., Jia, D., Muxworthy, A.R., Li, Y., Xia, B., Xie, Z., Hu, J., Zi, J., and Liu, W., 2018, The chemical remagnetization of Ediacaran Dolomite in the Taishan Paleo-Reservoir, South China: Journal of Geophysical Research: Solid Earth, doi:10.1029/2018JB015547.

# II. IMPACT PALYNOLOGY: UNCOMMON ALTERATION AND BIOGEOGRAPHICAL EVIDENCE FROM THREE MISSOURI 38TH PARALLEL STRUCTURES*[1,2]

Marissa K. Spencer[a] and Francisca E. Oboh-Ikuenobe[a]

[a]Missouri University of Science and Technology, Department of Geosciences and Geological and Petroleum Engineering, 1400 N. Bishop, Rolla, Missouri 65409

## ABSTRACT

Uniquely damaged palynomorphs and particulate organic matter in sediments from three unusually aligned meteorite impact structures in central Missouri - Crooked Creek, Decaturville, and Weaubleau - provide insights for unraveling complicated biostratigraphy and expanding knowledge about impact palynology. Extreme temperatures and highly energetic forces produced by meteorite impacts can damage organic material and disrupt stratigraphy. Although organic material may be altered by other earth processes, unusual damage such as bubbling and coarsening of surfaces and fusing of processes are most likely thermally induced (melting). The presence of these damages in acritarchs of the same type from the three Missouri structures suggests a link to meteorite impacts during the Ordovician that were likely fragments from the break-up of an L-chondrite asteroid. Furthermore, the ecological affinity of acritarchs indicates the presence of marine waters at the time of impact. The mixed assemblages of

* 1 This paper is intended for submission to *Palaeogeography, Palaeoclimatology, Palaeoecology*.
2. Spencer, M., Oboh-Ikuenobe, F.E., and Warny, S., 2021. "Goldilock palynomorphs" & the three geologic structures: a tale of meteor impact. 53rd Annual Meeting of the AASP-The Palynological Society: Beyond Miscellaneous: The Life and Legacy of Vaughn M. Bryant.

palynomorphs and particulate organic matter representing various paleoecological settings and ages provide clues about the traumatic effects of terrestrial meteorite impacts on biogeography.

## 1. INTRODUCTION

Meteorite impacts are dynamic, and intense, and create some of the most extreme forces known on earth. The magnitude of the effects on the rocks and biota in the impact crater is dependent on the size, speed, angle, and composition of the projectile, the composition, and competencies of the target rocks, and the presence of water (Kieffer and Simonds, 1980; Melosh, 1989; Wünnemann and Weiss, 2015; Rumpf et al., 2017; Collins et al., 2020; Pankhurst et al., 2022). With increasing crater size, the morphology generally becomes more complex (Melosh, 1989). While smaller projectiles form simple bowl shapes, larger meteorites form complex craters (2–4 km) with rings and central uplifts, and the largest produce basins because the ratio between depth and diameter decreases with increasing size (Riller et al., 2018). Impact sites are stratigraphically complex and comprise extremely mixed sediments of various ages and alteration states (Christeson et al., 2021) at radial distances and depths.

The 38th parallel structures are an unusually aligned structural zone extending across the US Midcontinent from Nevada (Retzler et al., 2015) to West-Central Virginia (Heyl, 1972) along the 38$^{th}$ latitude. Geologic structures within this zone include domes, craters, dike swarms, diatremes, folds, and faults; not all origins and relationships are known (Amstutz, 1965; Luczaj, 1998; Evans et al., 2008). Among these 38$^{th}$ Parallel Structures, shatter cone evidence in Crooked Creek and Decaturville in central Missouri

has been used to confirm meteorite impact (Hendriks, 1954; Offield and Pohn, 1979). Shatter cones offer confirmation since they occur solely at nuclear blasts and meteorite impact (Osinski and Ferrière, 2016) although planar features in resistant minerals (i.e., quartz, feldspar) also indicate shock metamorphism (French, 1998). Planar deformation features and other impact products suggest that the Weaubleau was also likely formed by meteorite impact (Morrow and Evans, 2007). These three Missouri structures (Figure 1) comprise sedimentary rocks (sampled for palynology for this study) and metamorphic rocks of Paleozoic age underlain by Precambrian granite basement. Speculation for the structures' alignment involves the type of impactor (comet, asteroid), the projectile origin (common or mixed) (Melosh, 1989), and break-up location and mechanism with theories ranging from serial impacts caused by asteroid break-up in the solar system (Rampino and Volk, 1996), comet or asteroid break-up related to planetary tidal forces (Bottke et al., 1997), and impact clustering (Melosh, 1989).

Understanding the timing and relationship of these structures is key to finding the planetary movements responsible for this unusual linear array; however, age determination of sedimentary structures is challenging (Osinski et al., 2007). Rocks and minerals suitable for age dating are scarce in sedimentary impact structures and are limited to the impact sheet and other shocked minerals, such as zircon, apatite, quartz, and micas in impactites (van Soest et al., 2011). Impact glass is scarce in sedimentary structures because volatiles restrict the formation of coherent melt (Kieffer and Simonds, 1980), and sedimentary rocks produce melt that differs in texture, chemical, and physical properties (Osinski and Pierrazo, 2013). Additionally, the target rock type limits

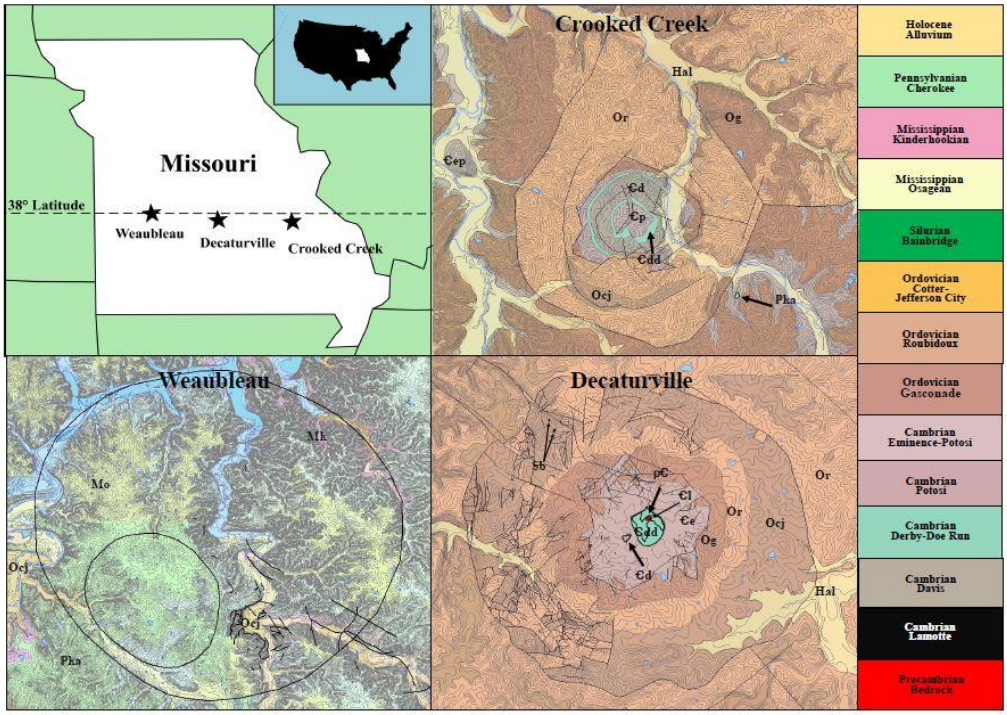


Figure 1. Location, geological maps and generalized stratigraphic column of the Crooked Creek, Decaturville, and Weaubleau geological structures along the 38th parallel in central Missouri. Holocene (Hal: alluvium), Pennsylvanian (ℙka: Cherokee Group, Krebs Subgroup, Atokan Stage), Mississippian (Mo: Osagean, Mk: Kinderhookian), Ordovician (Or: Roubidoux, Og: Gasconade, Ocj: Cotter-Jefferson City), Cambrian (Ꞓl: Lamotte, Ꞓd: Davis, Ꞓdd: Derby-Doe Run, Ꞓep: Eminence-Potosi, Ꞓp: Potosi), ρC: Precambrian granite pegmatite schist.

accessory and other minerals that are available for dating (i.e., zircon, mica, apatite). Although some of these minerals are resistant, they may be altered (granulation, metamictization, sericitization) by hydrothermal activity and other processes related to impact which complicate age dating (Geisler et al., 2007; Kenny et al., 2017, 2020; Černok et al., 2019; Kovaleva, 2020; Kubeš et al., 2021; Wittmann et al., 2021). Impact processes result in variable shock and temperature effects and poorly understood sedimentology and stratigraphy (Christeson et al., 2021). Studies of sedimentary impactites are rare (Beauford, 2012), and impact-affected material suitable for age dating

is limited in these structures. Biostratigraphy relies on stratigraphic continuity, but these sites have extremely mixed sediments and may lack a continuous overlying layer to provide time constraints. Additionally, unaltered fossils preserved at these sites may or may not be related to impact. The silicified (Reimold et al., 2005; Kring et al., 2020) and hardened structures may protect remnant unaltered post-impact fossils and sediments. Additionally, slumping and gravity along steep crater walls may result in post-impact sedimentary breccia formation (Shukla and Sharma, 2018) with the incorporation of younger non-impact material.

Palynology is emerging as an important branch of meteorite impact studies and provides valuable information about the depositional conditions during impact events. However, there is still a knowledge gap about impact effects on biostratigraphy. Impact-related palynological studies are limited and focus on age dating and paleoenvironmental interpretations (Nøhr-Hansen and Dam, 1997; Scott, 1999; Brandt et al., 2002; Vajda et al., 2004; Ocampo et al., 2006; Jolley et al., 2010; Bercovici et al., 2012; Vajda and Bercovici, 2014; Holm-Alwmark et al., 2019; Andreev et al., 2021; Smith et al., 2021). Even fewer studies, however, have addressed the effects of impact on palynomorphs (e.g., Edwards, 2012; Edwards and Powars, 2003; Smith et al., 2020). Although palynomorphs and particulate organic material may be affected by other earth processes (Barreto et al., 2012; Benca et al., 2018; Bingham-Koslowski et al., 2019; Marshall et al., 2020; Spina et al., 2022), damages resulting from meteorite impacts are atypical, and this information has important implications for understanding impact stratigraphy and biogeography. This study provides key information about the unusual effects of meteorite impact on palynomorphs and particulate organic matter in sediment samples (see

Appendix A) from the Decaturville, Crooked Creek, and Weaubleau Structures to constrain the timing of impact, the relationship between the three structures, and inferring the depositional environment. $^{40}Ar/^{39}Ar$ dating is used for additional age constraints (see Appendix B & C).

## 2. DYNAMICS OF IMPACT STRUCTURES

Meteorite impacts are dynamic, and intense with extreme effects. The kinetic impact forces are converted to thermal energy, resulting in high temperatures and damaging processes, which cause thermal and shock damages, vaporization of the target rocks, and formation of impactites. The rock layers involved are overturned, violently mixed, and heavily altered. The material undergoes highly energetic forces such as kinetic, thermal, shock, and electromagnetic radiation (Popova et al., 2013), causing vaporization temperatures of ten thousand degrees at the point of impact and prolonged heating of more than 2370ºC (Bunch et al., 2012; Timms et al., 2017). The sediments are also subjected to a complex geochemistry of siliceous (Libourel et al., 2019), acidic, sulfidic (Hörz et al., 2015; Lightfoot, 2017), and reducing chemical fluids. Surface and subsurface waters, along with pore fluids from the rock also develop into hydrothermal convection cells, pushing out these hot geochemically dynamic fluids for hundreds of kilometers (Kring et al., 2020) over 10's of 1000's years (Osinski et al., 2020). Other damaging impact conditions include high winds (Rumpf et al., 2017), particulate density currents: particulate, highly oxidizing, high temperature, and chemically reactive gases (Addison et al., 2010; Branney and Brown, 2011; Siegert et al., 2017; Mueller et al.,

2018), resurge-tsunamis (Kharif and Pelinovsky, 2005; Wünnemann et al., 2010; Weiss et al., 2015; Ernston, 2016; Gulick et al., 2019), phreatic and phreatomagmatic eruptions (Sato and Taniguchi, 1997; Grieve et al., 2010; Mueller et al., 2018), fires which range up to thousands of kilometers for a 3 km projectile (Svetsov and Shuvalov, 2019), contemporaneous erosion and faulting, and subsequent slump and debris flow due to gravity. These impact processes are complex and highly damaging with impact shock pressures that are unparalleled in other processes (French, 1998). The most relevant processes to this study are very high temperatures, complex geochemistry, and highly energetic forces.

## 3. MATERIALS AND METHODS

Six sedimentary rock core and cuttings samples from the center and rim of the Crooked Creek, Decaturville, and Weaubleau structures (Figure 1, Appendix A) were obtained from the Missouri Department of Natural Resources' McCracken Core Library. The samples were processed by Global Geolab (Medicine Hat, Canada) using standard palynological techniques of digestion in hydrochloric and hydrofluoric acids and centrifuging in heavy liquid ($ZnBr_2$) (Traverse, 2007). The oxidized and unoxidized fractions of the isolated organic residues were then strewn-mounted on separate glass sides and scanned for palynomorphs and particulate organic matter, respectively using transmitted light microscopy. A Nikon polarizing microscope attached to a Nikon Q-Imaging MicroPublisher 3.3 RTV digital camera was used to describe and photograph the palynomorphs and particulate organic matter. Damaged palynomorphs were grouped on

the severity of damage with those features associated with melting (bubbled, vesicular, and smoothed wall surface alteration; fused processes), which were interpreted as impact-related damages and were identified where possible. Palynomorphs were also grouped by environment into categories: (1) terrestrial indicators, such as spores, pollen, and fungal remains; and (2) aquatic marine (chitinozoans, acritarchs) and nonmarine (freshwater acritarchs and algae). The age ranges of palynomorphs were confirmed using Acritax (Pedder and Young, 2014) and Palynodata and White (2008). Particulate organic matter components such as nonmarine amorphous organic matter, marine amorphous organic matter, opaques, structured phytoclasts, structureless phytoclasts, degraded phytoclasts, terrestrial palynomorphs (pollen grains, spores, fungal remains), aquatic palynomorphs (freshwater algae and marine palynomorphs) were identified following the classification schemes of Tyson (1993, 1995) and Oboh-Ikuenobe et al., (2005). Data were supplemented with photographs and palynological data obtained from the literature (e.g., Jansonius and Hills, 1976 and supplements).

## 4. RESULTS

The core and cuttings samples from the three impact structures are primarily silt-sized sedimentary rock (Appendix A) and yield low palynomorph recovery (few in number). The recovered aquatic and terrestrial palynomorph types (acritarchs, cryptospores, chitinozoans, spores, pollen, and fungal hyphae and spores) suggest stratigraphic mixing and are indicative of Precambrian, Cambrian, Ordovician, Silurian, Devonian, Mississippian, Cretaceous, and Holocene ages (Figures 2-4). Except for the

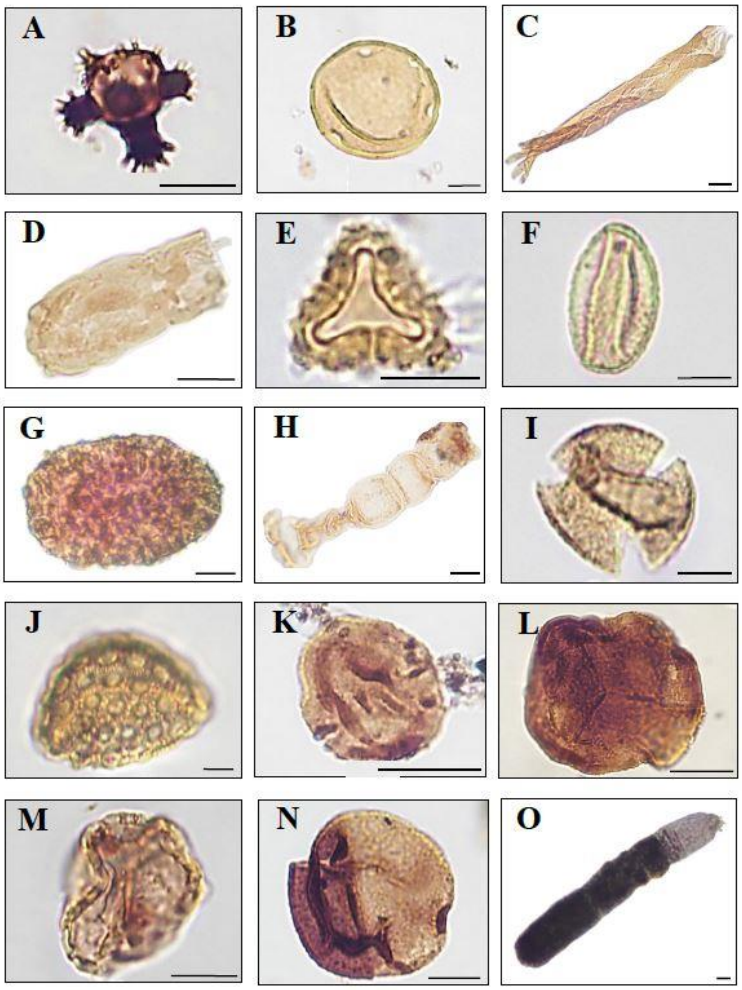


Figure 2. Photomicrographs of select palynomorphs of mixed ages and environments (aquatic and terrestrial) from Crooked Creek (CC) (figures A-E), Decaturville (D) (figures F-J), Weaubleau (W) (figures K-O). Included are the sample - slide number, and Lovins Field Finder (LF) and England Finder (EF) coordinates. Scale bars = 10 μm. A. *Baltisphaeridium jardiniae*, CC2-2505-CC795, LF 3J44. B. *Carya* sp., CC2-2505-CC795, LF 3K36. C. unidentified banded tubule, CC2-2505-CC795, LF 4T44. D. *Conchitina* sp., CC2-2505-CC795, EF 50.5, 14.6. E. *Trichotomosulcites subgranulatus* cf., CC2-2505-CC795, EF 63.2, 15.6. F. *Perfotricolpites* sp., D2-3198-C57, LF 4D22. G. *Camptotriletes juglandilis*, D1-2506-D771-37, 2M46. H. *Desmochitina minor*, D2-3198-C57, LF 1F28. I. *Rousea* sp., D2-3198-C57, LF 2F31. J. Stellatopollis sp.?, D1-2506-D771, LF 2M45. K. *Erdtmanitheca portucalensis* cf., W1-1690-NS1, LF 2M43. L. *Rhabdosporites langii*, W1-1690-NS, LF 2P29. M., unidentified cryptospore, W2-9652, LF 3T422. N., unidentified spore, W1-1690-NS1, LF 4O39. O. *Navifusa* sp., W1-1690-NS1, LF 2T30.

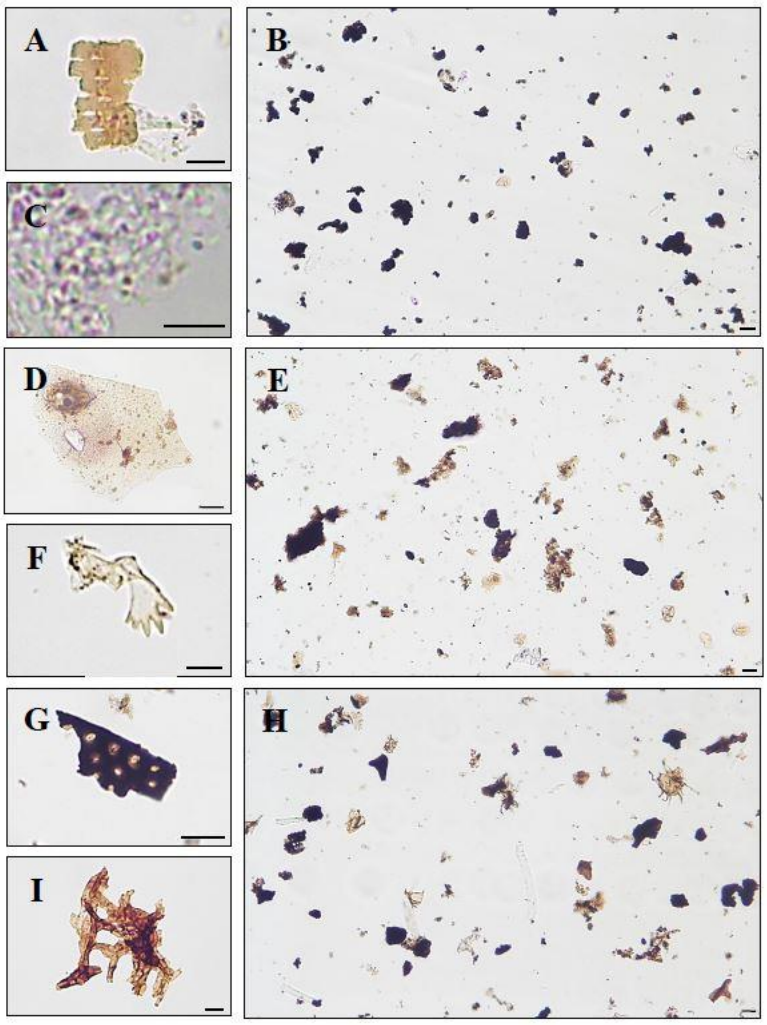


Figure 3. Photomicrographs of typical particulate organic matter from Crooked Creek (A-C), Decaturville (D-F), Weaubleau (G-I) impact sites. Included are the sample - slide number, and Lovins Field Finder (LF) and England Finder (EF) coordinates. Scale bar = 10 μm. A, unidentified banded tubule remains, CC2-2505-CC795, LF 2H43. B, typical particulate organic matter, CC2-2505-CC795, LF 1N29. C, marine amorphous organic matter, CC2-2505-CC795, LF 3U43. D, impact damaged structured phytoclast, D2, 3H41. E, typical particulate organic matter, D2-3198-C57, 2E26. F, likely polychaete worm mouthpart, C2-2505-CC795, LF 3N27. G, plant parenchyma, W1-1690-NS1, EF 16.3, 40.1. H, typical particulate organic matter, W1-1690-NS1, LF 4T33. I, fungal mycelium, W2-9652, LF 4C38.

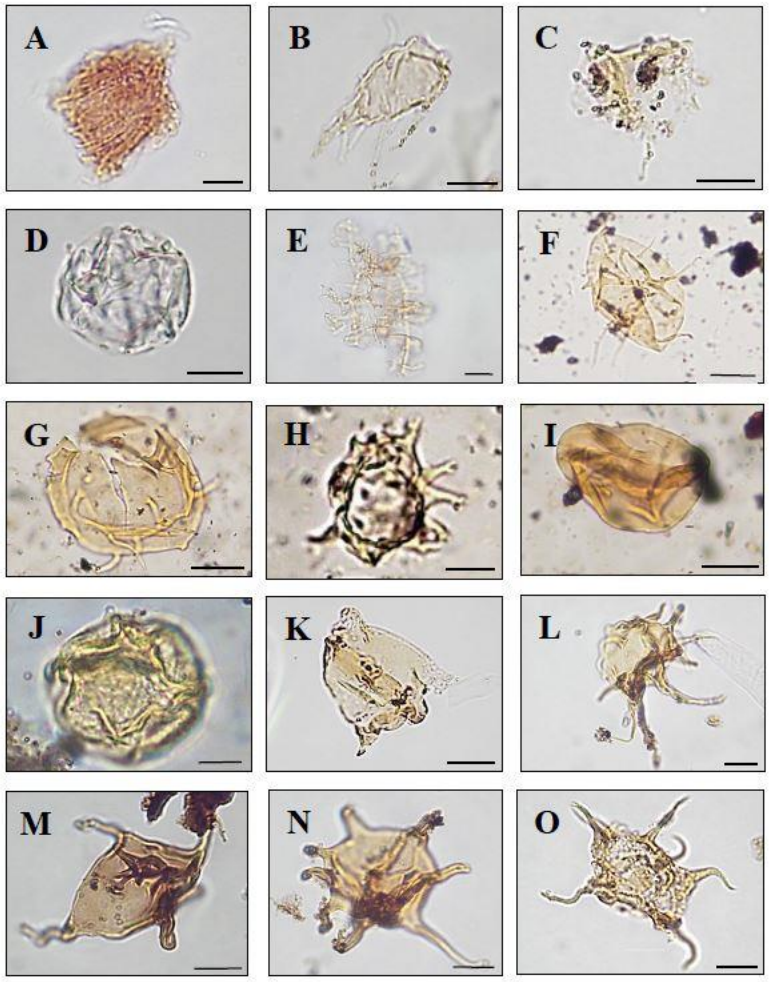


Figure 4. Photomicrographs of select impact-damaged palynomorphs from Crooked Creek (A - E), Decaturville (F - J) and Weaubleau (K - O) impact craters. Included are the sample location - slide number, and Lovins Field Finder (LF) or England Finder (EF) coordinates. Scale bars = 10 μm. A, unidentified acritarch, CC2-2505-CC795, LF 4V22. B, *Cornuferifusa* sp.?, CC2-2505-CC795, LF 3L42. C, unidentified acritarch, CC2-2505-CC795, EF 60.5, 8.4. D, *Multiplicisphaeridium* sp.?, CC2-2505-CC795, EF 62, 10.1. E, *Pheoclosterium fuscinulaegerum*, CC2-2505-CC795, LF 4S25. F, *Actinotodissus polimorphus*?, D2-3198-C57, LF 3C26. G, *Actinotodissus crinitus*?, D2-3198- C57, LF 4T38. H, *Polygonium nanum* cf., D2-3198-C57, LF 2R42. I, *Glaucotesta latiramosa*?, D2-3198-C57, LF 2D26. J, *Polygonium gracile*?, D2-3198-C57, LF 2U28. K, *Veryhachium trispinosum*, W1-1690-NS1, LF 1Y45. L, *Micrhystridium stellatum*?, W1-1690-NS1, LF 1H31. M, *Veryhachium rhombispinosum* cf., W1-1690-NS1, LF 1G43. N, *Baltispheridium perclarum* cf., W1-1690-NS1, LF 3J24. O, *Dorsendinium polorum* cf., W1-1690-NS1, LF 4H32.

Mississippian Embayment in southeast Missouri, Cretaceous rocks have not been documented in theMissouri 38th Parallel structures, or other parts of Missouri (Spencer, 2001). The identified acritarch species include the Cambrian form *Nellia* sp. and *Cryptotetrus* sp., the Ordovician *Veryhachium* cf. *arcarium* and *Pheoclosterium* cf. *fuscinulaegerum*, and the Silurian *Baltisphaeridium jardiniae* (Figure 2). Other identified palynomorphs are the Ordovician chitinozoan *Desmochitina minor*, the Devonian spore *Aneurospora* cf. *geriennei*, the Mississippian spores *Camptotriletes juglandis* (Figure 2) and *Spelaeotriletes triangulus*, and Cretaceous and younger angiosperms such as *Tricolpites* sp. Palynofacies components include degraded, structured, structureless and opaque phytoclasts, palynomorphs (pollen, spores, acritarchs and fungal remains), and marine and nonmarine amorphous organic matter (Figure 3). Some opaques exhibited a unique scalloped texture that is likely oxidized fragments of filamentous algae (Figure 3).

Palynomorphs and particulate organic matter exhibit a variety of damages (Figure 4) including those in common with other Earth processes processes such as thermal (Benca et al., 2018; Bingham-Koslowski et al., 2019; Marshall et al., 2020; Spina et al., 2022) mechanical (Luz et al., 2010; Barreto et al., 2012), and chemical processes (Batten, 1985; Emmings et al., 2019). These types of damage occur to the main bodies and surfaces of acritarchs, a few cryptospores, and chitinozoans and consist of darkening, boring, percussion marks, tearing, folding, and relict pyrite crystal impressions. Alternately, unusual impact-related damage such as vesicular texture, smoothed, or frosted wall alteration, and beaded or fused acritarch processes are attributed to melting; while frayed, missing, and rolled processes; and extreme wall alteration such as ghosting may be attributed to shock metamorphism. Many acritarchs that normally have smooth

wall surfaces exhibit uneven, rough, and vesicular walls (Figure 4), and have uneven darkening and alteration on the same palynomorph. While some acritarchs are relatively undamaged, many are severely damaged and nearly unrecognizable, except for their processes and a faint impression of their shape (Figure 4). Variable preservation is noted among the same species of some palynomorphs — some are well-preserved, some are degraded, and others are hardly recognizable. In addition to wall damage, there is intense damage to palynomorph processes. The processes are commonly bent, torn/ripped off, and fused to each other and the body of the palynomorph (Figure 4). These impact-related damages occur only in Ordovician acritarchs.

Particulate organic matter exhibit damages (Figure 3) similar to those of palynomorphs (Figure 4) and comprise a variety of organic components of mixed ages reflecting geologic periods before and after land plant evolution (Figure 3). Marine amorphous organic matter (Figure 3) are the most abundant organic components in all the three impact structures. The presence of tubules, filamentous algae, opaques that are likely oxidized filamentous cyanobacterial remains, and the absence of structured phytoclasts in the Crooked Creek and Weaubleau structures (Figure 3) are all consistent with deposition prior to land plants. The Decaturville samples contain both structured (terrestrially derived) and structureless (marine amorphous organic matter) (Figure 3), and also include tubules (Figure 3) reflective of depositional timing preceding the evolution of land plants.

# 5. PALEOBIOGEOGRAPHY

Understanding the stratigraphy of impact sites is challenging due to the efficient mixing of materials and variability of the damage processes. Smith et al. (2021) note that highly damaging impact processes can destroy flora and fauna and result in long recovery times (up to a million years) for organisms. It is like that the central Missouri impact materials (comprising mixed rocks of Precambrian and younger ages) were also subjected to several other geologic events that affected the mid-continent of the U.S. These geologic events include multiple transgressive-regressive sequences (Sauk, Tippecanoe, Kaskaskia, Absaroka, and Zuni), mountain-building episodes (rise of the Ozark Dome, Alleghenian and Ouachita Orogenies), and the rifting of the supercontinent Pangea (Sloss, 1963, 1988; Dolton and Finn, 1989; Hatcher et al., 1989; van Schmus, 1992; Hatcher, 2010). Once formed, the Decaturville, Crooked Creek, and Weableau impact craters were likely hardened due to the cooling of hot siliceous fluids created by the heat of impact. Their bowl shapes, with steep slopes and high angles between the central uplift and the crater rim created by listric and extensional faults, provided an ideal situation to trap sediments (Lindsay and Brasier, 2006; Dorn and Day, 2020; James et al., 2022). The types of palynomorphs and damages to their specimens, particulate organic material, and their alteration patterns (Figures 2-4), and the lithology of the sediments have been used to interpret the timing of impact and the paleoenvironment at the time of impact. Although palynomorphs of various affinities and ages (mixed assemblages) were present in the samples (Figures 2, 3), damages related to melting were restricted to Ordovician acritarchs (ie. *Acanthodiacrodium tadlaense, Baltisphaeridium perclarum,*

*Micrhystridium polygonale, Vermimarginata barbata, Veryhachium oklahomense, Veryhachium rhombispinosum, Veryhachium trispinosum*) (Figure 3). The oldest palynomorphs in the samples include cryptospores and ovoid, claviform, and flask-shaped chitinozoans (Figure 2). The oldest acritarchs at these sites had polygonal shapes with simple processes (e.g., *Veryhachium trispinosum*), whereas younger acritarchs such as the *Baltisphaeridium jardiniae* had more complex processes (Figure 2). Note that the impact likely destroyed much of the biota, which needed extended time for recovery.

The paleoenvironment in central Missouri at the time of meteorite impact was marine based on the lithology – primarily limestone and dolomite on Precambrian bedrock – and the presence of acritarchs, chitinozoans, and marine amorphous organic matter in the samples. The stratigraphy is interrupted by unconformities due to periods of erosion and/or lack of deposition and changes in the depositional environment over geological time, and after impact were also captured by the various types of palynomorphs (algae, spores, pollen, and fungi) (Figures 2-4). The scarcity (Silurian, Devonian, Mississippian) or absence of fossils (Pennsylvanian, Permian, Triassic, Jurassic) of certain age ranges may be due to a variety of paleoenvironmental or evolutionary changes. The age gaps may represent 1) a sudden change in the environment type (i.e., marine to terrestrial) where biota didn't have time or ability to adapt, 2) an absence of land plants because they hadn't yet evolved during that time 3) the environment may have been inhospitable or unsuitable for vegetation, 4) or the biota destroyed by impact, with an extended time of recovery.

# 6. DISCUSSION

Palynomorphs are highly resistant to damage, but they may be poorly preserved due to damage by earth processes, such as transportation by river and ocean currents and gravity flows, oxidation, reworking, and predation by fungi and bacteria (Batten, 1985; Luz et al., 2010; Barreto et al., 2012; Porter, 2016; Emmings et al., 2019). Effects of these processes manifest as mechanical body damage, broken and curled processes, darkening of the surface, percussion marks and other abrasion, boring, frosting from chemical etching, and relic pyrite impressions all of which can disrupt morphological and preservation evidence of palynomorph and particulate organic matter in sediments. Low productivity in aquatic environments and sparse terrestrial vegetation can also contribute to the low abundance and diversity of palynomorphs in the sedimentary record. The effects of Earth processes can be distinguished from novel impact-specific damages by identifying features attributed to melting and shock metamorphism which represent the high heat, pressures, and dynamic nature of impact. Impact damages can result in the rarity or absence of palynomorphs and affect their use for dating. Areal and temporal disruption of stratigraphic layers also occur and the impact site, resulting in sediment samples preserving mixed assemblages of palynomorphs representing various geologic ages and different depositional environments.

Studies at other impact sites (e.g., Chicxulub Crater and Chesapeake Bay) have recorded long-ranging absences of biota surrounding the impact horizon (Smith et al., 2021) and body and process damages in palynomorphs (Edwards and Powars, 2003; Edwards, 2012), respectively . Palynomorph specimens with body damage included those

that were torn, whereas others with surface damage were characterized by bubbling, vesicular (many holes), toasted, or roughened, and irregularly darkened areas. Note that while processes can be mechanically damaged and may be ripped off or appear bent or curved from being rolled, intense heat during impact causes melted and/or fused process ends and fusing of processes to the body.

The effects of impact in this study are variable among the low-diversity palynomorphs, even in groups of the same age. For example, some acritarch specimens are well preserved, while others are severely damaged and hardly recognizable, except for their processes and general outlines of their shapes. Interestingly, Hower et al. (2009) noted that the Pennsylvanian Middlesboro bolide impact in Kentucky impact had little effect on the coal rank (and by inference the kerogen). Although palynomorphs of varying ages are present in the Decaturville, Crooked Creek, and Weaubleau craters, the youngest impact-damaged palynomorphs are Ordovician acritarchs (Figure 2). This finding is contrary to the ages proposed by previous studies for the Crooked Creek (Early Ordovician to Pennsylvanian), Weaubleau (Mississippian), and Decaturville (Pennsylvanian to Permian/possibly younger than Cretaceous) (Beveridge, 1951; Hendriks, 1954; Snyder and Gerdemann, 1965; Offield and Pohn, 1979; Rampino and Volk, 1996; Luczaj, 1998; Evans et al., 2003; Mickus et al., 2005; Dulin and Elmore, 2007; Elmore and Dulin, 2007; Miller et al., 2007, 2010; Schmieder and Kring, 2020).

The acritarch specimens had a variety of damages, such as beaded, frayed, missing, and melted processes, as well as processes fused together or to the body. The acritarchs were commonly characterized by roughened vesicular surfaces and extreme body damage resulting in melted, balled-up, or faint impressions of their forms. As a

result of these damages and subsequent difficulties in identification, we have coined the term “Goldilock palynomorphs” to describe them. In the story of “Goldilocks and the Three Bears,” Goldilocks conducted a series of experiments to find those items that were just right (Pyle, 1918). Following this idea, damaged palynomorphs were classified into three groups: too damaged, not damaged enough; and those that were just right (melted but still identifiable, and thus useful to infer age). Thus, the presence of these melted marine acritarch specimens in limestone and dolomite sediments confirms a marine depositional environment during the time of impact.

Palynofacies analysis indicates that some particulate organic matter components were similarly affected, exhibiting similar textural and surface effects attributed to melting such as vesicular, darkening, toasting, and othered altered textures. Additionally, organic components reflected mixed environments with structured material, and nonmarine amorphous organic matter indicative of terrestrial/nonmarine environments occurring with marine amorphous organic matter components, and mixed ages (components that represent both pre- and post-land plant evolution in the same samples).

Previous studies noted isolated sediments with younger undamaged fossils within the same three Missouri 38$^{th}$ parallel structures that were presumed to be deposited at the time of impact (Beveridge, 1951; Hendriks, 1954; Snyder and Gerdemann, 1965; Offield and Pohn, 1979; Rampino and Volk, 1996; Luczaj, 1998; Evans et al., 2003; Mickus et al., 2005; Miller et al., 2007, 2010; Schmieder and Kring, 2020). We believe that younger sediments were likely deposited on top of the structures and only remnant sediments were preserved due to multiple episodes of flooding and subaerial erosion (transgressive-regressive sequences) which were well documented in this area of the Mid-Continent.

Silicates precipitated at these sites during the cooling of hot hydrothermal fluids (Reimold et al., 2005; Kring et al., 2020) and once hardened became resistant to weathering. The morphology of this hardened structure (steep sides and high angles) created an ideal catchment to trap sediments and protect and preserve remnant sediments and fossils.

## 7. CONCLUSIONS

The study of a low diversity palynomorph assemblage and particulate organic matter in the Decaturville, Crooked Creek and Weaubleau structures along the 38$^{th}$ Parallel in central Missouri provided the opportunity to study evidence of damages related to the timing of impact as well as the depositional environment. Unique damage representative of melting documented the extreme environment of impact Although stratigraphically mixed, the youngest of the most severely damaged palynomorphs (e.g., evidence of melting in acritarchs) present at the structures suggested an Ordovician age for the timing of impact and a marine depositional environment. The majority of the severely damaged acritarchs had similar ages and affinities. Thus, this study has constrained a coeval Ordovician age for impact structures that have been variously dated as Early Ordovician to Pennsylvanian (Crooked Creek), Mississippian (Weaubleau), Pennsylvanian to Permian/younger than Cretaceous (Decaturville).

## ACKNOWLEDGEMENTS

We thank the Missouri Geological Survey (Division of Natural Resources) for their assistance and for providing core and cuttings samples from McCracken Core Library. Financial support from the Department of Geosciences and Geological and Petroleum Engineering at the Missouri University of Science and Technology is gratefully acknowledged.

## REFERENCES

Addison, W.D., Brumpton, G.R., Davis, D.W., Fralick, P.W., and Kissin, S.A., 2010, Debrisites from the Sudbury impact event in Ontario, north of Lake Superior, and a new age constraint: are they base-surge deposits or tsunami deposits?, *in* Large Meteorite Impacts and Planetary Evolution IV, Geological Society of America, doi:10.1130/2010.2465(16).

Amstutz, G.C., 1965, Tectonic and petrographic observations on polygonal structures in Missouri: Annals of the New York Academy of Sciences, v. 123, p. 876–894, doi:10.1111/j.1749-6632.1965.tb20406.x.

Andreev, A., Dietze, E., Glushkova, O., Smirnov, V., Wennrich, V., and Melles, M., 2021, The environment at Lake El'gygytgyn Area (Northeastern Russian Arctic) prior to and after the meteorite impact at 3.58 Ma: Frontiers in Earth Science, v. 9, doi:10.3389/feart.2021.636983.

Askin, R.A., and Jacobson, S.R., 2003, Palynology, *in* Encyclopedia of Physical Science and Technology, Elsevier, p. 563–578, doi:10.1016/B0-12-227410-5/00930-3.

Barreto, C.F., Vilela, C.G., Baptista-Neto, J.A., and Barth, O.M., 2012, Spatial distribution of pollen grains and spores in surface sediments of Guanabara Bay, Rio de Janeiro, Brazil: Anais da Academia Brasileira de Ciências, v. 84, p. 627–644, doi:10.1590/S0001-37652012005000049.

Batten, D.J., 1985, Coccolith moulds in sedimentary organic matter and their use in palynofacies analysis: Journal of Micropalaeontology, v. 4, p. 111–116, doi:10.1144/jm.4.2.111.

Beauford, R.E., 2012, Carbonate melts and sedimentary impactite variation at Crooked Creek and Decaturville Impact Craters, Missouri, USA, *in* 43rd Lunar and Planetary Science Conference, The Woodlands, Lunar and Planetary Science.

Benca, J.P., Duijnstee, I.A.P., and Looy, C. v., 2018, UV-B–induced forest sterility: Implications of ozone shield failure in Earth's largest extinction: Science Advances, v. 4, doi:10.1126/sciadv.1700618.

Bercovici, A., Vajda, V., Pearson, D., Villanueva-Amadoz, U., and Kline, D., 2012, Palynostratigraphy of John's Nose, a new Cretaceous–Paleogene boundary section in southwestern North Dakota, USA: Palynology, v. 36, p. 36–47, doi:10.1080/01916122.2012.678695.

Bercovici, A., and Vellekoop, J., 2017, Methods in paleopalynology and palynostratigraphy: an application to the K-Pg Boundary, *in* Terrestrial depositional systems: deciphering complexities through multiple stratigraphic methods, Elsevier, p. 127–164, doi:10.1016/B978-0-12-803243-5.00003-0.

Beveridge, T.R., 1951, The geology of the Weaubleau Creek Area, Missouri. Missouri Division of Geological Survey and Water Resources, Volume 32, Second Series. 111 p.

Bingham-Koslowski, N., Miller, M.A., McCartney, T., and Carey, J.S., 2019, Revised biostratigraphic and thermal alteration interpretations for the Paleozoic of the Hopedale Basin, offshore Labrador, Canada: Bulletin of Canadian Petroleum Geology, v. 67, p. 185–214.

Bottke, W.F., Richardson, D.C., and Love, S.G., 1997, Can tidal disruption of asteroids make crater chains on the Earth and Moon? Icarus, v. 126, p. 470–474, doi:10.1006/icar.1997.5685.

Brandt, D., Holmes, H., Reimold, W.U., Paya, B.K., Koeberl, C., and Hancox, P.J., 2002, Kgagodi Basin: The first impact structure recognized in Botswana: Meteoritics & Planetary Science, v. 37, p. 1765–1779, doi:10.1111/j.1945-5100.2002.tb01162.x.

Branney, M.J., and Brown, R.J., 2011, Impactoclastic density current emplacement of terrestrial meteorite-impact ejecta and the formation of dust pellets and accretionary lapilli: evidence from Stac Fada, Scotland: The Journal of Geology, v. 119, p. 275–292, doi:10.1086/659147.

Bunch, T.E. et al., 2012, Very high-temperature impact melt products as evidence for cosmic airbursts and impacts 12,900 years ago: Proceedings of the National Academy of Sciences, v. 109, doi:10.1073/pnas.1204453109.

Černok, A., White, L.F., Darling, J., Dunlop, J., and Anand, M., 2019, Shock-induced microtextures in lunar apatite and merrillite: Meteoritics & Planetary Science, v. 54, p. 1262–1282, doi:10.1111/maps.13278.

Christeson, G.L., Morgan, J.V., and Gulick, S.P.S., 2021, Mapping the Chicxulub impact stratigraphy and peak ring drilling and seismic data: Journal of Geophysical Research: Planets, v. 126, doi:10.1029/2021JE006938.

Collins, G.S., Patel, N., Davison, T.M., Rae, A.S.P., Morgan, J. v., and Gulick, S.P.S., 2020, A steeply-inclined trajectory for the Chicxulub impact: Nature Communications, v. 11, p. 1480, doi:10.1038/s41467-020-15269-x.

Dolton, G.L., and Finn, T.M., 1989, Petroleum geology of the Nemaha Uplift, Central Midcontinent, U.S. Geological Survey Open-File Report 88-450D.:

Dorn, T., and Day, M., 2020, Intracrater sediment trapping and transport in Arabia Terra, Mars: Journal of Geophysical Research: Planets, v. 125, doi:10.1029/2020JE006581.

Dulin, S., and Elmore, R.D., 2007, Paleomagnetism of the Weaubleau structure, southwestern Missouri, *in* Special Paper 437: The Sedimentary Record of Meteorite Impacts, Geological Society of America, p. 55–64, doi:10.1130/2008.2437(04).

Edwards, L.E., 2012, Dinocyst taphonomy, impact craters, cyst ghosts and the Paleocene–Eocene thermal maximum (PETM): Palynology, v. 36, p. 80–95, doi:10.1080/01916122.2012.679205.

Edwards, L.E., and Powars, D.S., 2003, Impact damage to dinocysts from the Late Eocene Chesapeake Bay Event: PALAIOS, v. 18, p. 275–285, doi:10.1669/0883-1351(2003)018<0275:IDTDFT>2.0.CO;2.

Elmore, R.D., and Dulin, S., 2007, New paleomagnetic age constraints on the Decaturville impact structure and Weaubleau structure along the 38th parallel in Missouri (North America): Geophysical Research Letters, v. 34, doi:10.1029/2007GL030113.

Emmings, J.F., Hennissen, J.A.I., Stephenson, M.H., Poulton, S.W., Vane, C.H., Davies, S.J., Leng, M.J., Lamb, A., and Moss-Hayes, V., 2019, Controls on amorphous organic matter type and sulphurization in a Mississippian black shale: Review of Palaeobotany and Palynology, v. 268, p. 1–18, doi:10.1016/j.revpalbo.2019.04.004.

Ernston, K., 2016, Evidence of a meteorite impact-induced tsunami in Lake Chiemsee (Southeast Germany) strengthened, *in* 47th Lunar and Planetary Science Conference, https://www.hou.usra.edu/meetings/lpsc2016/pdf/1263.pdf (accessed June 2022).

Evans, K., Davis, G., Miao, X., Mickus, K., Miller, J., and Morrow, J., 2008, Re-evaluating the 38th Parallel serial impact hypothesis, *in* AGU Fall Meeting Abstracts, American Geophysical Union.

Evans, K.R., Mickus, K.L., Rovey, I.C.W., and Davis, G.H., 2003, The Weaubleau-Osceola Structure: evidence of a Mississippian meteorite impact in Southwestern Missouri.:

French, B., 1998, Traces of catastrophe: a handbook of shock-metamorphic effects in terrestrial meteorite impact structures: Washington, DC, Smithsonian Institute, 31–60 p.

Geisler, T., Schaltegger, U., and Tomaschek, F., 2007, Re-equilibration of zircon in aqueous fluids and melts, Elements, v. 3, p. 43–50, doi:10.2113/gselements.3.1.43.

Grieve, R.A.F., Ames, D.E., Morgan, J.V., and Artemieva, N., 2010, The evolution of the Onaping Formation at the Sudbury impact structure: Meteoritics & Planetary Science, v. 45, p. 759–782, doi:10.1111/j.1945-5100.2010.01057.x.

Gulick, S.P.S. et al., 2019, The first day of the Cenozoic: Proceedings of the National Academy of Sciences, v. 116, p. 19342–19351, doi:10.1073/pnas.1909479116.

Hatcher, R.D., 2010, The Appalachian Orogen: a brief summary, *in* From Rodinia to Pangea: the lithotectonic record of the Appalachian Region, Geological Society of America, doi:10.1130/2010.1206(01).

Hatcher, R.D., Thomas, W.A., and Viele, G.W., 1989, The Appalachian-Ouachita Orogen in the United States (R. D. Hatcher, W. A. Thomas, & G. W. Viele, Eds.): Boulder, Colorado 80301, Geological Society of America, doi:10.1130/DNAG-GNA-F2.

Hendriks, H.E., 1954, The geology of the Steelville quadrangle Missouri: Missouri Geological Survey and Water Resources, 36, p. 88.

Heyl, A. v., 1972, The 38th Parallel Lineament and its relationship to ore deposits: Economic Geology, v. 67, p. 879–894, doi:10.2113/gsecongeo.67.7.879.

Holm-Alwmark, S. et al., 2019, An Early Jurassic age for the Puchezh-Katunki impact structure (Russia) based on $^{40}$Ar/$^{39}$Ar data and palynology: Meteoritics & Planetary Science, v. 54, p. 1764–1780, doi:10.1111/maps.13309.

Hörz, F., Archer, P.D., Niles, P.B., Zolensky, M.E., and Evans, M., 2015, Devolatilization or melting of carbonates at Meteor Crater, AZ? Meteoritics & Planetary Science, v. 50, p. 1050–1070, doi:10.1111/maps.12453.

Hower, J.C., Greb, S.F., Kuehn, K.W., and Eble, C.F., 2009, Did the Middlesboro, Kentucky, bolide impact event influence coal rank? International Journal of Coal Geology, v. 79, p. 92–96, doi:10.1016/j.coal.2009.05.003.

James, S., Chandran, S.R., Santosh, M., Pradeepkumar, A.P., Praveen, M.N., and Sajinkumar, K.S., 2022, Meteorite impact craters as hotspots for mineral resources and energy fuels: a global review: Energy Geoscience, v. 3, p. 136–146, doi:10.1016/j.engeos.2021.12.006.

Jansonius, J., and Hills, L.V., 1976, Genera file of fossil spores and pollen (with supplements): Special Publication, Department of Geology, University of Calgary, Canada.

Jolley, D., Gilmour, I., Gurov, E., Kelley, S., and Watson, J., 2010, Two large meteorite impacts at the Cretaceous-Paleogene boundary: Geology, v. 38, p. 835–838, doi:10.1130/G31034.1.

Kenny, G.G., Karlsson, A., Schmieder, M., Whitehouse, M.J., Nemchin, A.A., and Bellucci, J.J., 2020, Recrystallization and chemical changes in apatite in response to hypervelocity impact: Geology, v. 48, p. 19–23, doi:10.1130/G46575.1.

Kenny, G.G., Morales, L.F., Whitehouse, M.J., Petrus, J.A., and Kamber, B.S., 2017, The formation of large neoblasts in shocked zircon and their utility in dating impacts: Geology, v. 45, p. 1003–1006, doi:10.1130/G39328.1.

Kharif, C., and Pelinovsky, E., 2005, Asteroid impact tsunamis: Comptes Rendus Physique, v. 6, p. 361–366, doi:10.1016/j.crhy.2004.12.016.

Kieffer, S.W., and Simonds, C.H., 1980, The role of volatiles and lithology in the impact cratering process: Reviews of Geophysics, v. 18, p. 143, doi:10.1029/RG018i001p00143.

Kovaleva, E., 2020, Textural Identification of polycrystalline magmatic, tectonically-deformed, and shock-related zircon aggregates: Minerals, v. 10, p. 469, doi:10.3390/min10050469.

Kring, D.A. et al., 2020, Probing the hydrothermal system of the Chicxulub impact crater: Science Advances, v. 6, doi:10.1126/sciadv.aaz3053.

Kubeš, M., Leichmann, J., Wertich, V., Mozola, J., Holá, M., Kanický, V., and Škoda, R., 2021, Metamictization and fluid-driven alteration triggering massive HFSE and REE mobilization from zircon and titanite: Direct evidence from EMPA imaging and LA-ICP-MS analyses: Chemical Geology, v. 586, p. 120593, doi:10.1016/j.chemgeo.2021.120593.

Li, T.-J., Huang, Z.-L., Chen, X., Li, X.-N., and Liu, J.-T., 2021, Paleoenvironment and organic matter enrichment of the Carboniferous volcanic-related source rocks in the Malang Sag, Santanghu Basin, NW China: Petroleum Science, v. 18, p. 29–53, doi:10.1007/s12182-020-00514-1.

Libourel, G., Nakamura, A.M., Beck, P., Potin, S., Ganino, C., Jacomet, S., Ogawa, R., Hasegawa, S., and Michel, P., 2019, Hypervelocity impacts as a source of deceiving surface signatures on iron-rich asteroids: Science Advances, v. 5, doi:10.1126/sciadv.aav3971.

Lightfoot, P.C., 2017, The relationship between the impact melt sheet and the Ni-Cu-PGE sulfide mineral systems at Sudbury, *in* Nickel Sulfide Ores and Impact Melts, Elsevier, p. 442–508, doi:10.1016/B978-0-12-804050-8.00005-5.

Lindsay, J., and Brasier, M., 2006, Impact craters as biospheric microenvironments, Lawn Hill Structure, Northern Australia: Astrobiology, v. 6, p. 348–363, doi:10.1089/ast.2006.6.348.

Luczaj, J., 1998, Argument supporting explosive igneous activity for the origin of "cryptoexplosion" structures in the midcontinent, United States: Geology, v. 26, p. 295, doi:10.1130/0091-7613(1998)026<0295:ASEIAF>2.3.CO;2.

Luz, C.F.P. da, Barth, O.M., and Silva, C.G., 2010, Modern processes of palynomorph deposition at lakes of the northern region of the Rio de Janeiro State, Brazil: Anais da Academia Brasileira de Ciências, v. 82, p. 679–690, doi:10.1590/S0001-37652010000300016.

Mander, L., Wesseln, C.J., McElwain, J.C., and Punyasena, S.W., 2012, Tracking taphonomic regimes using chemical and mechanical damage of pollen and spores: an example from the Triassic–Jurassic Mass Extinction: PLoS ONE, v. 7, p. e49153, doi:10.1371/journal.pone.0049153.

Marshall, J.E.A., Lakin, J., Troth, I., and Wallace-Johnson, S.M., 2020, UV-B radiation was the Devonian-Carboniferous boundary terrestrial extinction kill mechanism: Science Advances, v. 6, doi:10.1126/sciadv.aba0768.

Melosh, H.J., 1989, Impact cratering: a geologic process: Oxford University Press, 245 p.

Mickus, K.L., Evans, K.R., and Rovey, C.W., I., 2005, Gravity and magnetic analysis of the Weaubleau-Osceola Structure, Missouri , *in* SEPM Research Conference: the sedimentary record of meteorite impacts, SEPM.

Miller, J.F., Evans, K.R., Ethington, R.L., Repetski, J.E., Sandberg, C.A., and Thompson, T.L., 2007, Critical stratigraphic data from reworked conodonts in impact breccias across Missouri's Ozark Dome, *in* Geological Society of America Annual Meeting, Geological Society of America.

Miller, J.F., Thompson, T.L., and Ethington, R.L., 2010, Conodonts and other fossils from cores in the resurge breccia at the Weaubleau impact structure, St. Clair County, Missouri, *in* Geological Society of America North-Central Section and South-Central Section Joint Annual Meeting, Geological Society of America.

Morrow, J., and Evans, K., 2007, Preliminary shocked-quartz petrography, upper Weaubleau breccia, Missouri, USA, *in* Meteoritical Society 2007 Annual Meeting, Meteoritical Society.

Mueller, S.B., Kueppers, U., Huber, M.S., Hess, K.-U., Poesges, G., Ruthensteiner, B., and Dingwell, D.B., 2018, Aggregation in particle rich environments: a textural study of examples from volcanic eruptions, meteorite impacts, and fluidized bed processing: Bulletin of Volcanology, v. 80, p. 32, doi:10.1007/s00445-018-1207-3.

Nøhr-Hansen, H., and Dam, G., 1997, Palynology and sedimentology across a new marine Cretaceous-Tertiary boundary section on Nuussuaq, West Greenland: Geology, v. 25, p. 851, doi:10.1130/0091-7613(1997)025<0851:PASAAN>2.3.CO;2.

Oboh-Ikuenobe, F.E., Obi, C.G., and Jaramillo, C.A., 2005, Lithofacies, palynofacies, and sequence stratigraphy of Palaeogene strata in Southeastern Nigeria: Journal of African Earth Sciences, v. 41, p. 79–101, doi:10.1016/j.jafrearsci.2005.02.002.

Ocampo, A., Vajda, V., and Buffetaut, E. Unravelling the Cretaceous-Paleogene (KT) turnover, evidence from flora, fauna and geology, *in* biological processes associated with impact events, Berlin/Heidelberg, Springer-Verlag, p. 197–219, doi:10.1007/3-540-25736-5_9.

Offield, T., and Pohn, H., 1979, Geology of the Decaturville impact structure, Missouri.: Missouri Division of Geological Survey and Water Resources

Osinski, G.R., Cockell, C.S., Pontefract, A., and Sapers, H.M., 2020, The role of meteorite impacts in the origin of life: Astrobiology, v. 20, p. 1121–1149, doi:10.1089/ast.2019.2203.

Osinski, G.R., and Ferrière, L., 2016, Shatter cones: (mis)understood? Science Advances, v. 2, doi:10.1126/sciadv.1600616.

Osinski, G., and Pierrazo, E., 2013, Impact cratering: processes and products (G. R. Osinski & E. Pierazzo, Eds.): Wiley, doi:10.1002/9781118447307.

Osinski, G.R., Spray, J.G., and Grieve, R.A.F., 2007, Impact melting in sedimentary target rocks: an assessment, *in* Special Paper 437: The Sedimentary Record of Meteorite Impacts, Geological Society of America, p. 1–18, doi:10.1130/2008.2437(01).

Pankhurst, M.J., Stevenson, C.J., and Coldwell, B.C., 2022, Meteorites that produce K-feldspar-rich ejecta blankets correspond to mass extinctions: Journal of the Geological Society, v. 179, doi:10.1144/jgs2021-055.

Pedder, B, and Young, J., 2014, Acritax:, https://www.mikrotax.org/Acritax/ (accessed June 2022).

Popova, O.P. et al., 2013, Chelyabinsk airburst, damage assessment, meteorite recovery, and characterization: Science, v. 342, p. 1069–1073, doi:10.1126/science.1242642.

Porter, S.M., 2016, Tiny vampires in ancient seas: evidence for predation via perforation in fossils from the 780–740 million-year-old Chuar Group, Grand Canyon, USA: Proceedings of the Royal Society B: Biological Sciences, v. 283, p. 20160221, doi:10.1098/rspb.2016.0221.

Pyle, K., 1918, Goldilocks and the three bears, *in* Mother's nursery tales: New York, E.P. Dutton and Company , 207–213 p.

Rampino, M.R., and Volk, T., 1996, Multiple impact event in the Paleozoic: collision with a string of comets or asteroids? Geophysical Research Letters, v. 23, p. 49–52, doi:10.1029/95GL03605.

Reimold, W.U., Koeberl, C., Gibson, R.L., and Dressler, B.O., 2005, Economic mineral deposits in impact structures: a review, *in* Impact tectonics, Berlin/Heidelberg, Springer-Verlag, p. 479–552, doi:10.1007/3-540-27548-7_20.

Retzler, A.J., Tapanila, L., Steenberg, J.R., Johnson, C.J., and Myers, R.A., 2015, Post-impact depositional environments as a proxy for crater morphology, Late Devonian Alamo impact, Nevada: Geosphere, v. 11, p. 123–143, doi:10.1130/GES00964.1.

Riller, U. et al., 2018, Rock fluidization during peak-ring formation of large impact structures: Nature, v. 562, p. 511–518, doi:10.1038/s41586-018-0607-z.

Rumpf, C.M., Lewis, H.G., and Atkinson, P.M., 2017, Asteroid impact effects and their immediate hazards for human populations: Geophysical Research Letters, v. 44, p. 3433–3440, doi:10.1002/2017GL073191.

Sato, H., and Taniguchi, H., 1997, Relationship between crater size and ejecta volume of recent magmatic and phreato-magmatic eruptions: implications for energy partitioning: Geophysical Research Letters, v. 24, p. 205–208, doi:10.1029/96GL04004.

Schmieder, M., and Kring, D.A., 2020, Earth's impact events through geologic time: a list of recommended ages for terrestrial impact structures and deposits: Astrobiology, v. 20, p. 91–141, doi:10.1089/ast.2019.2085.

van Schmus, W.R., 1992, Tectonic setting of the Midcontinent Rift System: Tectonophysics, v. 213, p. 1–15, doi:10.1016/0040-1951(92)90247-4.

Scott, L., 1999a, Palynological analysis of the Pretoria Saltpan (Tswaing Crater) sediments and vegetation history in the bushveld savanna biome, South Africa., *in* p. 143–166.

Scott, L., 1999b, Vegetation history and climate in the Savanna biome South Africa since 190,000 ka: a comparison of pollen data from the Tswaing Crater (the Pretoria Saltpan) and Wonderkrater: Quaternary International, v. 57–58, p. 215–223, doi:10.1016/S1040-6182(98)00062-7.

Shukla, M.K., and Sharma, A., 2018, A brief review on breccia: it's contrasting origin and diagnostic signatures: Solid Earth Sciences, v. 3, p. 50–59, doi:10.1016/j.sesci.2018.03.001.

Siegert, S., Branney, M.J., and Hecht, L., 2017, Density current origin of a melt-bearing impact ejecta blanket (Ries suevite, Germany): Geology, v. 45, p. 855–858, doi:10.1130/G39198.1.

Sloss, L.L., 1988, Sedimentary cover—North American Craton (L. L. Sloss, Ed.): Boulder, Colorado, Geological Society of America, doi:10.1130/DNAG-GNA-D2.

Sloss, L.L., 1963, Sequences in the cratonic interior of North America: GSA Bulletin, v. 74, p. 93–114, doi:10.1130/0016-7606(1963)74[93:SITCIO]2.0.CO;2.

Smith, V., Warny, S., Jarzen, D.M., Demchuk, T., Vajda, V., and Gulick, S.P.S., 2020, Paleocene–Eocene palynomorphs from the Chicxulub impact crater, Mexico. Part 2: angiosperm pollen: Palynology, v. 44, p. 489–519, doi:10.1080/01916122.2019.1705417.

Smith, V., Warny, S., Vellekoop, J., Vajda, V., Escarguel, G., and Jarzen, D.M., 2021, Palynology from ground zero of the Chicxulub impact, southern Gulf of Mexico: Palynology, v. 45, p. 283–299, doi:10.1080/01916122.2020.1813826.

Snyder, F.G., and Gerdemann, P.E., 1965, Explosive igneous activity along an Illinois-Missouri-Kansas axis: American Journal of Science, v. 263.

van Soest, M.C., Hodges, K. v., Wartho, J.-A., Biren, M.B., Monteleone, B.D., Ramezani, J., Spray, J.G., and Thompson, L.M., 2011, (U-Th)/He dating of terrestrial impact structures: the Manicouagan example: Geochemistry, Geophysics, Geosystems, v. 12, p. n/a-n/a, doi:10.1029/2010GC003465.

Spencer, C.G., 2001, Roadside geology of Missouri: Mountain Press, 288 p.

Spina, A., Brogi, A., Capezzuoli, E., Ventruti, G., Zucchi, M., Aldinucci, M., Cirilli, S., Schito, A., and Liotta, D., 2022, Use of palynology and thermal maturity in deformed geological units: A case study from the Permian succession in the Monte Leoni area (Middle Tuscan Ridge, inner Northern Apennines, Italy): Sedimentary Geology, p. 106210, doi:10.1016/j.sedgeo.2022.106210.

Svetsov, V., and Shuvalov, V., 2019, Thermal radiation from impact plumes: Meteoritics & Planetary Science, v. 54, p. 126–141, doi:10.1111/maps.13200.

Timms, N.E., Erickson, T.M., Pearce, M.A., Cavosie, A.J., Schmieder, M., Tohver, E., Reddy, S.M., Zanetti, M.R., Nemchin, A.A., and Wittmann, A., 2017, A pressure-temperature phase diagram for zircon at extreme conditions: Earth-Science Reviews, v. 165, p. 185–202, doi:10.1016/j.earscirev.2016.12.008.

Traverse, A., 2007, Paleopalynology: Dordrecht, Springer Netherlands, doi:10.1007/978-1-4020-5610-9.

Tyson, R.V., 1993, Palynofacies analysis: *in* Applied Micropaleontology (D. G. Jenkins, Ed.): Dordrecht, The Netherlands, Kluwer Academic Publishers, 153–191 p.

Tyson, R.V., 1995, Sedimentary organic matter: organic facies and palynofacies: Dordrecht, Springer Netherlands, doi:10.1007/978-94-011-0739-6.

Vajda, V., and Bercovici, A., 2014, The global vegetation pattern across the Cretaceous–Paleogene mass extinction interval: a template for other extinction events: Global and Planetary Change, v. 122, p. 29–49, doi:10.1016/j.gloplacha.2014.07.014.

Vajda, V., Raine, J.I., Hollis, C.J., and Strong, C.P., 2004, Global effects of the Chicxulub impact on terrestrial vegetation — review of the palynological record from New Zealand Cretaceous/Tertiary Boundary, *in* p. 57–74, doi:10.1007/978-3-662-06423-8_4.

Weiss, R., Lynett, P., and Wünnemann, K., 2015, The Eltanin impact and its tsunami along the coast of South America: insights for potential deposits: Earth and Planetary Science Letters, v. 409, p. 175–181, doi:10.1016/j.epsl.2014.10.050.

White, J.M., 2008, Palynodata Datafile: 2006 version:, doi:10.4095/225704.

Wittmann, A. et al., 2021, Shock impedance amplified impact deformation of zircon in granitic rocks from the Chicxulub impact crater: Earth and Planetary Science Letters, v. 575, p. 117201, doi:10.1016/j.epsl.2021.117201.

Wünnemann, K., Collins, G.S., and Weiss, R., 2010, Impact of a cosmic body into Earth's ocean and the generation of large tsunami waves: insight from numerical modeling: Reviews of Geophysics, v. 48, p. RG4006, doi:10.1029/2009RG000308.

Wünnemann, K., and Weiss, R., 2015, The meteorite impact-induced tsunami hazard: Philosophical Transactions of the Royal Society A: Mathematical, Physical and Engineering Sciences, v. 373, p. 20140381, doi:10.1098/rsta.2014.0381.

# III. INTEGRATION OF PALYNOLOGICAL AND FORAMINIFERAL ANALYSES TOWARD EVALUATION OF THE HYDROCARBON POTENTIAL IN THE ORANGE BASIN, SW AFRICA*

Marissa K. Spencer[1*], Damián Cárdenas[1,2], Francisca E. Oboh-Ikuenobe[1], Tapas Chatterjee[3]

[1]Geosciences and Geological and Petroleum Engineering, Missouri University of Science and Technology, Rolla, Missouri, USA

[2] Smithsonian Tropical Research Institute, Panamá, Panama

[3] Department of Earth Sciences, University of the Western Cape, Bellville, South Africa

*Corresponding author

## ABSTRACT

Changes in the paleogeography during the breakup of Gondwana and the development of the proto-South Atlantic have been of enduring significance to scientists. The realignment of these landmasses during the Mesozoic, which includes the formation of the Orange Basin in southern Africa, had a profound effect on the environment. These paleoenvironmental differences likely affected fossil preservation and hydrocarbon maturation. Although there are known hydrocarbon accumulations within the Orange Basin, the basin is still largely underexplored and has much future potential. Palynology is an invaluable tool for inferring paleoenvironmental conditions and hydrocarbon potential, and therefore, is used in this study to evaluate this key offshore South African

* This manuscript has been published by Springer in *Advances in Petroleum Source Rock Characterizations: Integrated Methods and Case Studies – A Multidisciplinary Source Rock Approach* (Edited by H. El Atfy and B.I. Ghassal)

area. A total of forty-three samples from six conventional cores from four exploratory wells (K-A2, K-A3, K-H1, K-E1) within three blocks were analyzed for their palynomorph, particulate organic matter (kerogen) and foraminiferal contents. Integration of the palynomorph, palynofacies, and foraminiferal data have provided information that suggest the sediments were early Cenomanian in age, deposited in a shallow marine (inner-middle shelf) setting, and characterized by gas-prone types II and III kerogen in this frontier basin.

## 1. INTRODUCTION

The Orange Basin is a major sedimentary basin in the South Atlantic on the western passive margin of southern Africa. Located near the international border of South Africa and Namibia, it covers an area of around 160,000 square miles (Kuhlmann et al. 2010) between the Walvis and Agulhas Ridges along the coast offshore of western Southern Africa (Figure 1). Sedimentation in the Orange Basin is Late Jurassic to Quaternary age and consists of lacustrine sediments overlying basic and alkaline volcanic rock left from rift flood basalts, and fluvio-deltaic sandstones and conglomerates contributed by the Orange River (Muntingh 1993, Jungslager 1999, Van der Spuy 2003, Adekola et al. 2012, Brownfield 2016). During the Early Cretaceous (Barremian–Aptian), fluvial deposits and marine interbedded sandstones and shales form transgressive–regressive cycles. In addition, a major flooding event is recorded in the early Aptian which resulted in the progradation of additional siliciclastic material (Van der Spuy,

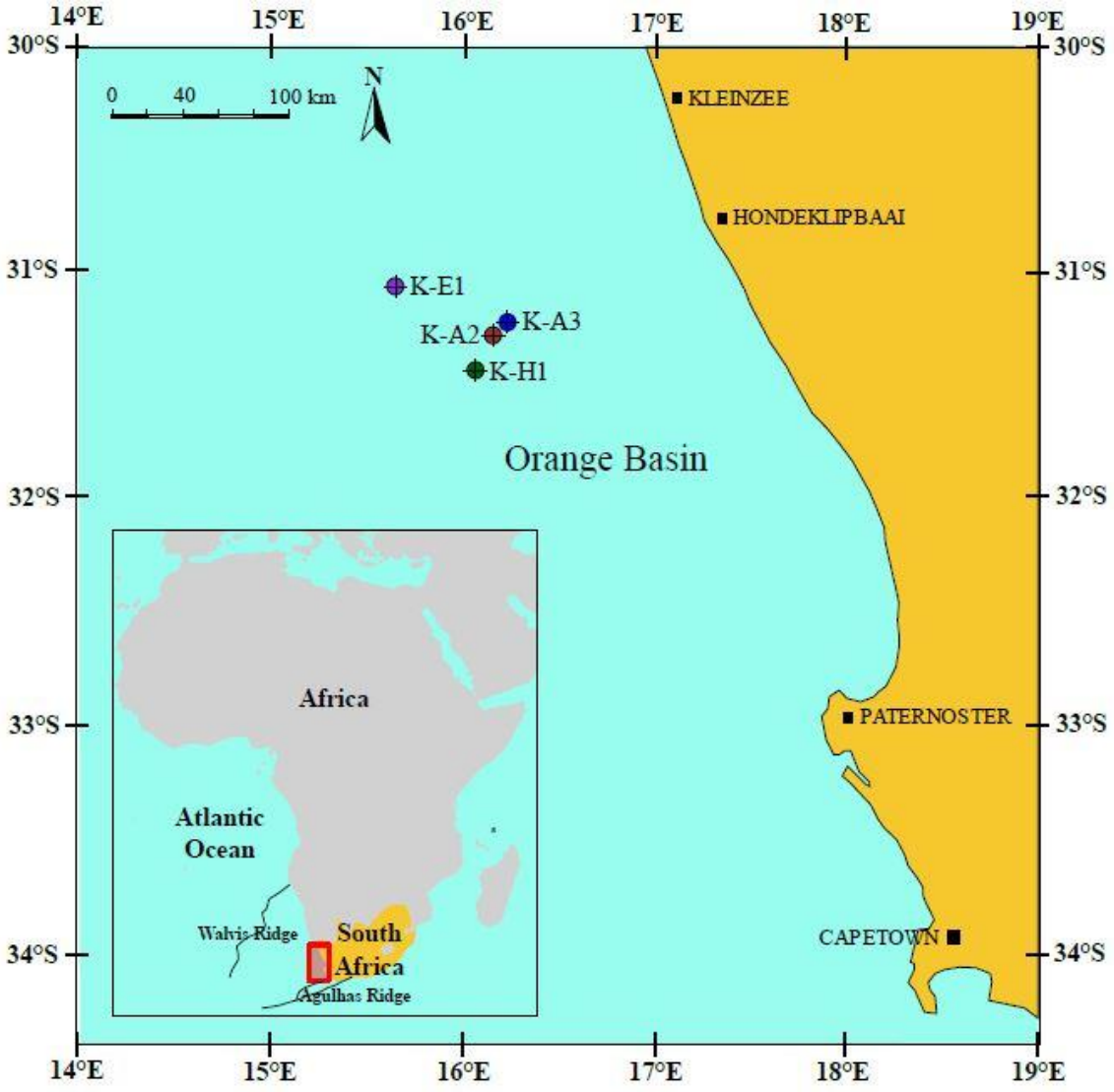


Figure 1. Location map of the Orange Basin, off South Africa, showing the four studied wells (K-A2, K-A3, K-E1, K-H1).

2003); sedimentation reached a total depth of more than 7 km in the northern parts of the basin and approximately 3 km in the south (Figure 2, Muntingh 1993, Brown et al. 1996).

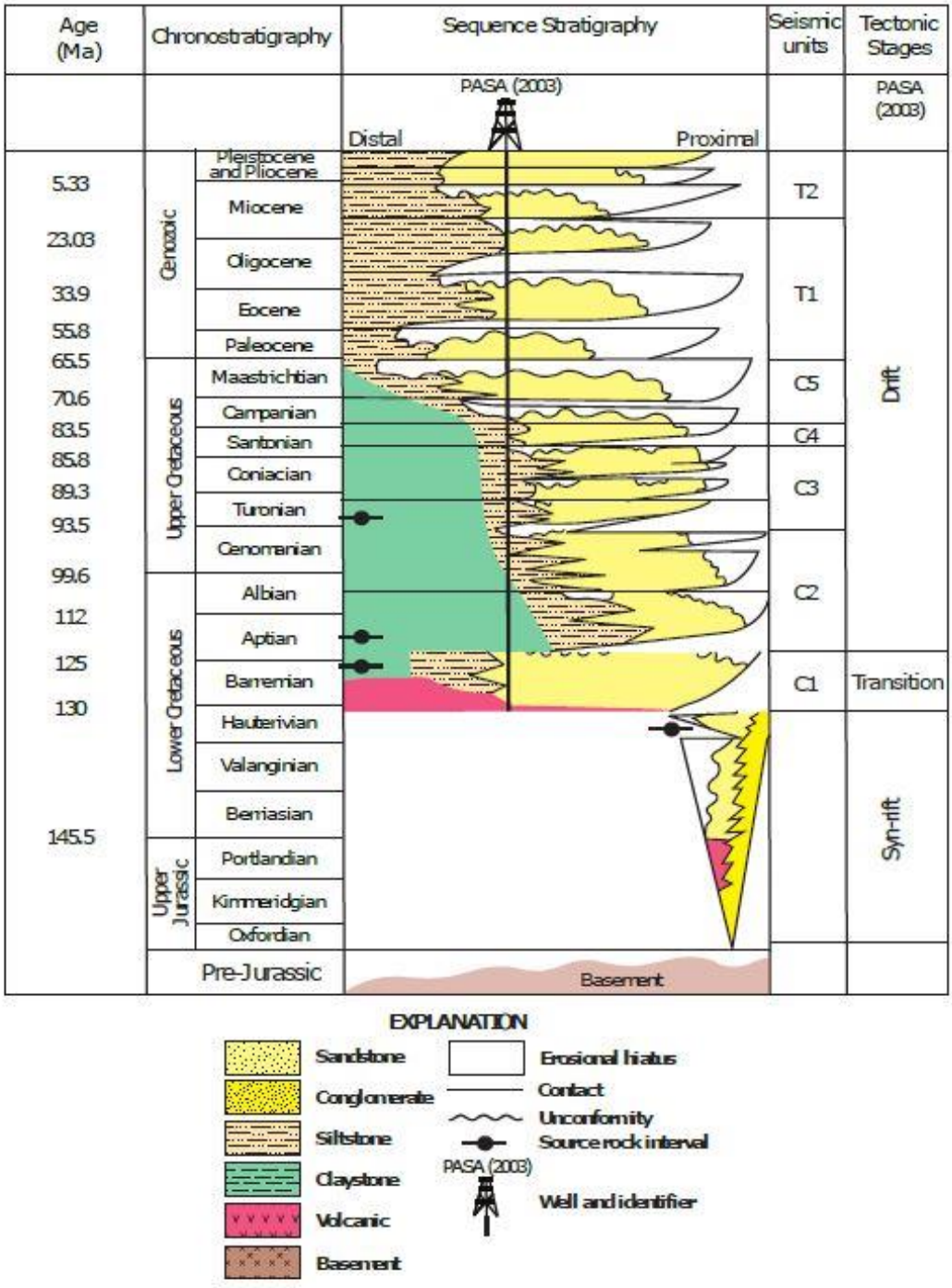


Figure 2. Stratigraphic column of the Orange Basin (after Brownfield, 2016).

The Orange Basin has not been well explored in spite of its proven hydrocarbon reserves, and little is known of its potential. The studies that have considered various aspects of the basin's hydrocarbon systems include Jungslager (1999), Van der Spuy (2003), Paton et al. (2007), and Kuhlmann et al. (2010). There is also limited biostratigraphic information for the basin; this is derived from studies on palynology (Davey and Rogers 1975, Davey 1978, MacLachlan and Pieterse 1978, Benson 1990, Bamford and Corbett 1994, 1995, De Villiers and Cadman 2001, Oboh-Ikuenobe and De Villiers 2003, Zavada 2004, Sandersen et al. 2011, Adekola et al. 2014) and foraminifera (McMillan 2003, Stevenson and McMillan 2004, McMillan, 2008).

This study focuses on the lithology, palynomorphs, particulate organic matter, and foraminifera in wells K-A2, K-A3, K-H1, and K-E1 (Figure 1) located between 15 degrees and 17 degrees latitude and around 31 degrees longitude within blocks 3A and 2C of the Orange Basin. The aim of the study is to provide information about the paleoenvironment and hydrocarbon potential of a previously understudied area of the basin. Palynofacies analysis is very useful in discerning paleoenvironmental conditions and proximity to paleoshoreline, particularly when paucity of microfossils limits interpretations. The characteristics of phytoclasts, such as their sizes, shapes, and oxidation levels, are used to infer their distance from source and the paleoshoreline (Tyson and Follows 2000). Additional valuable biostratigraphic information provided by foraminifera is integrated with palynological data to better constrain the age, paleoenvironmental reconstruction, and hydrocarbon potential of the sediments.

# 2. GEOLOGIC SETTING

The Orange Basin developed as part of a rift-drift sequence during the breakup of the supercontinent Gondwana, which resulted in the separation of South America and Africa in the Late Jurassic, and the development of the South Atlantic in the Early Cretaceous (Muntigh 1993, Muntingh and Brown 1993, Brown et al. 1996, Brownfield 2016). This breakup created the space in the basin (Campher 2009) for diverse and thick Upper Jurassic to Lower Cretaceous siliciclastic marine, lacustrine, and volcanic sediments (Muntigh and Brown 1993, Paton et al. 2007, Brownfield 2016). The development of the structure of the basin involved two major phases consisting of rifting and then later drift phases (Campher et al. 2009, Brownfield 2016). The rifting began in the Jurassic and continued into the Early Cretaceous, forming north-south trending grabens and half-grabens, and ceased in the late Hauterivian (Brownfield 2016). An injection of basalt and unconformity occurred at the margin sometime in the Early Cretaceous, followed by a marine ingression and flooding in the mid-Cretaceous resulting from thermal subsidence and eustasy along the margin; this culminated in the Atlantic being fully open by the Late Cretaceous (Kuhlmann et al. 2010).

A major uplift occurred along the margin during this time as the continent moved over the Africa Superplume, resulting in at least one kilometer of uplift in the Orange Basin that created a shelf-slope topography documented by deltaic progradation of Albian age in the basin (Baby et al. 2020). The development of canyons and normal faults, as well as listric faults and toe thrusts, were prevalent along the shelf edge. The movement of the tectonic plates resulted in the movement of Africa northward. This

position change resulted in climate fluctuations in the southern portion of the basin, from arid to temperate, tropical, and then back to temperate conditions (Scotese 2002, Boucot et al. 2013). This was controlled in part by the changes in the equatorial distance and the development of ocean currents (Benguela, Mozambique and Antarctic Subpolar gyres) once the continents were far enough apart (Gordon 1973, Fischer and Uenzelmann-Neben 2018).

# 3. MATERIALS AND METHODS

## 3.1. PALYNOLOGY

Thirty-seven core samples from the six conventional cores of the four wells (one each from K-E1 and K-H1; two cores each from K-A2 and K-A3) were analyzed for their palynomorph and particulate organic matter (kerogen) contents. Fifteen grams of samples were digested in hydrochloric and hydrofluoric acids to dissolve carbonates and silicates, respectively (Traverse 2007). A portion of the organic residue was oxidized with Schultze solution ($KClO_3$ plus $HNO_3$) and sieved using a 10 μm mesh. The oxidized and unoxidized (kerogen) organic residues were strew-mounted on glass slides that were used for palynomorph identification and palynofacies analysis, respectively under transmitted light microscopy. The slides of the sieved residues were scanned for routine identification of palynomorphs (to the species level whenever possible) based on existing literature, reference indices and palynological databases (Ibrahim et al. 2015, Jansonius and Hills 1976 and supplements, Jaramillo and Rueda 2019, Frederiksen et al. 1982, Fensome et al. 2019, Slimani et al. 2010). Additionally, the chronostratigraphic ranges of taxa were

confirmed using Palynodata and White (2008), Fossilworks, the Paleobiology database, and AlgaeBase (Guiry and Guiry 2021). For palynofacies analysis, 300 particles of particulate organic matter components were point counted in each kerogen slide. Eight types of particulate organic matter components were identified (Table 1, Figure 3), following the classification schemes of Tyson (1993, 1995) and Oboh-Ikuenobe et al. (2005). The components are terrestrial amorphous organic matter, marine amorphous organic matter (AOM), opaques, structured phytoclasts, structureless phytoclasts, degraded phytoclasts, terrestrial palynomorphs (pollen grains, spores, freshwater algae, fungal remains), and marine palynomorphs (dinoflagellate cysts, foraminiferal test linings). Additional 300 point-counts per slide of phytoclasts and opaques were obtained to generate data for lath-shaped and equidimensional particles. Ternary plots with AOM—Phytoclasts—Palynomorphs (Tyson 1995) and marine amorphous organic matter (AMOM)—Phytoclasts/Nonmarine Palynomorphs—Marine Palynomorphs (El Beialy et al. 2016) as end members (Figure 4) were used to characterize the kerogen and interpret the paleoenvironmental conditions. The particulate organic matter data was used for cluster analysis (Wards, stratigraphic constraints) using the Paleontological Statistics Software Package for Education and Data Analysis (PAST© 2001) to identify palynofacies assemblages. Cluster analysis was chosen as the most appropriate for this study since the software assigns and compares the distances between objects and subsequently can show the relationships between these objects on the dendrogram (Sokal and Michener, 1958). Sample distances are represented on the left side (Q-mode) of the cluster dendrogram while component abundances on the right. Furthermore, Ward's

method was chosen based on its ability to constrain well-defined clusters by utilizing the lowest sum of squares within each group.

### 3.2. FORAMINIFERAL ANALYSIS

The 27 shale and claystone core samples analyzed for foraminifera (six of which were not analyzed for palynology) were selected after careful examination of well logs and composite logs (well completion report) and detailed megascopic analysis. Prior to the megascopic examination, all the samples were washed with water to remove drilling mud contamination, and the overall lithological characters of each sample were recorded. The lithological properties that were documented included general textural elements (color of the grains and overall appearance, angularity, grain size, nature of cement, etc.), percentage-wise lithology (sand, siltstone, shale, claystone, limestone fragments, presence of fossil and algal remains), presence of accessory materials like carbonaceous matter, oxidized ferruginous grains, and anoxic (pyritized) materials, which were important for the interpretation of the depositional environment.

Sample processing techniques for conventional core samples depend on the nature of the samples (Kummel and Raup 1965, Feldmann et al. 1989, Harris and Sweet 1989, Green, 2001). The main aim is to disintegrate rock fragments into individual grains as much as possible in order to remove the binding cement material and facilitate the separation of the microfossils. While processing the conventional core samples, 20 grams of core fragments were washed in water and their geological characteristics (texture, mineral or lithological composition) were recorded. Since most of the core fragments

Table 1. Classification and description of the particulate organic matter components identified in this study. See Figure 3 for examples of these components.

| | | | |
|---|---|---|---|
| **Palynomorphs** | | | |
| Terrestrial | Sporomorphs | | Fungal remains |
| | Pollen | Spores | Filamentous hyphae (C), spores, or mycelia, of brown color and ranging from 5 µm to more than 100 µm in size. |
| | Yellow grains (A) of terrestrial plant origin (gymnosperm and angiosperm). | Pale yellow to orange-brown grains (B) of terrestrial plant origin (bryophytes and pteridophytes). | |
| Nonmarine aquatic | Micro- and megaspores | | Algae |
| | Spores (D) produced by heterosporous embryophytic plants (water ferns) | | Cysts, zygospores, or coenobia (E) of orange-brown to brown color produced by algae |
| Marine | Dinoflagellate cysts | | Palynomorphs |
| | Cysts (F) produced by dinoflagellates which may be smooth or ornamented with tabulation and/or processes | | Palynomorph of animal-like protists, microflora and foraminiferal test lining (G) |
| **Palynodebris** | | | |
| Structured organic material | Phytoclasts | | Zooclasts |
| | Degraded | Structured | Fragment of animal origin (i.e. insect) and may be yellow or brown (O & P) |
| | Broken-down plant material that is nearly structureless and may be yellow to brown in color (H) | Translucent angular material of terrestrial plant origin with internal structure (I) | |
| | Opaques | | |
| | Black particles (J-L) which may be phytoclasts including woody material such as cuticles, tracheids (M), parenchyma (N), or palynomorphs oxidized or affected by diagenesis | | |
| Structureless organic material | Amorphous Organic Matter (AOM) | | Resin |
| | Diaphanous or translucent kerogen particles (Q & R) of marine origin including dinoflagellates and acritarchs with variable texture (fluffy, clotted or granular) and colors including clear, gray, and brown | | Yellow to brown translucent and structureless angular particles (S), sometimes with conchoidal fracture along edges, produced from tree sap |

were of relatively large size, they were broken down into smaller fragments using a wooden hammer before soaking the sample in water. The core pieces were not powdered as this could potentially have destroyed the foraminifera tests. The washed samples were kept in separate enamel bowls with water. Approximate 15 ml of hydrogen peroxide (30%) was added to the content in the enamel bowls and soaked for 48 hours at standard room temperature conditions. The hydrogen peroxide helped disintegrate the sedimentary particles by breaking the sediment lattice and removing the cemented material. A small amount of caustic soda/laboratory detergent was also added to the solution to assist with separation from the clay matrix of the sample. After 48 hours of soaking, the samples were rapidly boiled for about 45 minutes on an electric stove in the laboratory to intensify the disintegration and then allowed to cool. After cooling, the entire content of the boiled

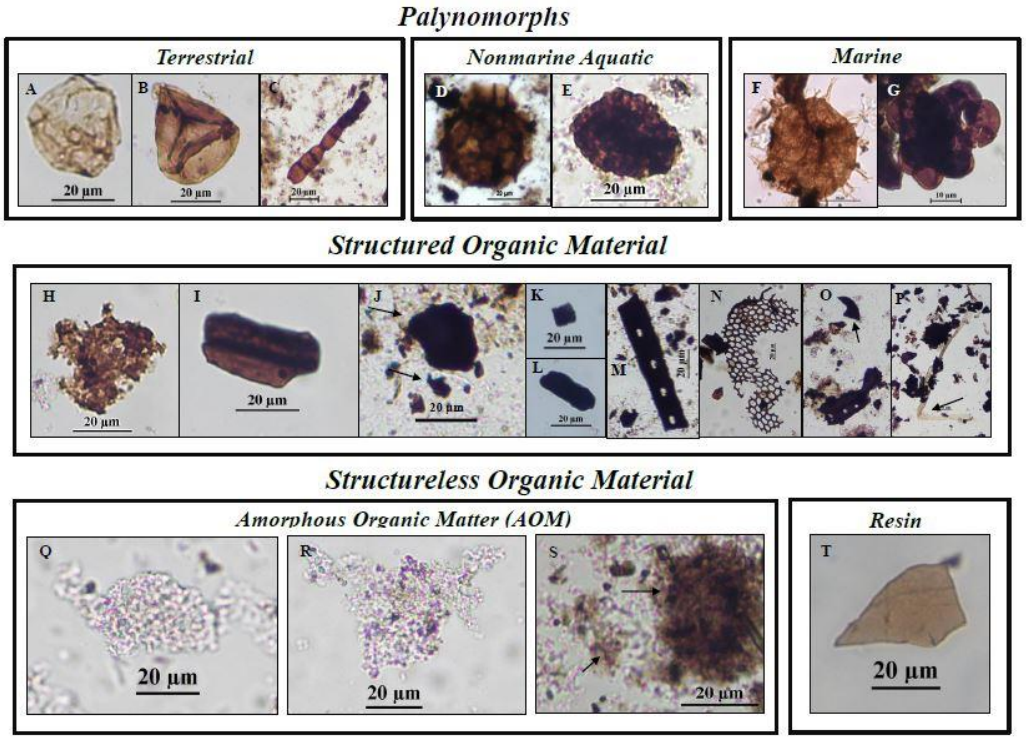


Figure 3. Photomicrographs of the types of particulate organic matter components identified in this study. Some components occur in minor amounts but were not point counted. A, Stephanoporate pollen. B, Trilete spore. C, Fungal hypha. D, Water fern (*Balmeisporites* sp.). E, Algal coenobium. F, Dinoflagellate cyst. G, Microforaminiferal test lining. H, Degraded phytoclast. I, Structured phytoclast. J, Opaque particles. K, Equant-shaped opaque particle. L, Lath-shaped opaque particle. M, Tracheid. N, Parenchyma. O, P, Zooclasts. Q, R, Marine amorphous organic matter. S, Nonmarine amorphous material. T, Resin.

samples were placed in a fine 50 µm sieve and rinsed under running water in a sink to remove the clay materials that were separated out of the chemically treated and boiled samples, in order to retain the disintegrated sediment fragments and microfossils. The washed content in the sieve was transferred to the enamel bowl once again, dried in the oven and then allowed to cool. The contents of the bowls were kept in transparent sample tubes with proper identification tags. Extreme caution was taken while processing the large number of samples to avoid sieve contamination and mixing of identification labels.

The samples were identified by well number, depth interval, or core segment number/depth, and were microscopically examined for biostratigraphy.

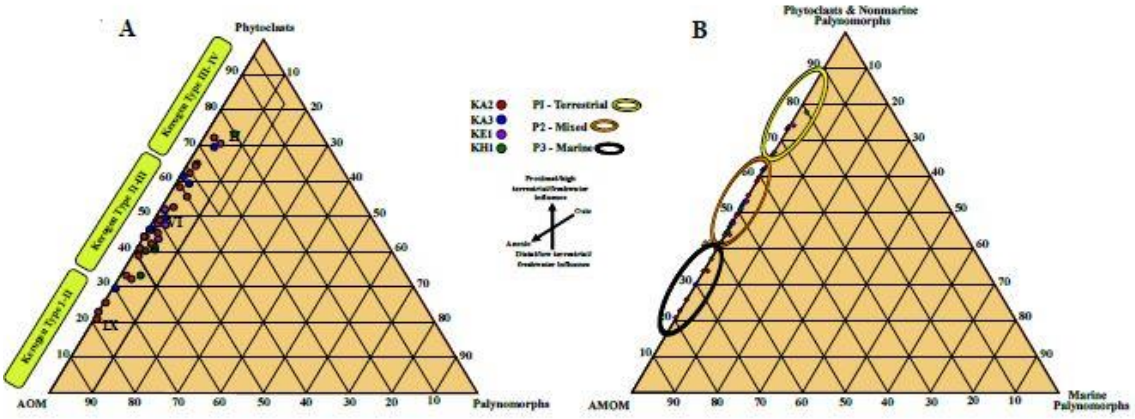


Figure 4. Ternary plots of particulate organic matter in the samples of wells K-H1, K-E1, K-A2, K-A3. A. AOM-Palynomorph-Phytoclast plot (after Tyson, 1995). B. Marine Amorphous Marine Organic Matter [AMOM]-Phytoclast and Nonmarine Palynomorph-Marine Palynomorph plot (after El Beialy et al. 2016) and inferred palynofacies assemblages. Yellow oval = palynofacies 1, orange oval = palynofacies 2, black oval = palynofacies 3.

## 4. RESULTS

### 4.1. LITHOLOGY

The lithology in wells K-A2, K-A3, K-H1, and K-E1 is dominated by fine-grained sandstone and siltstone interbedded with shale and claystone (Figures 5–7). The rate of sedimentation in the studied sections, which experienced terrestrial inputs from the nearby continent, is generally relatively high (Gallagher and Brown 1999, Paton et al. 2007, Campher et al. 2009, Rouby et al. 2009, Brownfield 2016). Carbonaceous streaks,

mixed shallow marine algal fragments, and pyritized foraminiferal tests were noted in the core samples.

Core 1 of well K-A2 (3984.1–3991.85 m) comprises mainly very fine-grained sandstone intercalated with shale and siltstone (Figure 5, left). The shale is dark gray and fissile with disseminated pyrite grains towards the bottom of each interval. The sandstone is light gray to white, feebly argillaceous, tight towards the base, and moderately sorted with subangular grains. Parallel shale laminations and carbonaceous particles occur in the middle sandstone interval at 3987.31 m. The upper sandstone interval (3985.25–3984 m) contains fine-grained silty patches, is moderately hard and feebly calcareous, and very tight with poor visual porosity and rare carbonaceous matter. The siltstone is light gray and feebly calcareous with parallel shale lamination in the middle; it has carbonaceous particles and common pyrite grains in the upper portion. Bioturbation is widespread in this core. Some interlaminated siltstone and shale preserve load casts, as well as climbing ripples and wavy laminations (Salie 2018).

Core 2 of well K-A2 (4076.1–4083.1 m) is dominated by intercalated siltstone and shale in the lower portion, followed by alternating layers of sandstone and siltstone, coarsening-upward sandstone with intercalations of siltstone and very thin shale (Figure 5, right). The siltstone in the lower portion of the core is medium gray with white patches and is feebly calcareous. The sandstone in the upper half of the core is light gray, massive, very tight, and is locally silty with subangular to subrounded grains. The shale is dark gray, bulky, feebly carbonaceous, and often grades to siltstone.

The dominant lithology in core 1 of well K-A3 (2906–2914.5 m) is medium- to very fine-grained sandstone, which has interbeds of shale and a thin siltstone below

2911.7 m (Figure 6, left). The initial fining-upward sequence is succeeded by a coarsening upward sequence. The sandstone varies from white to light gray in color (mud drapes forming flaser laminations), consists of well sorted and subangular grains, and is feebly calcareous with fine carbonaceous patches in places. The shale is dark gray and fissile with some carbonaceous layers. Core 2 of well K-A3 (3875.5–3884 m) is also dominantly sandstone with thin intercalations of siltstone, claystone (silty shale), and shale (Figure 6, right). The sandstone is light gray to white with subangular to subrounded grains and a few shale clasts, and has planar laminations. The siltstone is

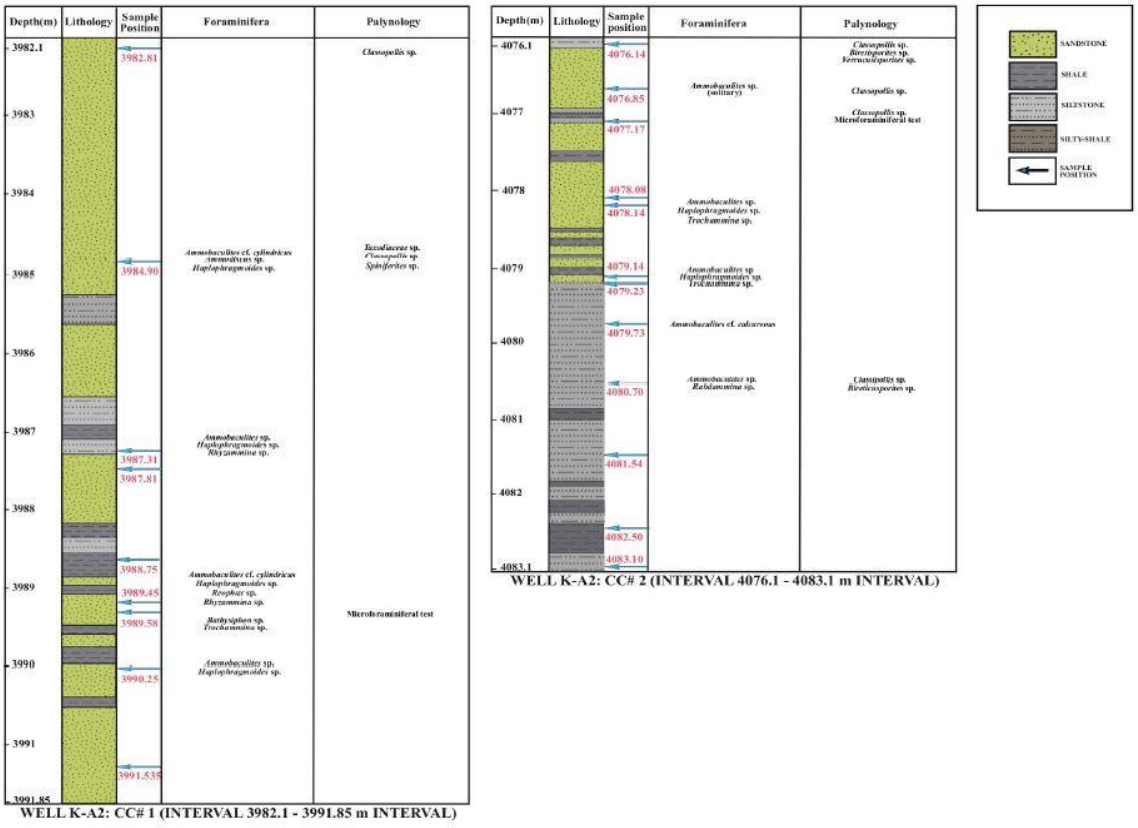


Figure 5. Lithologic column of the well K-A2 showing the locations of samples and key foraminiferal and palynomorph taxa.

gray and laminated. The dark gray to black shale is hard and fissile, contains pyrite grains, and transitions to a claystone.

The well K-H1 core spans 3066 m through 3083 m. It is dominantly sandstone which alternates with siltstone and shale layers between ~3073.8 m and 3080.6 m (Figure 7, left). The sandstone is gray to light gray, fine-grained, moderately sorted with planar laminations, and has subangular to subrounded grains surrounded by mild calcareous cement; it also has common fine pyrite grains. The siltstone is dark gray, locally fissile and transitions into claystone. The shale is dark gray and non-calcareous, and has a few pyrite grains.

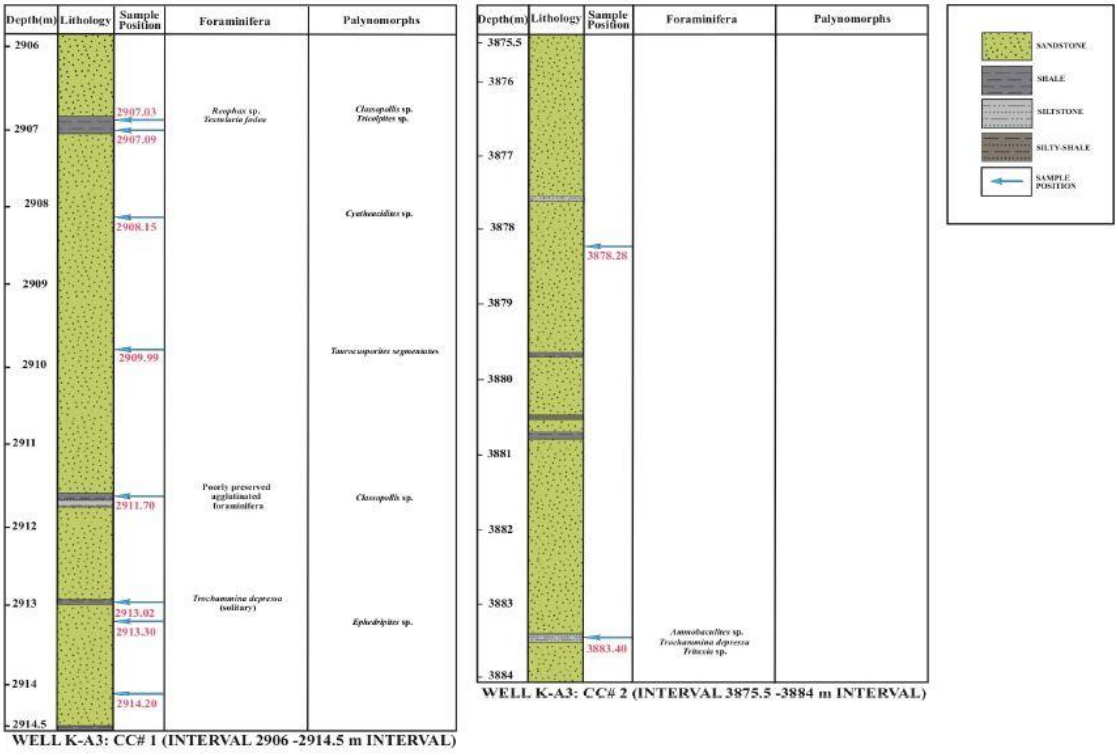


Figure 6. Lithologic column of the well K-A3 showing the locations of samples and key foraminiferal and palynomorph taxa.

In the well K-E1 core (Figure 7, right), alternating shale and sandstone transition to alternating sandstone and siltstone near the top of this segment. The siltstone is light gray to pale yellow in color, hard and compact, and argillaceous and feebly carbonaceous in places. The sandstone is light yellow to white, fine-grained, with subangular to subrounded grains, and is very tight with poor visual porosity. Fine argillaceous patches and rare carbonaceous fine flaser and wavy laminations also occur in places. The shale is dark gray, hard, and compact with some carbonaceous layers. There is occasional lenticular bedding, and low angle cross bedding is more apparent with decreasing depth (Salie 2018).

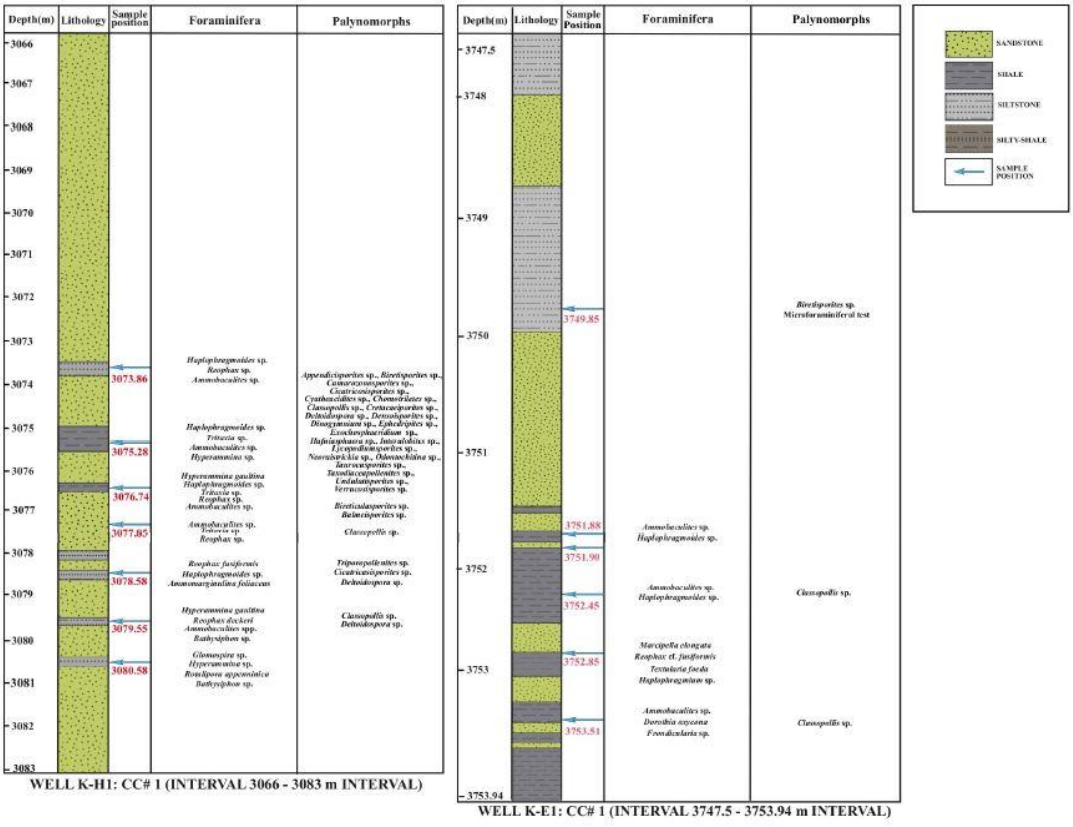


Figure 7. Lithologic column of the wells K-E1 and K-H1 showing the locations of samples and key foraminiferal and palynomorph taxa.

## 4.2. PALYNOMORPHS

Palynomorph abundances and diversity vary from low to barren in the four studied sections (Table 2). The recovered palynomorphs (Figures 8–10), which are primarily nonmarine in origin, include spores of pteridophytes (*Appendicisporites erdtmanni*, *Appendicisporites* sp., *Balmeisporites* sp., *Biretisporites potoniaei*, *Camarozonosporites* sp., *Cicatricasisporites* sp., *Cyatheacidites* sp., *Deltoidospora* sp., *Densoisporites* sp. *Gleicheniidites* sp., *Lycopodium* sp., *Undulatisporites* sp., *Verrucosisporites* sp.), and bryophytes (*Interlobites* sp., *Taurocusporites segmentatus*, *Taurocusporites* sp.). Gymnosperm pollen grains (*Classopollis classoides*, *Classopollis* sp., *Ephedripites* sp., *Taxodiaceaepollenites hiatus*), angiosperm pollen grains (*Cretacaeiporites polygonalis*, *Tricolpites* sp.), and fungal remains are present. Few nonmarine algae (*Chomotriletes minor*) and marine palynomorphs (the dinoflagellate cysts *Dinogymnium* sp., *Exochosphaeridium* sp., *Hafniasphaera* sp., *Spiniferites* sp., *Odontochitina operculata*) and foraminiferal test linings occur. *Classopollis* sp. is the most common taxon.

## 4.3. PALYNOFACIES ANALYSIS

The abundances of the particulate organic matter components identified in Section 3.1 (Table 2, Figure 3) provide information about the depositional conditions. Structured phytoclasts, degraded phytoclasts, opaques, and zooclasts such as insect parts (noted but not counted in this study) are associated with proximity to terrestrial environments. Structureless organic material such as amorphous organic matter or resin (tree sap) are characterized as marine or nonmarine in origin, respectively. Marine amorphous organic

Table 2. Quantitative Distribution of Particulate Organic Matter Components. Well locations shown in Figure 1. Lithology shown in Figure 5,6,7. AOM = Amorphous Organic Matter, MAR = Marine palynomorphs, SPORO = Pollen and spores, FUN = Fungal remains, STR = Structured, DEG = Degraded, OPA = Opaques, EO = Equidimensional, LO = Lath, + = Present but not point counted.

| Well & depth (m) | Lithology | AOM | Palynomorphs | | | Phytoclasts | | | Opaque Shapes | |
|---|---|---|---|---|---|---|---|---|---|---|
| | | | MAR | SPORO | FUN | STR | DEG | OPA | EO | LO |
| KA3 2907.03 | Sandstone & Shale | 81 | + | 11 | + | 85 | 29 | 94 | 133 | 167 |
| KA3 2908.15 | Sandstone | 210 | + | 2 | + | 22 | 43 | 23 | 209 | 91 |
| KA3 2909.99 | Sandstone | 142 | + | 3 | + | 48 | 28 | 79 | 109 | 191 |
| KA3 2911.70 | Silty Shale | 159 | + | 2 | 1 | 39 | 23 | 76 | 134 | 166 |
| KA3 2913.30 | Silty Shale | 114 | 1 | 8 | + | 57 | 21 | 99 | 117 | 183 |
| KA3 2914.20 | Sandstone | 145 | + | 7 | + | 62 | 12 | 74 | 142 | 158 |
| KA3 3878.28 | Sandstone | 115 | 1 | 1 | + | 25 | 98 | 60 | 155 | 145 |
| KA3 3883.40 | Shale | 161 | + | 1 | + | 7 | 109 | 22 | 154 | 146 |
| KH1 3073.86 | Silty Shale | 148 | + | 2 | 3 | 38 | 25 | 84 | 173 | 127 |
| KH1 3075.28 | Clay | 61 | 6 | 13 | 1 | 73 | 65 | 81 | 129 | 171 |
| KH1 3076.74 | Silty Shale | 100 | + | 6 | + | 70 | 11 | 113 | 165 | 135 |
| KH1 3077.85 | Sandstone & Silty Shale | 166 | 2 | 9 | 2 | 46 | 18 | 57 | 142 | 158 |
| KH1 3078.58 | Silty Shale & Sandstone | 165 | 1 | 10 | + | 53 | 14 | 57 | 163 | 137 |
| KH1 3079.85 | Sandstone & Silty Shale | 187 | 1 | 12 | 1 | 40 | 13 | 46 | 179 | 121 |
| KH1 3080.58 | Silty Shale | 173 | + | 4 | 3 | 57 | 11 | 52 | 159 | 141 |
| KE1 3749.85 | Silty Shale | 159 | + | 9 | 2 | 60 | 15 | 55 | 160 | 140 |
| KE1 3751.90 | Shale | 153 | + | + | 4 | 56 | 11 | 76 | 162 | 138 |
| KE1 3752.45 | Shaley Mudstone | 75 | 4 | 10 | + | 90 | 53 | 68 | 144 | 156 |
| KE1 3752.85 | Shale | 142 | + | 2 | 1 | 61 | 26 | 68 | 155 | 145 |
| KE1 3753.51 | Shale & Sandstone | 148 | + | 10 | + | 69 | 14 | 59 | 146 | 154 |
| KA2 3982.81 | Sandstone | 176 | + | 2 | + | 14 | 66 | 42 | 173 | 127 |
| KA2 3984.90 | Mudstone & Sandstone | 157 | + | 8 | + | 46 | 43 | 46 | 140 | 160 |
| KA2 3987.31 | Silty Shale | 167 | + | 1 | + | 9 | 68 | 55 | 151 | 149 |
| KA2 3987.81 | Siltstone | 236 | + | 2 | + | 16 | 30 | 16 | 130 | 170 |
| KA2 3988.75 | Shaley Mudstone | 109 | + | 5 | + | 34 | 76 | 76 | 159 | 141 |
| KA2 3989.45 | Shale & Sandstone | 180 | + | 2 | 2 | 39 | 56 | 21 | 123 | 177 |
| KA2 3990.25 | Shale & Sandstone | 197 | + | 3 | 1 | 25 | 34 | 40 | 127 | 173 |
| KA2 3991.535 | Sandstone | 195 | 2 | 7 | + | 46 | 29 | 21 | 129 | 171 |
| KA2 4076.14 | Silty Shale | 122 | + | 3 | 1 | 53 | 73 | 48 | 97 | 203 |
| KA2 4076.85 | Sandstone | 102 | + | 6 | + | 56 | 55 | 81 | 95 | 205 |
| KA2 4077.17 | Silty Shale | 77 | + | 7 | + | 79 | 72 | 65 | 120 | 180 |
| KA2 4078.08 | Sandstone | 150 | + | 3 | 1 | 50 | 31 | 65 | 111 | 189 |
| KA2 4079.14 | Mudstone | 166 | + | 8 | + | 51 | 35 | 40 | 118 | 182 |
| KA2 4079.73 | Silty Shale | 135 | + | 7 | 1 | 69 | 36 | 52 | 117 | 183 |
| KA2 4080.70 | Silty Shale | 121 | + | 12 | 1 | 84 | 33 | 49 | 108 | 192 |
| KA2 4081.54 | Mudstone | 168 | + | + | + | 15 | 69 | 48 | 161 | 139 |
| KA2 4082.50 | Sandstone & Mudstone | 223 | + | 1 | + | 13 | 49 | 14 | 174 | 126 |
| KA2 4083.10 | Silty Shale | 232 | + | + | + | 4 | 49 | 15 | 158 | 142 |

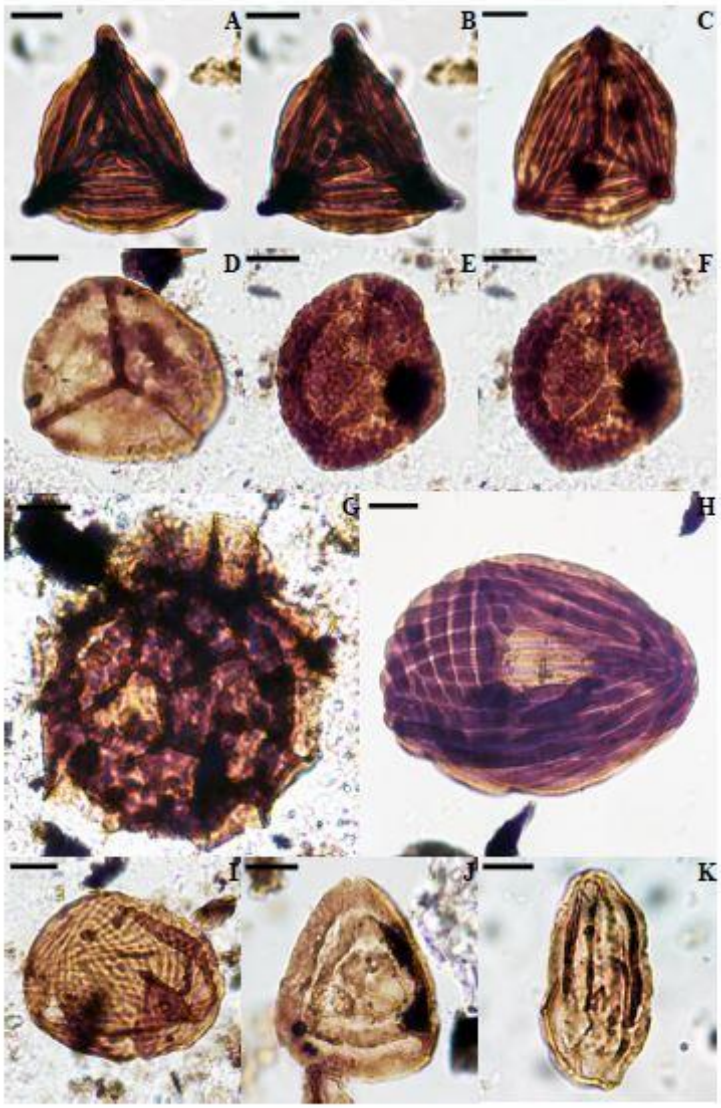


Figure 8. Photomicrographs of selected taxa. Well sample numbers are noted EF = England Finder® coordinates. Scale bar is 10 μm. A, B, *Appendicisporites erdtmanii*, KH1 3075.28-2, EF1T25. C, *Appendicisporites trichacanthus*, KH1 3075.28B, EF4P45. D, *Biretisporites potoniaei*, KH1 3075.28D, EF4L44. E, F, *Camarozonosporites* sp., KH1 3075.28B, EF2M36. G, *Balmeisporites* sp., KH1 3076.74D, EF1P39. H, *Cicatricosisporites* sp., KH1 3075.28D, EF3O33. I, *Cicatricosisporites venustus*, KH1 3075.28A, EF4Q28. J, *Cyatheacidites* sp., KH1 3075.28D, EF4B50. K, *Ephedripites* sp., KH1 3075.28C, EF2U41.

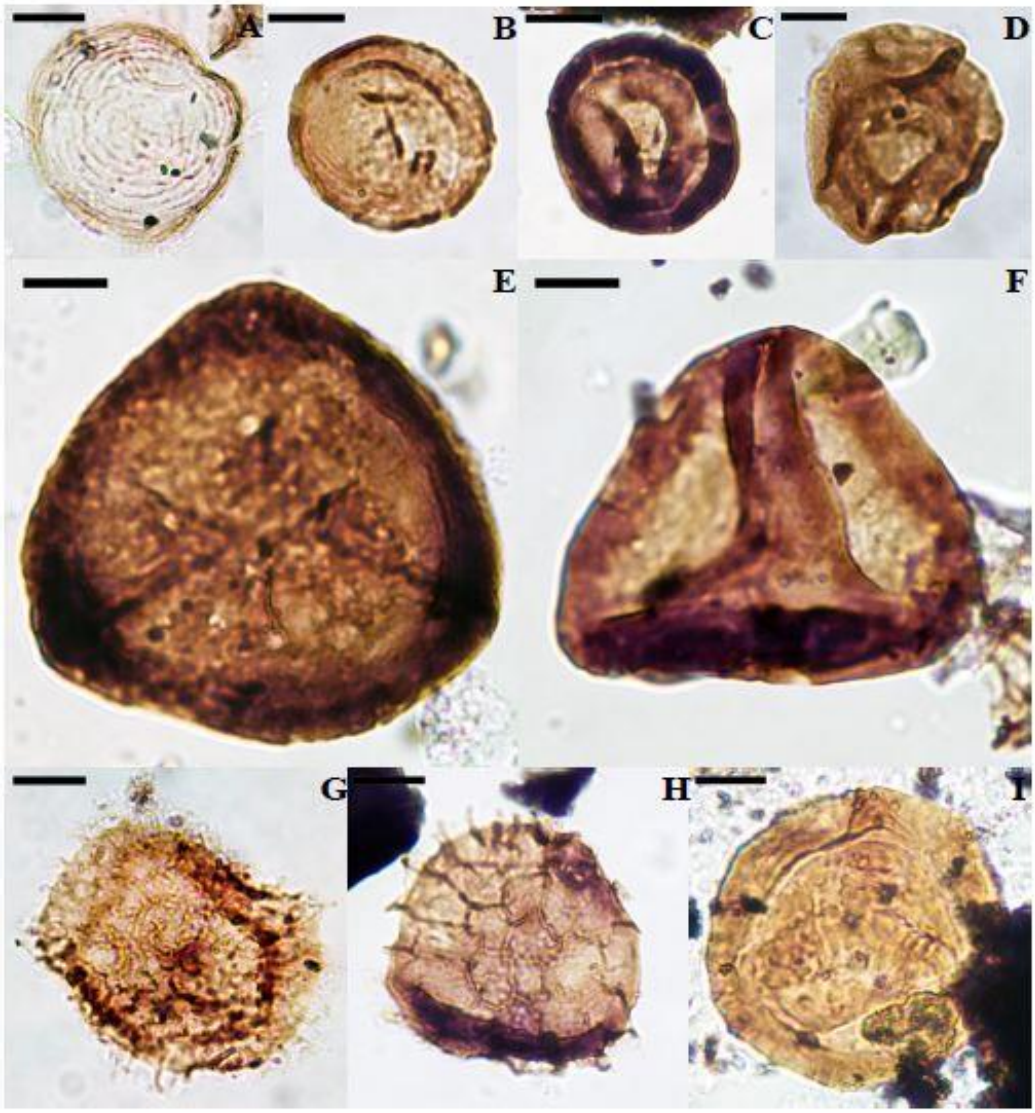


Figure 9. Photomicrographs of selected taxa. Well sample numbers are noted EF = England Finder® coordinates. Scale bar is 10 μm. A, *Chomotriletes minor*, KH1 3075.28A, EF2F31. B, *Classopollis classoides*, KH1 3075.28B, EF2R52. C, *Classopollis* sp., KH1 3752.45C, EF1O30. D, *Cretacaeiporites polygonalis*, KH1 3075.28B, EF1S35. E, *Densoisporites* sp., KH1 3075.28-2, EF3N30. F, *Gleicheniidites* sp., KH1 3076.74D, EF4L40. G, *Exochosphaeridium* sp., KH1 3075.28B, EF1B40. H, *Lycopodiumsporites reticulumsporites*, KH1 3075.28D, EF2E51. I, *Taurocusporites segmentatus*, KA3 2909.99E, EF1K47

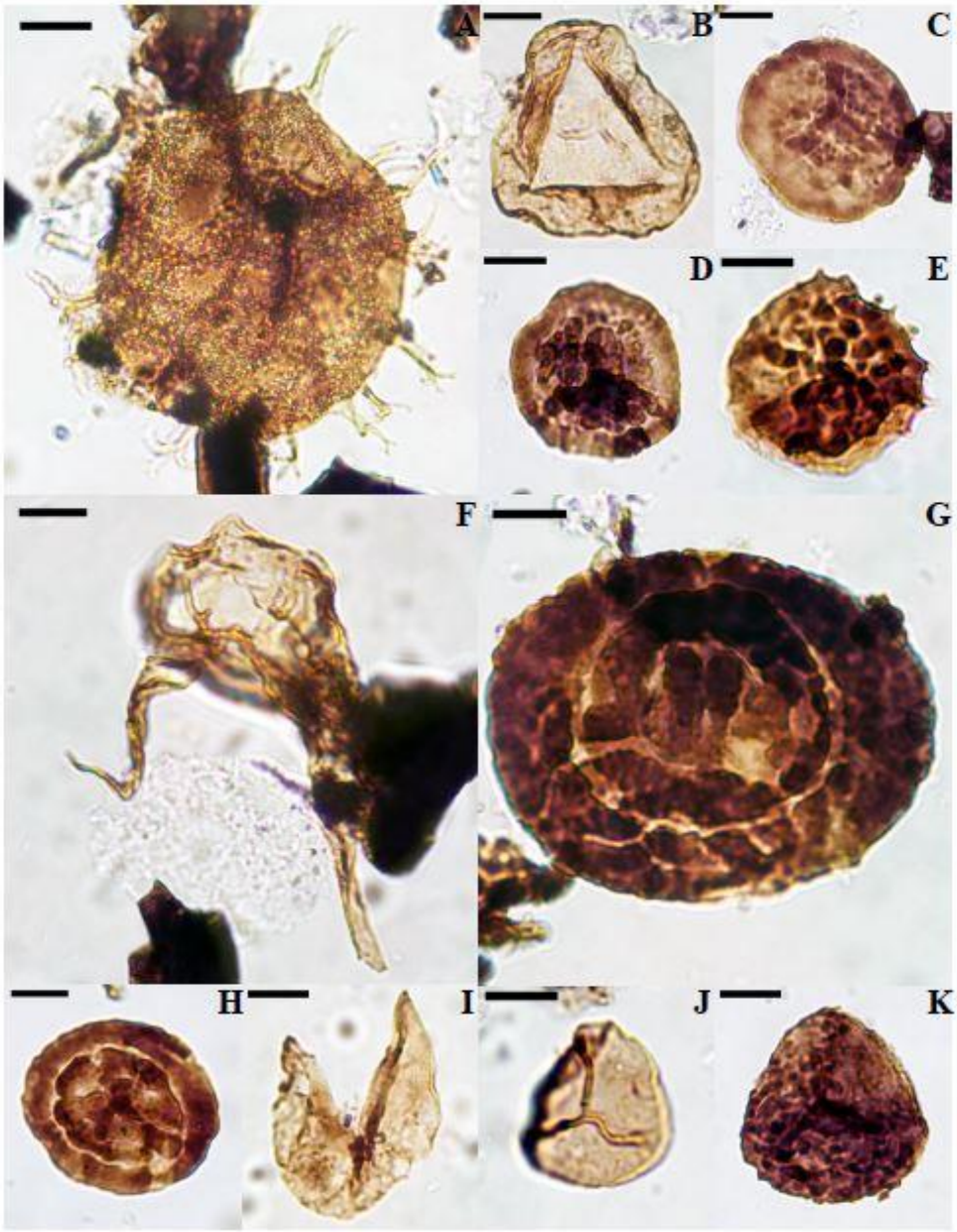


Figure 10. Photomicrographs of selected taxa. Well sample numbers are noted. EF = England Finder® coordinates. Scale bar is 10 μm.A, *Hafniasphaera* sp., KH1 3075.28A, EF2R43. B, *Deltoidospora* sp., KH1 3075.28-2, EF2O32. C, *Interulobites* sp., KH1 3752.45D, EF3U33. D, *Interulobites* sp., KH1 3075.28D, EF3S46. E, *Neoraistrickia* sp., KH1 3075.28-2, EF1E42. F, *Odontochitina operculata*, KH1 3075.28-2, EF3S37. G, *Taurocusporites* sp. A, KH1 3075.28A, EF2V43. H, *Taurocusporites* sp. B, KH1 3075.28B, EF4E31. I, *Taxodiaceaepollenites hiatus*, KH1 3075.28-2, EF2H45. J, *Undulatisporites* sp., KH1 3075.28D, EF4W40. K, *Verrucosisporites* sp., KH1 3075.28D, EF3E27.

matter is the dominant component in this study, followed by phytoclasts (Table 2). The sizes and shapes (lath-shaped, equidimensional) of the phytoclasts, including opaques, are affected by the hydroenergetic regime and distance of transportation. Equidimensional to lath-shaped opaque ratios decrease offshore overall, from well K-A3 and K-A2 to well K-E1 (Table 2). Previous studies have benefited from the use of multivariate statistical analyses for interpreting palynofacies results (Oboh 1992, Kovach and Batten 1994, Oboh-Ikuenobe and De Villiers 2003, Oboh-Ikuenobe et al. 2005). These analyses provide comparison of complex datasets with multiple variables that are of particular use in ecological studies (James, 1990; Ramette, 2007). The multivariate analytical methods chosen are unique to the dataset and depend on the aim of the study. Based on cluster analysis, three palynofacies assemblages are constrained (I, II, III in Figure 11), and an image of a representative sample from each assemblage is shown in Figure 12. Palynofacies assemblage I (Figures 11, 12) is dominated by nonmarine, mainly terrestrial components (between 60 and 80 %), with only about 20 to 40 % AOM. The AOM is mostly dispersed, although some clumped nonmarine AOM is present. The opaques are moderately rounded and include tracheids and both structured and structureless material such as resin. This assemblage is divided into two subgroups (A and B). Subgroup B differs from subgroup A due to increased numbers of structured phytoclasts, terrestrial palynomorphs, and marine palynomorphs, and a decrease in AOM and opaques. Palynofacies II (Figures 11, 12) is characterized by approximately 40% to 60 % AOM, and has two subgroups (A and B) as a result of differences in numbers of degraded Palynofacies assemblage III (Figures 11, 12) comprises the highest abundance (60-80 %) of marine components, the lowest nonmarine input, and the lowest abundance

of opaques. This assemblage contains a mix of angular and well-rounded opaques, and dispersed and granular marine AOM. It is also further divided into two subgroups: subgroup A is differentiated by the absence of palynomorphs, whereas subgroup B contains few palynomorphs, scattered resins, and structured phytoclasts.

### 4.4. FORAMINIFERAL ANALYSIS

Foraminiferal frequency is moderate to low in most of the core samples in all the four well sections. In general, all the samples are dominated by agglutinated foraminifera, and pyritized tests are present in some intervals. Several agglutinated foraminifera species are recorded in well K-A2, such as *Ammobaculites* cf. *cylindricus*, *Ammobaculites* spp., *Ammodiscus* spp., *Bathysiphon* sp., *Haplophragmoides* sp., *Reophax* sp., and *Trochammina* sp. There is a gradual decrease in foraminiferal frequency from the lower part of the interval to the top. One core sample in well K-A3 (CC#2, depth 3883.41m) records very coarse textured agglutinated foraminifera. Some samples above this depth contain the agglutinated foraminifera *Trochammina depressa*, *Textularia* sp., and *Ammobaculites* spp. In the other core (CC#1: samples at 2907.03 m, 2911.70 m. and 2913.02 m), very rare agglutinated foraminifera are present.

In well K-H1, there is moderate to low frequency of taxa, with few calcareous benthic forms. The early Cenomanian planktonic foraminifera *Rotalipora appenninica* and *Rotalipora gandolfi* (*Rotalipora brotzeni* Zone, Caron 1985) are present at depth 3080.58 m. Agglutinated foraminifera, such as *Ammobaculites* spp., *Glomospira* sp., *Haplophragmoides* spp., *Hyperammina gaultina*, *Reophax* sp., and *Tritaxia* sp. dominate the remaining samples. Calcareous benthics, including *Lenticulina angulosa* and

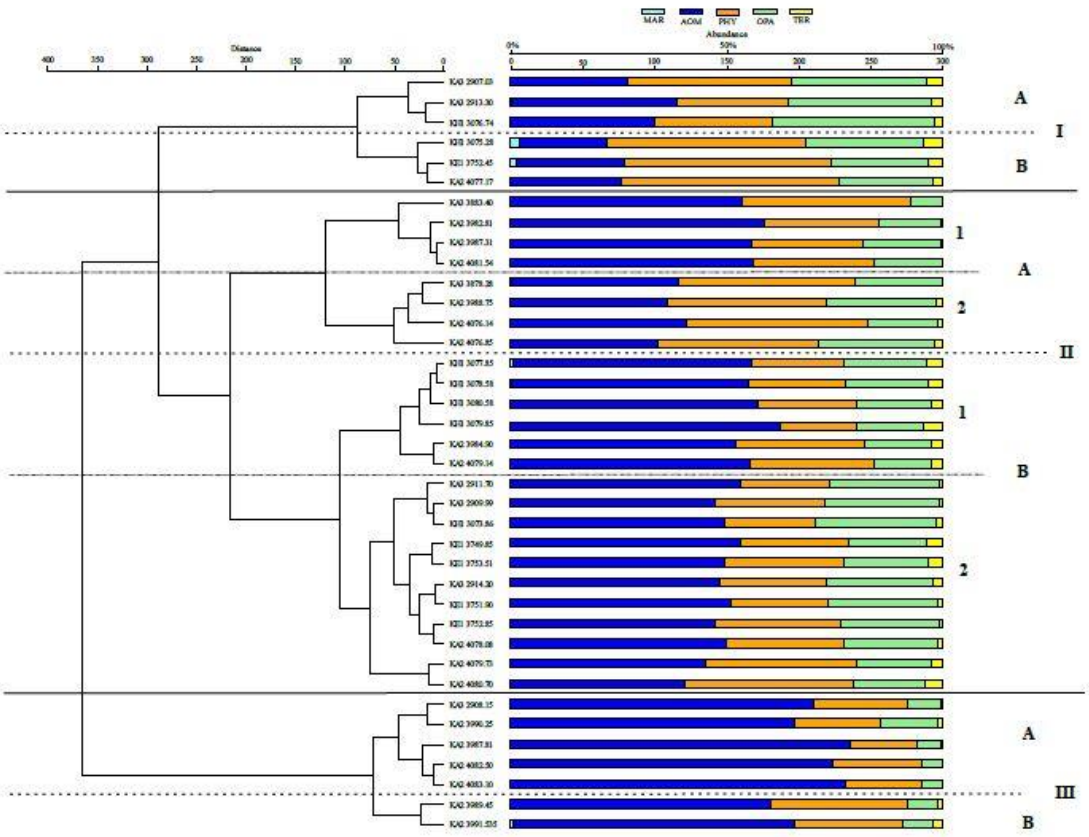


Figure 11. Q-mode cluster analysis (Ward's/Euclidean method) and abundance of particulate organic matter components characterizing the samples. MAR: Marine palynomorphs; AOM: Amorphous Organic Matter; PHY: Structured and degraded phytoclasts; OPA: Opaques; TER: terrestrial/nonmarine palynomorphs. Three palynofacies assemblages, each with two subgroups A and B, are recognized. I: Nonmarine, primarily terrestrially dominated, II: Mixed terrestrial and marine, III: Marine dominated.

*Lenticulina* cf. *nodosa,* are recorded in the basal part of the section. In well K-E1, the agglutinated benthic foraminifera *Ammobaculites subaquale, Haplophragmoides* spp., *Reophax* cf. *fusiformis, Textularia foeda, Dorothia oxycona,* and *Frondacularia* sp. are recorded in varying proportion in most of the samples.

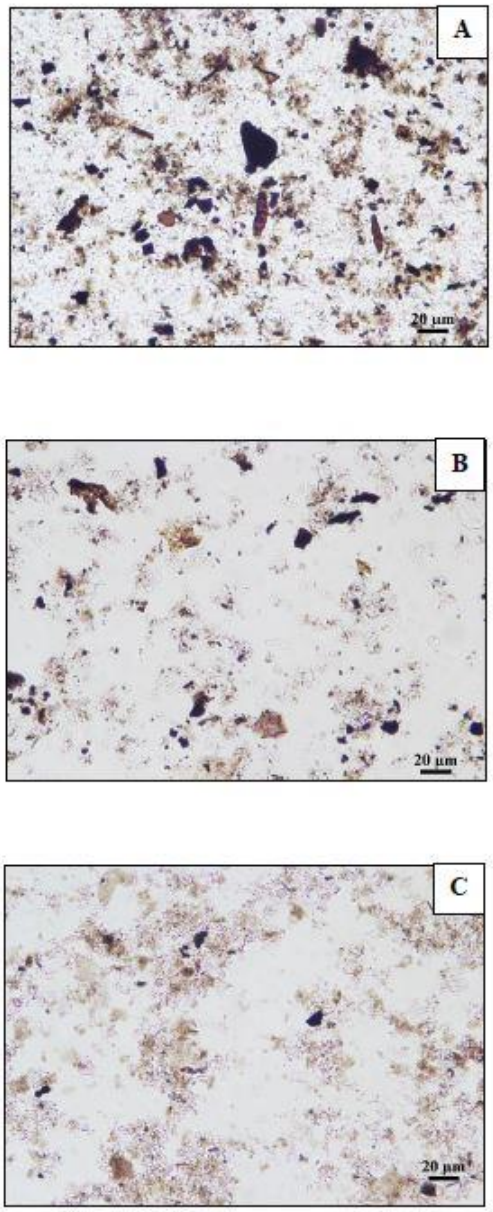


Figure 12. Photomicrographs of representative palynofacies assemblages. Well sample numbers are noted. EF = England Finder® coordinates. Scale bar is 20 µm. A, Palynofacies assemblage I with primarily nonmarine organic components; well K-E1 3752.85E, EF4S32. B, Palynofacies assemblage II with mixed terrestrial and marine organic components; well K-H1 3079.85B, EF1P46. C, Palynofacies assemblage III with mainly marine organic components; well K-A2 4082.50A, EF4K29.

# 5. DISCUSSION

Palynomorph and foraminiferal data provide the information used to constrain the age of the sediments in the studied wells. In addition, these two proxies have been integrated with lithological and palynofacies analyses to interpret the depositional environment, in addition to inferring the hydrocarbon potential of this segment of the Orange Basin.

## 5.1. AGE CONSTRAINT

The majority of the identified agglutinated foraminifera and palynomorph taxa are long ranging, from the Late Jurassic through the Late Cretaceous. The presence of the planktonic foraminifera *Rotalipora appenninica* and *Rotalipora gandolfi* at 3080.58 m in well K-H1, however, indicates an early Cenomanian age (Caron 1985). In addition, the presence of the angiosperm pollen *Cretacaeiporites polygonalis*, which is constrained to the Albian–Coniacian (Ibrahim et al. 2015), at 3075.28 in well K-H1 supports this age assignment. Therefore, the inferred age of the studied sequences is early Cenomanian.

## 5.2. PALEOENVIRONMENTAL CONDITIONS

The multiple proxies generated from the lithological descriptions of the sediments, microfossils, and particulate organic matter provide useful information about the depositional environment, sedimentary processes (e.g., energetic, and redox conditions), the origins, duration of transport, and/or source proximity of particulate organic matter and palynomorphs, and indirect inferences about the paleoclimatic

conditions at the time of sedimentation. The overall lithology of alternating fine-grained sandstone, siltstone, shale, and claystone in the four wells (Figures 2-4) is consistent with fluvio-marine type deposits reported from other African basins (e.g., Oboh-Ikuenobe et al. 2005, Khalifa and Catuneanu 2008). While the dominance of sandstone in the wells, except well K-E1, suggests high energy of deposition, the presence of flaser laminations and mud drapes in the sandstone units, and occasional wavy laminations in some heteroliths suggest short periods of quiescence. While mostly shallow marine, the depositional structures suggest periodic tidal and deltaic influences. We see no clear evidence of turbiditic deposition.

The types of nonmarine and marine microfossils in the sediments, as well as palynofacies analysis and the presence of glauconite (Salie 2018), suggest marginal to shallow marine (shelf) depositional environment subject to input of sedimentary material from the adjacent continent in this part of the Orange Basin during the early Cenomanian. The thicker overburden in the study area (Campher et al. 2009) that accompanied the high rate of sedimentation in southwestern Africa during the mid-Cretaceous (Dingle and Hendry 1984) was likely the result of increased topography along the coast, sedimentation outpacing the space created in the basin by rifting, and higher sea levels (Miller et al. 2003, An et al. 2017). The absence of bioturbation except in well K-A2 provides additional evidence of higher sedimentation rate and changing water conditions related to fluctuations in sea level (Tonkin 2012). Higher sea level is also documented by the carbonaceous streaks, marine algal fragments, and calcareous cement in the sandstone beds in wells K-H1 and K-A2 and the upper portion of well K-A3. However, the presence of pyrite crystals (Table 1) in the samples, in addition to the high amounts of

AOM (well K-E1) and few marine microfossils (Figure 11), suggest low depositional energy and reducing conditions with high potential for preservation of organic material (Tyson 1995, Zobaa et al. 2011, 2013). Since some pyritized foraminiferal tests and pyritized particulate organic matter were also recovered, the pyrite crystals may be early diagenetic in origin.

Palynofacies analysis supports deposition on the continental shelf. Two ternary plots of the particulate organic matter provide information about the types of kerogen and depositional conditions. However, Figure 7B (following El Beialy et al. 2016) with palynofacies assemblages I, II, and III delineated provides more accurate data with respect to the origins of the particulate organic matter than Figure 7A (following Tyson 1995; see discussion in Section 5.3). Marine amorphous organic matter (AMOM) represents the redox state at the time of deposition, while the combination of phytoclasts and nonmarine palynomorphs reflects terrestrial and nonmarine aquatic input, and the relationship with marine palynomorphs and AMOM provides a proxy for the distance between the basin and the paleoshoreline (El Beialy et al. 2016). The appearance of preserved AOM can be related to its origin and how it is preserved, with its abundance in sediments attributed to an increase in paleoproductivity (Powell et al. 1990, 1992). Granular AOM is likely representative of benthic microbial mats (Pacton et al. 2007, 2011; Emmings et al. 2019) and may have been transported via flooding, turbidites, debris flows, bottom currents, or coastal upwelling (Tyson 1995, Emmings 2019). Additionally, the shapes and sizes of opaque particles yield information about their distance from source. According to Tyson (1995), relatively high ratios of equidimensional to lath-shaped opaque particles (Table 2) typically represent a short

distance of transport from source where the equidimensional particles have the largest sizes. In this study, the lath-shaped particles are larger (10-150 μm length for longest axis) compared to the equidimensional particles (2-50 μm length for longest axis), suggesting a longer transport distance for the terrestrial material.

Palynofacies assemblages II (largest with samples from all four wells) and III (mainly K-A2 samples) are characterized by mixed marine (>40% AMOM)/nonmarine components and preponderance (>60%) of AMOM, respectively. Foraminiferal test linings are present in some intervals. Assemblages II and III plot in the proximal suboxic-anoxic shelf (VI) and distal suboxic-anoxic basin (IX) fields, respectively in Figure 7. Although nonmarine (terrestrial/aquatic) organic components (Figure 11, Table 2) dominate palynofacies assemblage I (with fewest samples from all four wells), AMOM comprises 20-40% of the total organic material, and the assemblage plots in the marginal dysoxic-anoxic basin field (II). The presence of insect parts, cuticles, and tracheids also support this continental contribution to the basin (Table 1).

Detailed palynomorph analysis provides information about the source areas from which the spores, pollen grains and algae were derived. The few palynomorph taxa recovered in this study, including the gymnosperm *Classopollis* sp., the pteridophytes *Deltoidospora* sp., *Cicatricasisporites* sp. and *Cyatheacidites* sp., the bryophytes *Interlobites* sp. and *Taurocusporites* sp., the nonmarine algae *Chomotriletes* sp. and *Balmeisporites* sp., as well as fungal remains are typically found in coastal environments (e.g., fluvial, deltaic) with arid hinterlands (El-Soughier 2013, Carvalho et al. 2017). Due to the configuration of the continents during the Cretaceous, the climate on the continental interior from which these palynomorphs originated was likely arid (Eldridge

and Scotese, 2002) with sparse vegetation (El Beialy et al. 2016). The recovered gymnosperms *Ephedripites* sp. and *Classopollis* sp. are associated with dry to semi-arid coastal environments and support this scenario (Srivastava 1976, Schrank 2010, Warny et al. 2019). It is possible that the absence to low abundances of palynomorphs in the samples may be reflective of the dilution effect of abundant AMOM and phytoclasts, or the aridity and sparse vegetation in the hinterland.

The dominance of benthic agglutinated-walled foraminifera in this study is an enigma, particularly because forms such as *Ammobaculities* spp., *Trochamina* sp., and *Haplophragmodies* sp. are indicative of low salinity and pH. They also typically suggest short distance of transport since the agglutinated forms do not fare well with travel (McMillan 2008). The agglutinated taxa provide additional support for a possible coastal or marginal marine interpretation. For example, *Ammobaculites* spp., *Haplophragmoides* sp., *Reophax* sp., and *Trochaminna* sp. are associated with hypoxic waters, and *Ammodiscus* sp. and *Glomospira* sp. are typically found in brackish delta plain and estuaries (Nagy et al. 2010). Although benthic forms such as *Ammodiscus* and *Trochammina* may adapt to periods of hypoxia, lower salinity, and disruption by storms in restricted marine shelf environments with deltaic influence (Nagy et al. 2010), some authors (e.g., Stevenson and McMillan 2004) explain their presence as due to river-incised fill. Note that the presence of calcareous benthic forms *Lenticulina angulosa* and *Lenticulina* cf. *nodosa*, and the planktonic species *Rotalipora appenninica* and *Rotalipora gandolfi* in well K-H1 is consistent with fully marine, inner to middle shelf conditions.

The foregoing discussion based on the lithology of the studied intervals in the four wells, the palynofacies, palynomorph and foraminifera data from of the studied samples, and the available information on mid-Cretaceous sediments elsewhere in the Orange Basin (e.g., Campher et al. 2009, Kuhlmann et al. 2010) suggests that the sediments were likely deposited in a highly dynamic shallow marine (inner shelf to middle shelf) paleoenvironment. This paleoenvironment experienced fluctuations in depositional energy and redox conditions, periodic continental runoff, and episodes of low salinity. Sedimentary structures, such as flaser and wavy laminations, support the deposition of the sediments in wells K-A2, K-A3, and K-E1 in the very shallow shelf closest to the Walvis Ridge. Sediments in well K-H1, which was farther from the Ridge, were deposited under more open marine (inner to middle shelf) conditions. Warm temperate to subtropical, semi-arid climate was prevalent in the hinterland.

### 5.3. HYDROCARBON POTENTIAL

Figure 7 depicts the character of the particulate organic matter (kerogen I-IV) in the samples; it shows that type I kerogen is most common in sediments that are rich in AMOM and marine palynomorphs, whereas type IV kerogen dominates terrestrially/nonmarine derived sediments. The positions of the samples characterizing the three palynofacies assemblages (see Figures 11, 12) in Figure 7 were used to infer the types of kerogen and hydrocarbon potential. Palynofacies I has the potential to produce type III kerogen, which is gas prone, whereas palynofacies assemblage II is characterized by types II-III kerogen given its mixed nature, which are oil-gas prone. Palynofacies

assemblage III has the potential to produce type I-II kerogen and the components are highly oil prone.

While this paleoenvironment has the potential to produce types II and III kerogen, there appears to be very low productivity. The low abundances of palynomorphs and foraminifera, supports this inference, which, together with the presence of pyrite crystals and pyritized microfossils, may also be indicative of conditions of lower salinity, lower levels of oxygenation and, or thermal maturity of sediments (Gupta and Machain-Castillo 1993, Zobaa et al. 2011). We used the color of *Classopollis* spp., the most common palynomorphs in Type II and III kerogen samples to infer a thermal alteration index (TAI) of around 3. Although a preponderance of terrestrially-derived organic material and palynomorphs indicate a greater likelihood to produce gas rather than oil (Kandiyoti et al. 2006, Vandenbroucke and Largeau 2007), the low abundance of palynomorphs in these sediments belies the potential for hydrocarbon. We note here that Kuhlmann et al. (2010) used lithological interpretations of Cenomanian to Turonian outer shelf sediments in nearby blocks in the southern Orange Basin to infer gas prone source rocks.

## 6. CONCLUSIONS

Integrated lithology and biostratigraphy of wells K-A2, K-A3, K-H1, and K-E1 provides key information for the interpretation of this complex area within the Orange Basin. Data from terrestrial and marine palynomorphs, benthic and planktonic foraminifera, and other organic material constrain the age and depositional conditions of this marginal marine setting with evidence of a reducing and arid nature and an inner to

middle shelf transition during the early Cenomanian (based on the planktonic foraminifera *Rotalipora appenninica* and *Rotalipora gandolfi*). Additionally, this information provides insight into the hydrocarbon potential and productivity revealing the potential for type II and III kerogen, albeit low productivity.

## ACKNOWLEDGEMENTS

The samples studied for this project were provided by of PetroSA. We especially thank Dr. Mohamed Zobaa (University of Texas of the Permian Basin) for assisting with the taxonomic identification of palynomorphs. We also thank Dr. Annette Götz (Landesamt für Bergbau, Energie und Geologie) for her insightful comments that improved the quality of this work. Funding provided by Geoscience and Geological and Petroleum Engineering Department at Missouri University of Science and technology, the Department of Earth Science at the University of the Western Cape, and the University of Missouri South African Education Program are gratefully acknowledged.

## REFERENCES

Adekola SA, Akinlua A, Mangelsdorf K (2012) Organic geochemical evaluation of Cretaceous shale samples from the Orange Basin, South Africa. Applied Geochemistry 27:1633–1644

Adekola SA, Akinlua A, Fadiya SL, Fajemila OT, Ugwu GC (2014) Palynological and paleoenvironmental analyses of selected shale samples based on terrestrial palynomorphs from two wells in the offshore Orange Basin of South Africa. Ife Journal of Science 16(1):44–59

An K, Chen H, Lin X, Wang F, Yang S, Wen Z, Wang Z, Zhang G, Tong X (2017) Major transgression during Late Cretaceous constrained by basin sediments in northern Africa: implication for global rise in sea level. Frontiers of Earth Science 11:740–750

Baby G, Guillocheau F, Braun J, Robin C, Dall'Asta M (2020) Solid sedimentation rates history of the Southern African continental margins: Implications for the uplift history of the South African Plateau. Terra Nova 32:53–65

Bamford MK, Corbett IB (1994) Fossil wood of Cretaceous age from the Namaqualand continental shelf, South Africa. Palaeontologia Africana 31:83–95

Bamford MK, Corbett IB (1995) More fossil wood from the Namaqualand coast, South Africa: onshore material. Palaeontologia Africana 32:67–74

Benson JM (1990) Palynofacies characteristics and palynological source rock assessment of the Cretaceous sediments of the northern Orange Basin (Kudu 9A-2 and 9A-3 boreholes). Communications of the Geological Survey of Namibia 6:31–39

Boucot A, Xu C, Scotese, C (2013) Phanerozoic Paleoclimate: An Atlas of Lithologic Indicators of Climate. In: Nichols GJ, Ricketts B (eds) Concepts in Sedimentology and Paleontology, SEPM (Society for Sedimentary Geology), 11:478

Brown LF, Brown Jr LF, Benson JM, Brink GJ, Doherty S, Jollands A, Jungslager EHA, Keenan JHG, Muntingh A, Van Wyk NJS (1996) Sequence stratigraphy in offshore South Africa divergent basins. An Atlas on Exploration for Cretaceous Lowstand Traps. AAPG Studies in Geology 41:138–184

Brownfield ME (2016) Assessment of undiscovered oil and gas resources of the Orange River Coastal Province, southwest Africa. In: Brownfield ME (eds) Geologic assessment of undiscovered hydrocarbon resources of Sub-Saharan Africa, U.S. Geological Survey Digital Data Series 69–GG, 8:14

Campher CJ, di Primio R, Kuhlmann G, van der Spuy D, Domoney R (2009) Geological modeling of the offshore Orange Basin, west coast of South America. American Association of Petroleum Geologists Search and Discovery 10191:1-5

Campher C (2009) Geological modeling of the offshore Orange Basin, west coast of South Africa. M.Sc. thesis, University of the Western Cape, Cape Town, South Africa

Caron M (1985) Cretaceous planktic foraminifera. In: Bolli HM, Saunders JB, Perch-Nielsen K (ed) Plankton Stratigraphy. Cambridge University Press, Cambridge, p 17–86

Carvalho MA, Lana CC, Bengtson P, Sá NP (2017) Late Aptian (Cretaceous) climate changes in northeastern Brazil: A reconstruction based on indicator species analysis (IndVal). Palaeogeography, Palaeoclimatology, Palaeoecology 485:543–560

Davey R (1978) Marine Cretaceous palynology of Site 361, DSDP Leg 40, off Southwestern Africa. In: Bolli HM, Ryan WBF (ed) Initial Reports of the Deep Sea Drilling Project, Leg 40. Ocean Drilling Program, College Station TX, p 889–913

Davey RJ, Rogers J (1975) Palynomorph distribution in Recent offshore sediments along two traverses off South West Africa. Marine Geology 18(4):213–225

De Villiers SE, Cadman A (2001) An analysis of the palynomorphs obtained from Tertiary sediments at Koingnaas, Namaqualand, South Africa. Journal of African Earth Sciences 33:17–47

Dingle RV, Hendy QB (1984) Late Mesozoic and Tertiary sediment supply to the eastern Cape Basin (SE Atlantic) and palaeodrainage systems in southwestern Africa. Marine Geology 56:13–26

El Beialy SY, Zobaa MK, Taha AA (2016) Depositional paleoenvironment and hydrocarbon source potential of the Oligocene Dabaa Formation, north Western Desert, Egypt: A palynofacies approach. Geosphere 12(1):346–353

Eldridge J, Walsh D, Scotese CR (2002) PALEOMAP Paleogeographic Atlas. www.scotese.com

El-Soughier MI (2014) Palynology and palynofacies of the Upper Cretaceous succession of the El-Noor-1X borehole, northwestern Egypt. Arabian Journal Geosciences 7:1297–1311

Emmings JF, Hennissen JAI, Stephenson MH, Poulton SW, Vane CH, Davies SJ, Leng MJ, Lamb A, Moss-Hayes V (2019) Controls on amorphous organic matter type and sulphurization in a Mississippian black shale. Review of Palaeobotany and Palynology 268:1–18

Feldmann R, Chapman R, Hannibal J (1989) Paleotechniques. The Paleontological Society Special Publication No. 4, 5 p

Fensome RA, Williams GL, MacRae RA (2019) The Lentin and Williams Index of fossil dinoflagellates. AASP Contributions Series No. 50, 1173 p

Fischer M, Uenzelmann-Neben G (2018) Late Cretaceous onset of current controlled sedimentation in the African–Southern Ocean gateway. Marine Geology 395:380–396

Fossilworks, Gateway to the Paleobiology Database. http://fossilworks.org/bridge.pl?a=home. Accessed 4 January 2021

Frederiksen NO, Bybell LM, Christopher RA, Crone AJ, Edwards LE, Gibson TG, Hazel JE, Repetski JE, Russ DP, Smith CC, Ward LW (1982) Biostratigraphy and paleoecology of lower Paleozoic, Upper Cretaceous, and lower Tertiary rocks in U.S. Geological Survey New Madrid test wells, southeastern Missouri. Tulane Studies in Geology and Paleontology 17:23–45

Gallagher K. Brown RW (1999) The denudation history of the Atlantic Margins of southern Africa and south-east Brazil and their relationship to offshore sedimentation, In: Cameron N (ed) Oil and Gas Habitats of the South Atlantic Special Publication. Geological Society of London, The Royal Society, London, vol 357

Gordon W (1973) Marine Life and Ocean Surface Currents in the Cretaceous. The Journal of Geology 81(3):269–284

Green OR (2001) Staining Techniques Used in Micropalaeontology. In: A Manual of Practical Laboratory and Field Techniques in Palaeobiology. Springer, Dordrecht, p 211-218

Guiry MD, Guiry GM (2021) *AlgaeBase*. World-wide electronic publication, National University of Ireland, Galway. https://www.algaebase.org. Accessed 4 January 2021

Gupta BK, Machain-Castillo ML (1993) Benthic foraminifera in oxygen-poor habitats. Marine Micropaleontology 20(3–4):183–201

Harris A, Sweet W (1989) Mechanical and chemical techniques for separating microfossils from rock, sediment, and residue matrix. The Paleontological Society Special Publications, 4 (1): 70–86

Herngreen GFW, Chlonova AF (1981) Cretaceous microfloral provinces. Pollen et Spores 23:441–555

Ibrahim MIA, Zobaa MK, El-Noamani ZM, Tahoun SS (2015) A review of the angiosperm pollen genus Cretacaeiporites Herngreen, with one new species from the Upper Cretaceous of Egypt. Palynology 41(1): 101–116

Jansonius J, Hills LV (1976) Genera file of fossil spores and pollen (with supplements). Special Publication, Department of Geology, University of Calgary, Canada

Jaramillo C, Rueda M (2019) A Morphological Electronic Database of Cretaceous-Tertiary and Extant pollen and spores from Northern South America, v. 2019. https://biogeodb.stri.si.edu/jaramillosdb/web/morphological/. Accessed 4 January 2021

Jungslager EHA (1999) Petroleum habitats of the Atlantic margin of South Africa. Geological Society, London, Special Publications 153:153–168

Kandiyoti R, Herod AA, Bartle K (2006) Solid fuels and heavy hydrocarbon liquids: thermal characterisation and analysis. Solid fuels and heavy hydrocarbon liquids: thermal characterisation and analysis, Energy, Elsevier, Oxford

Khalifa MA, Catuneanu O (2008) Sedimentology of the fluvial and fluvio-marine facies of the Bahariya Formation (Early Cenomanian), Bahariya Oasis, Western Desert, Egypt. Journal of African Earth Sciences 51(2):89–103

Kuhlmann G, Adams S, Campher C, van der Spuy D, di Primio R, Horsfield B (2010) Passive margin evolution and its controls on natural gas leakage in the southern Orange Basin, blocks 3/4, offshore South Africa. Marine and Petroleum Geology 27(4):973–992

Kummel B, Raup D (1965) Handbook of paleontological techniques. WH Freeman and Co, London

Londeix L, Pourtoy D, Fenton JPG (1996) The presence of Dinogymnium (Dinophyceae) in Lower Cretaceous sediments from the northwest Tethys (southeast France and western Switzerland) and Gulf of Mexico areas: stratigraphic and systematic consequences. Review of Palaeobotany and Palynology 92:367–382.

McLachlan IR, Pieterse E (1978) Preliminary palynological results Deep Sea Drilling Project, Initial Reports, U.S. Government Print Office, Washington, 40:857–881

McMillan IK (2003) Foraminiferally defined biostratigraphic episodes and sedimentation pattern of the Cretaceous drift succession (Early Barremian to Late Maastrichtian) in seven basins on the South African and southern Namibian continental margin. South African Journal of Science 99:537–576

McMillan IK (2008) Aragonitic-walled benthic foraminifera (E.pistomina) in the Cretaceous 'mud belt' off southern Africa, and postmortem cross-shelf transport of tests. African Natural History 4:17–24

McLachlan IR, Pieterse E (1978) Preliminary palynological results: Site 361, Leg 40, Deep Sea Drilling Project. In: Bolli, H. & Ryan, W.B.F., et al. (ed), Initial Reports of the Deep-Sea Drilling Project 40, Washington DC, U.S. Government Printing Office, p 857–881

Mathison S, Chmura G (1995) Utility of microforaminifera test linings in palynological preparations. Palynology 19:77–84

Miller KG, Sugarman PJ, Browning JV, Kominz MA, Hernández JC, Olsson RK, Wright JD, Feigenson MD, Van Sickel W (2008) Late Cretaceous chronology of large, rapid sea-level changes: Glacioeustasy during the greenhouse world. Geology 31(7):585–588

Muntingh A (1993) Geology, prospect in Orange Basin offshore western South Africa. Oil and Gas Journal 91:105–109

Muntingh A, Brown Jr. LF (1993) Sequence stratigraphy of petroleum plays, postrift Cretaceous rocks (lower Aptian to upper Maastrichtian), Orange basin, western offshore, South Africa. In: P. Weimer and H. W. Posamentier (ed), Siliciclastic sequence stratigraphy – recent developments and applications. American Association of Petroleum Geologists Memoir, 58, p 71–97

Nagy J, Hess S, Alve E (2010) Environmental significance of foraminiferal assemblages dominated by small-sized Ammodiscus and Trochammina in Triassic and Jurassic delta-influenced deposits. Earth-Science Reviews 99(1–2):31–49

Oboh-Ikuenobe FE, De Villiers SE (2003) Dispersed organic matter in samples from the western continental shelf of Southern Africa: palynofacies assemblages and depositional environments of Late Cretaceous and younger sediments. Palaeogeography, Palaeoclimatology, Palaeoecology, 201:67–88

Oboh-Ikuenobe FE, Obi CG, Jaramillo CA (2005) Lithofacies, palynofacies, and sequence stratigraphy of Paleogene strata in southern Nigeria. Journal of African Earth Sciences 41:79–101

Pacton M, Fiet N, Gorin GE (2007) Bacterial Activity and Preservation of Sedimentary Organic Matter: The Role of Exopolymeric Substances. Geomicrobiology Journal 24(7-8):571–581

Pacton M, Gorin GE, Vasconcelos C (2011) Amorphous organic matter — Experimental data on formation and the role of microbes. Review of Palaeobotany and Palynology 166(3–4):253–267

Palynodata and White (2008) Palynological Literature Information Collection. Springfield, Massachusetts, USA: Palynodata Incorporation, https://doi.org/10.4095/225704. Accessed 4 January 2021

PAST© 2001, Hammer Ø, Harper DAT, Ryan PD (2001) Past: Paleontological Statistics Software Package for Education and Data Analysis. Palaeontologia Electronica, 4:1, art. 4: 9 p., 178kb. http://palaeo-electronica.org/2001_1/past/issue1_01.htm. Accessed 4 January 2021

Paton DA, di Primio R, Kuhlmann G, van der Spuy D, Horsfield B (2007) Insights into the Petroleum System Evolution of the Southern Orange Basin, South Africa. South African Journal of Geosciences :261–274

Powell AJ, Dodge JD, Lewis J (1990) Late Neogene to Pleistocene palynological facies of the Peruvian continental margin upwelling, Leg 112. In: Suess E, Von Huene R et al. (eds) Proceedings of the Ocean Drilling Program, Scientific Results, vol 112. Ocean Drilling Program, College Station, pp 297-321

Powell AJ, Lewis J, Dodge JD (1992) The palynological expressions of post-Palaeogene upwelling: A review. In Summerhayes CP, Prell WL, Emeis KC (eds) Upwelling systems: evolution since the Early Miocene. Geological Society Special Publication 64(1):215-226

Rouby D, Bonnet S, Guillocheau F, Gallagher K, Robin C, Biancotto F, Braun J (2009) Sediment supply to the Orange sedimentary system over the last 150 My: An evaluation from sedimentation/denudation balance. Marine and Petroleum Geology 26:782–794

Salie S (2018) The effects of minerals on reservoir properties in block 3A and 2C, within the Orange Basin, South Africa. Dissertation, University of the Western Cape

Sanderson A (2006) A palynological investigation of the offshore Cretaceous sequence on the south-west coast of South Africa. Dissertation, University of the Witwatersrand

Sandersen A, Scott L, McLachlan IR, PJ, Hancox PJ (2011) Cretaceous biozonation based on terrestrial palynomorphs from two wells in the offshore Orange Basin of South Africa. Palaeontologia Africana 46:21–41

Schrank E (2010) Pollen and spores from the Tendaguru Beds, Upper Jurassic and Lower Cretaceous of southeast Tanzania: palynostratigraphical and paleoecological implications. Palynology 34(1):3–42

Slimani H, Louwye S, Abdelkabir T (2010) Dinoflagellate cysts from the Cretaceous–Paleogene boundary at Ouled Haddou, southeastern Rif, Morocco: biostratigraphy, paleoenvironments and paleobiogeography. Palynology 34:90–124

Sokal RR, Michener CD (1958) A Statistical Methods for Evaluating Relationships. University of Kansas Science Bulletin 38:1409–1448

Stevenson I R, McMillan IK (2004) Incised valley fill stratigraphy of the Upper Cretaceous succession, proximal Orange Basin, Atlantic mar- gin of southern Africa. Journal of the Geological Society 161:185–208

Srivastava SK (1976) The fossil pollen genus Classopollis. Lethaia 9:437–457

Tonkin NS (2012) Trace Fossils as Indicators of Sedimentary Environments. In: Knaust D, Bromley RG (eds), Developments in Sedimentology, vol 64. Elsevier, London. pp 507-528

Traverse A (2007) Palaeopalynology, 2nd ed. Springer, Dordrecht

Tyson RV (1993) Palynofacies analysis. In: Jenkins DG (ed) Applied micropaleontology. Kluwer Academic Publishers, Dordrecht, p 153–191

Tyson RV (1995) Sedimentary Organic Matter; Organic Facies and Palynofacies. Chapman and Hall, London

Tyson RV, Follows B (2000) Palynofacies prediction of distance from sediment source: A case study from the Upper Cretaceous of the Pyrenees. Geology 28:569–571

Van der Spuy D (2003) Aptian source rocks in some South African Cretaceous basins. In: Arthur TJ, Macgregor DS and Cameron NR (eds) Petroleum geology of Africa: new themes and developing technologies, vol 207. Geological Society Special Publications, London, pp 185–202

Van der Spuy D (2005) Prospectivity of the Northern Orange Basin, offshore South Africa. Poster presented at Africa Session, Forum 23, 18th World Petroleum Congress, 25-29 September, Johannesburg, South Africa

Vandenbroucke M, Largeau C (2007) Kerogen origin, evolution and structure, Organic Geochemistry 38(5):719–833

Warny S, Jarzen DM, Haynes SJ, MacLeod KG, Huber BT (2019) Late Cretaceous (Turonian) angiosperm pollen from Tanzania: a glimpse of past vegetation from a warmer climate. Palynology 43(4):608–620

Zavada MS (2004) The earliest occurrence of angiosperms in Southern Africa. South African Journal of Botany 70:646–653

Zobaa M, Oboh-Ikuenobe F, Ibrahim M (2011) The Cenomanian/Turonian oceanic anoxic event in the Razzak Field, north Western Desert, Egypt: Source rock potential and paleoenvironmental association. Marine and Petroleum Geology 28(8):1475–1482

Zobaa MK, El Beialy SY, El Sheikh HA, El Beshtawy MK (2013) Jurassic Cretaceous palynomorphs, palynofacies, and petroleum potential of the Sharib1X and Ghoroud1X wells, north Western Desert, Egypt. Journal of African Earth Sciences 78:51–6

# SECTION

# 3. CONCLUSIONS

In the three case studies, applied palynology has provided key information to aid in interpreting age and paleoenvironment, evaluating hydrocarbon potential and contributing novel techniques to resolve challenging questions through correlation with other proxies.

The documentation of the novel effects of meteorite impact on palynomorphs and particulate organic matter in this work contributes to an understudied area (impact palynology). The mixed types and preservation states of palynomorph and particulate organic matter types (terrestrial and aquatic) provide evidences for stratigraphic mixing, paleoenvironmental conditions, and impact-related thermal damage inflicted on organic material in the form of melted Ordovician acritarchs.

Melted Ordovician acritarchs from the three Missouri 38$^{th}$ Parallel structures (Crooked Creek, Decaturville and Weaubleau) correlated with $^{40}Ar/^{39}Ar$ stepwise heating of impact spherules from the Crooked Creek crater provide a link with an Ordovician L-chondrite break-up and the subsequent Ordovician Meteorite Event and provide compelling evidence for the relationship of the 38$^{th}$ Parallel structures in Missouri with implications for geologic understanding of the U.S. midcontinent.

Correlation between palynological and foraminiferal studies provided valuable information about the age, paleoenvironment, and hydrocarbon potential of the Orange Basin, a frontier basin offshore in western South Africa. Through the combination of

lithology and biostratigraphy, the environment was constrained to a marginal marine setting with evidence of reducing and arid conditions and an inner to middle shelf transition during the early Cenomanian. The information provided by this study revealed primarily type III kerogen and some II kerogen, although low productivity that was likely limited by environment rather than preservation.

# APPENDIX A.

# PALYNOLOGY SAMPLE INFORMATION

Table A1. The locations and lithological information of palynological samples. Identifiers for the sample numbers are as follows: D = Decaturville; CC = Crooked Creek; W = Weaubleau.

| Sample no. | Location | Lithology | Depth (m) | Sample type |
|---|---|---|---|---|
| D1-2506-D771 | SE ¼ SE ¼ SE ¼ SE ¼, S31 T37N R16W, Camden County, Missouri, 37.895, -92.725 | Limestone | 11.28 m | Core |
| D2-3198-C57 | SW ¼ SW ¼ SW ¼, S32 T37N R16W, Camden County, Missouri, 37.89508, -92.7137 | Limestone | 21.34-21.95 m | Core |
| CC1-2504-CC794 | C NW ¼ SE ¼ SE ¼, S8 T37N R4W, Crawford County, Missouri, 37.849, -91.383 | Marl | 3.66 m | Core |
| CC2-2505-CC795 | NW ¼ NW ¼ SW ¼ SE ¼, S17 T36N R4W, Crawford County, Missouri, 37.835, -91.385 | Marl | 21.34 m | Core |
| W1-1690-NS1 | NW ¼ NW ¼ NE ¼ NE ¼, S12 T37N R26W, St. Clair County, Missouri, 37.99118, -93.7352 | Limestone | 14.94 m | Core |
| W2-9652 | C NE ¼, S10 T37N R25W, St. Clair County, Missouri 37.98666, -93.6625 | Shale/ Limestone/ Chert | 15.24-18.90 m | Cuttings |

# APPENDIX B.

# SPHERULE SAMPLE INFORMATION

Table B1. The locations and lithological information of spherule samples. Identifiers for the sample numbers are as follows: D = Decaturville; CC = Crooked Creek; W = Weaubleau.

| Sample no. | Location | Litholo-gy | Depth (m) | Sample type | Crater Loca-tion |
|---|---|---|---|---|---|
| DOB1 | State Highway 5, Camden County, Missouri, 37.895, -92.725 | Polymict breccia (marl matrix) | Surface | Outcrop | Rim |
| CC-79-5 | Crawford County, Missouri 37.835, -91.385 McCracken Core Library, DNR Missouri Geological Survey, Rolla MO | Lime-stone | 560 m | Core | Central uplift |
| CC-002166 | Crawford County, Missouri 37.8339, -91.396 McCracken Core Library, DNR, Missouri Geological Survey, Rolla, MO | Dolo-mite | 240 m | Cuttings | Central uplift |
| WOB1 | State Highway 13, St. Clair County, Missouri 37.942176, -93.634577 | Polymict breccia (marl matrix) | Surface | Outcrop | Rim/center |

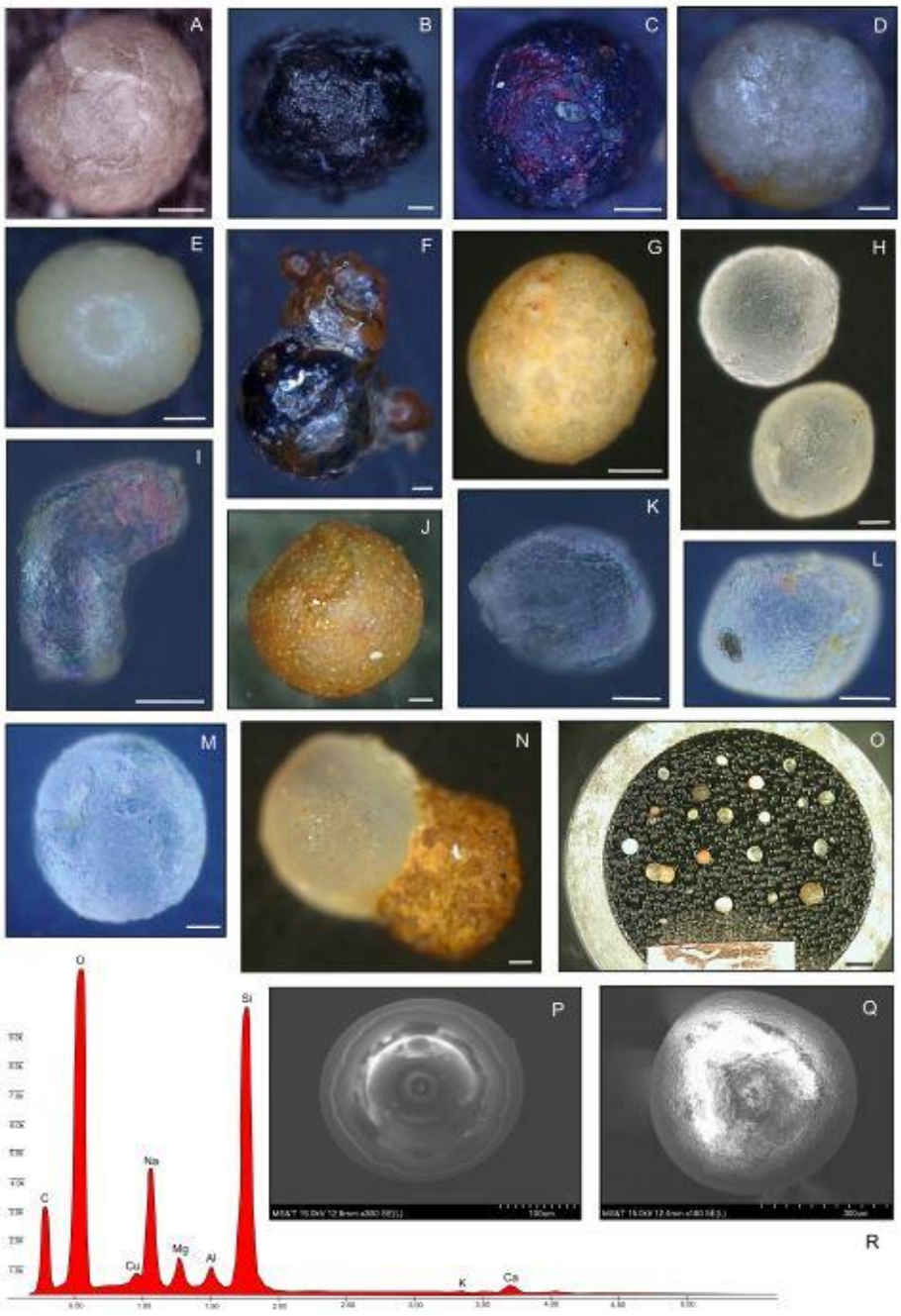


Figure B1. Images of selected spherules from Crooked Creek (A-D), Decaturville (E-H, N,O,P,Q) and Weaubleau (I-M) impact structures, SEM-EDS stub with some Decaturville spherules including EDS results from included glassy spherule with sodic glass composition.

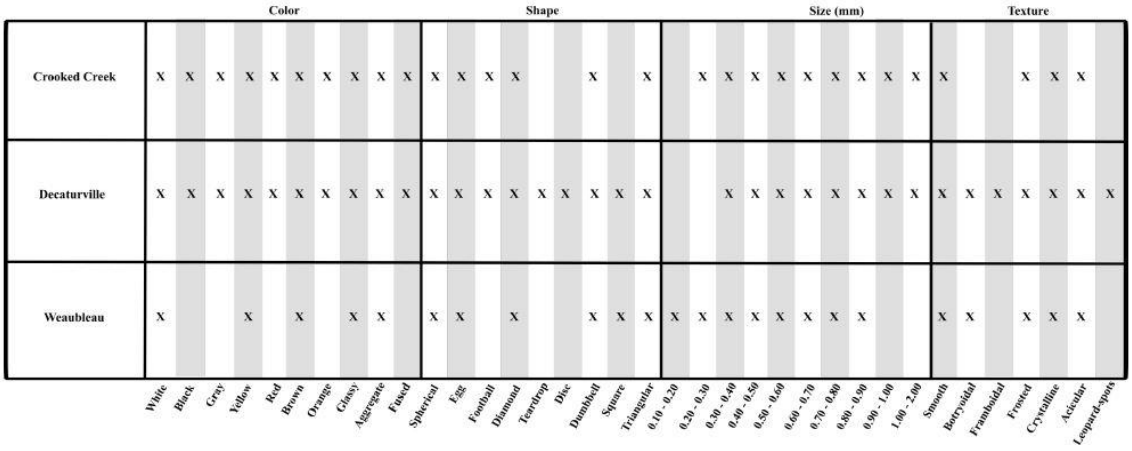


Figure B2. Spherule characteristics for Crooked Creek, Decaturville and Weaubleau impact structures.

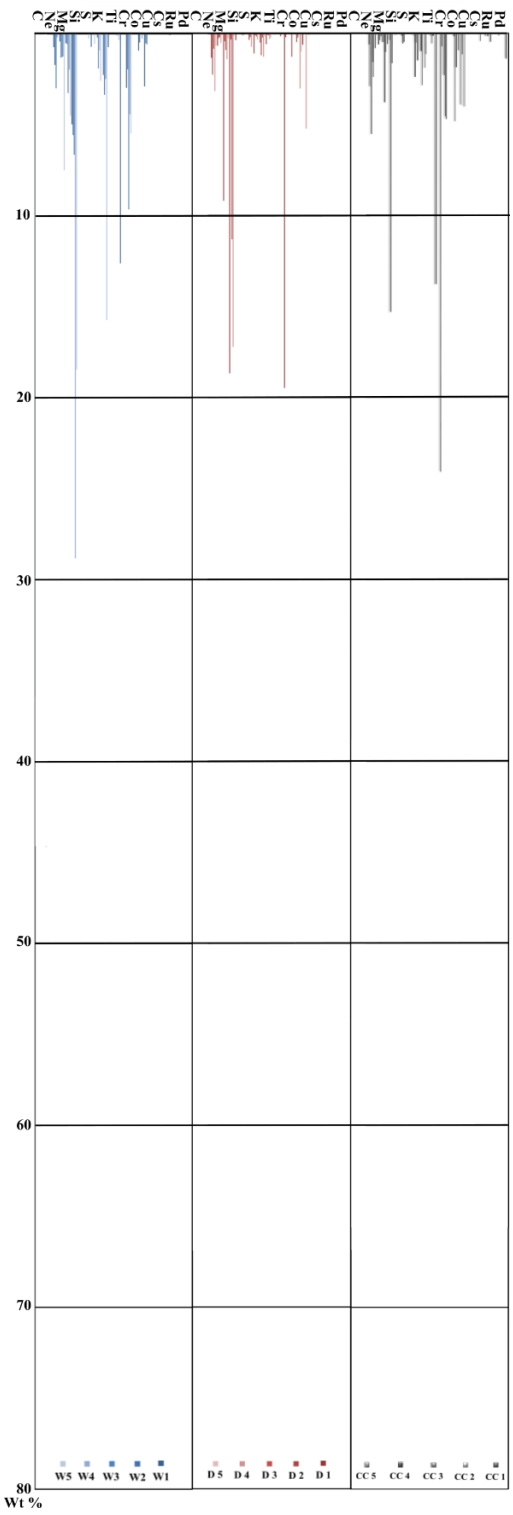


Figure B3. SEM-EDS Results for Crooked Creek (C), Decaturville (D) and Weaubleau (W) impact spherules. Additional data can be accessed online at https://scholarsmine.mst.edu/research_data/.

# APPENDIX C.

# $^{40}$AR/$^{39}$AR STEPWISE HEATING METHODOLOGY, DATA ACCESS AND REFERENCES

## 1. $^{40}Ar/^{39}Ar$ STEPWISE HEATING METHODOLOGY

$^{40}Ar/^{39}Ar$ analyses were performed at the University of Vermont Noble Gas Geochronology Laboratory. The spherules were loaded into aluminum foil packets, arranged in a suprasil vial, and placed in an aluminum canister for irradiation. Samples were irradiated at the Oregon State University Radiation Center in the CLOCIT facility for 18 hours with multigrain aliquots of Fish Canyon Tuff Sanidine to act as a flux monitor (28.201 ± 0.046; Kuiper et al. (2008). Laser step heating for $^{40}Ar/^{39}Ar$ dating was conducted with a Santa Cruz Laser Microfurnace 75 W diode laser system. Samples were loaded directly into wells in a copper sample holder. The gas released during heating was purified with SAES getters and argon isotopes were analyzed on a Nu Instruments Noblesse magnetic sector noble gas mass spectrometer in peak-hopping mode during step-heating analyses. Data from samples and flux monitors were corrected for blanks, mass discrimination, atmospheric argon, neutron-induced interfering isotopes, and the decay of $^{37}Ar$ and $^{39}Ar$. Correction factors used to account for interfering nuclear reactions for the irradiated samples are from Rutte et al. (2018), and decay constants are from Min et al. (2000) and Stoenner et al. (1965). Mass discrimination was calculated by analyzing known aliquots of atmospheric argon for which the measured $^{40}Ar/^{36}Ar$ (299.2 ± 0.44) was compared with an assumed atmospheric value of 298.56 (Lee et al., 2006). A linear interpolation was used to calculate J factors for samples based on sample position between flux monitor packets in the irradiation tube. The data analyses were achieved using both an in-house data reduction program and Isoplot 3.0 (Ludwig, 2003). Data and additional information may be accessed at https://scholarsmine.mst.edu/research_data/.

# REFERENCES

Lee, J.Y., Marti, K., Severinghaus, J.P., Kawamura, K., Yoo, H.S., Lee, J.B. and Kim, J.S., 2006. A redetermination of the isotopic abundances of atmospheric Ar. Geochimica et Cosmochimica Acta, 70(17), pp.4507-4512.

Min, K., Mundil, R., Renne, P.R. and Ludwig, K.R., 2000. A test for systematic errors in $^{40}Ar/^{39}Ar$ geochronology through comparison with U/Pb analysis of a 1.1-Ga rhyolite. Geochimica et Cosmochimica Acta, 64(1), pp.73-98.

Stoenner, R.W., Schaeffer, O.A. and Katcoff, S., 1965. Half-lives of argon-37, argon-39, and argon-42. Science, 148(3675), pp.1325-1328.

Kuiper, K.F., Deino, A., Hilgen, F.J., Krijgsman, W., Renne, P.R. and Wijbrans, A.J., 2008. Synchronizing rock clocks of Earth history. science, 320(5875), pp.500-504.

Rutte, D., Becker, T.A., Deino, A.L., Reese, S.R., Renne, P.R. and Schickler, R.A., 2018. The New CLOCIT Irradiation Facility for 40Ar/39Ar Geochronology: Characterisation, Comparison with CLICIT and Implications for High-Precision Geochronology. Geostandards and Geoanalytical Research, 42(3), pp.301-307.

# APPENDIX D.

# PENNSYLVANIAN ROCK SAMPLES

Table D1. Surface Pennsylvanian rock and sediment locations around the Missouri 38th Parallel Structures studied for presence of spherules.

| Location (Lat/Long) | Rock/sediment |
|---|---|
| 37.891436/-93.606671 | clay |
| 37.886749/-93.611658 | clay |
| 37.975831/-93.498670 | clay, limestone, shale and sandstone |
| 38.003697/-92.064746 | clay, limestone, shale and sandstone |
| 37.971679/-91.739331 | clay |

# APPENDIX E.

# GEOCHEMISTRY MAP AND SOURCE DATA ACCESS

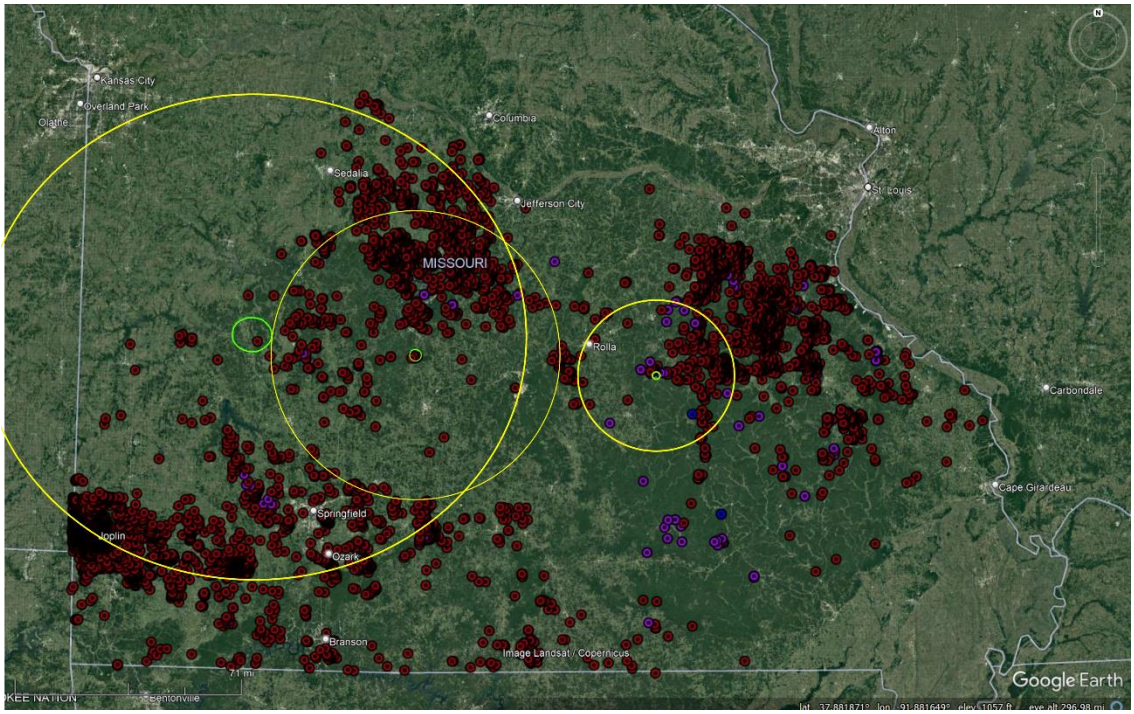


Figure E1. Google Earth Pro image of the presence of zinc (red), cobalt (blue) and copper (purple) based on the geochemistry of soil, water, and rock in relation to the three Missouri 38th Parallel structures. Green circles represent the crater extent for Weaubleau, Decaturville and Crooked Creek (left to right) craters in Missouri. Yellow circles highlight the pattern of geochemistry data that may be related to impact generated hydrothermal activity. Missouri data portion of the National Geochemistry Database: https://gis-modnr.opendata.arcgis.com/datasets/modnr::national-geochemical-survey/about. Last accessed 03/26/2023.

# VITA

Marissa Kay Spencer was born in Dexter, Missouri. She received her Bachelor of Science in Geology & Geophysics in 2014 from the Department of Geosciences and Geological and Petroleum Engineering, Missouri University of Science and Technology, Rolla, Missouri, USA. Marissa received a PhD in Geology and Geophysics in May 2023 from the Department of Geosciences and Geological and Petroleum Engineering, Missouri University of Science and Technology for her research using biogeochronology and geochemistry. Marissa's professional appointments include Teaching and Research Assistant, Department of Geosciences and Geological and Petroleum Engineering, Missouri University of Science and Technology (2016-2018), and Teaching Assistant, Department of Materials Science, Missouri University of Science and Technology (2018-2021).